NUMERICAL APPROXIMATIONS FOR THE FRACTIONAL LAPLACIAN IN SPACE-FRACTIONAL REACTION-DIFFUSION EQUATIONS

by

Saham S. Alzahrani

A Dissertation Submitted in Partial Fulfillment

of the Requirements for the Degree of

Doctor of Philosophy in Computational Science

Middle Tennessee State University

Fall 2019

Dissertation Committee:

Prof. Abdul Khaliq, Chair

Department of Mathematical Sciences

Prof. Yuri Melnikov

Department of Mathematical Sciences

Prof. Tibor Koritsanszky

Department of Chemistry

Dedicated to

my beloved parents, husband,

and kids.

ACKNOWLEDGMENTS

I would like to express my sincere appreciation to all those who have supported me throughout the Ph.D. program. I would particularly like to single out my advisor Professor Abdul Khaliq. I want to thank you for your support, invaluable suggestions, and collaboration. I want also to thank you for all of the opportunities that I was offered to accomplish my research. Without your endless help and guidance, this dissertation would never have been possible. I am deeply grateful to Professor John Wallin, Director of the Computational Science program, for his assistance during my study. I am thankful to the committee members, Professors Yuri Melnikov and Tibor Koritsanszky, for their help with reviewing this dissertation. I would like to thank the co-authors of my research papers, Professor Khaled Furati from King Fahd University of Petroleum and Minerals (KFUPM) and my colleague Toheeb Biala, for their invaluable comments and suggestions.

My deepest gratitude goes to my lovely family for making my success possible. I am grateful to my parents for their constant love and prayers. I am thankful to my dear husband, Rami, who encouraged and motivated me while pursuing his own Ph.D., and to my wonderful kids, Laith, Laura and Ghaith, for their unending inspiration. I want to thank my brothers, sisters, and friends for their continuous encouragement.

Finally, I am grateful to Taibah University for their scholarship, and to my country, Saudi Arabia, for providing the financial support through my education.

DECLARATION

I declare that this dissertation has not been submitted at any other university for any degree. The results presented in this dissertation are published in the following refereed journals:

- S. S. Alzahrani, A. Q. M. Khaliq, High-order time stepping Fourier spectral method for multi-dimensional space-fractional reaction-diffusion equations. *Computers & Mathematics with Applications*, 77(3):615-630, 2019.

- S. S. Alzahrani, A. Q. M. Khaliq, Fourier spectral exponential time differencing methods for multi-dimensional space-fractional reaction-diffusion equations. *Journal of Computational and Applied Mathematics*, 361:157-175, 2019.

- S. S. Alzahrani, A. Q. M. Khaliq, T. A. Biala, K. M. Furati, Fourth-order time stepping methods with matrix transfer technique for space-fractional reaction-diffusion equations. *Applied Numerical Mathematics*, 146:123-144, 2019.

ABSTRACT

The systems of non-linear time-dependent space-fractional differential equations have been employed to model important physical phenomena in many fields of engineering and science. The analytical solutions of most of these systems are unknown, and evaluating an analytical solution for some fractional differential equations is complicated and difficult to calculate because it is in the trigonometric series form. Thus, developing numerical solutions for such nonlinear systems is essential. There have been growing interests recently to develop efficient and robust numerical schemes for solving the nonlinear systems of fractional differential equations.

In this study, several novel numerical schemes are proposed to solve the systems of multidimensional non-linear space-fractional reaction-diffusion equations efficiently. The non-local nature of the fractional operator adds new features to the mathematical models but also introduces additional difficulties in their implementation where large, dense matrices are required at each time step. To overcome this challenge, the Fourier spectral approach is applied to discretize the fractional Laplacian. This approach gives a diagonal representation of the fractional operator while achieving spectral convergence and the implementation to multi-dimensions is similar to one-dimensional problems. Since this approach lacks capability to implement on non-homogeneous boundary conditions, a second-order matrix transfer technique (MTT) for non-homogeneous boundary conditions is used for the space discretization. A fourth-order MTT based on a compact scheme is also employed for the discretization of the fractional Laplacian.

To deal with the nonlinearities, exponential time differencing schemes (ETD) are employed for the reason that while the approaches achieve the expected accuracy, solving nonlinear systems at each time step is no longer needed. The Fourier spectral approach is combined with two second-order ETD schemes to solve space-fractional reaction-diffusion equations with non-smooth initial data and is also combined with a forth-order ETD scheme to provide highly efficient solutions for multidimensional

systems. The second-order MTT is combined with the forth-order ETD scheme to solve problems with non-homogeneous boundary conditions. Moreover, the fourth-order compact scheme MTT is combined with forth-order ETD schemes to show the effectiveness of the L-stable scheme when the initial data is non-smooth and to illustrate that the A-stable scheme is not reliable for some time steps. A novel reliability constraint is introduced to avoid the oscillations present in the solutions when the A-stable scheme is employed.

Theoretical and numerical investigation of the convergence and stability of the numerical schemes have been discussed. Extensive numerical experiments are performed on wide well-known systems of time-dependent space-fractional reaction-diffusion equations to demonstrate the reliability, efficiency and accuracy of the developed schemes.

CONTENTS

List of Tables

List of Figures

CHAPTER 1

INTRODUCTION

Fractional calculus indicates the generalization of integrals and derivatives of the integer-order to rational-order [1]. In 1695, the possibility of the fractional derivative was first discussed in a letter from Leibniz to L'Hôpital [2, 3, 4], in which it was asked what the derivative of $d^n y/dx^n$ is when $n = 1/2$. Later, Leibniz mentioned the derivative of the general order in a letter to J. Bernoulli. Euler and Lagrange *et al.* provided some relevant observations on this problem. In 1812, Laplace introduced a definition of fractional derivative based on the concept of integral, and Lacroix proposed a definition by employing the gamma function that is consistent with the fractional derivative of Riemann-Liouville. Fourier, in 1822, introduced the definition of fractional derivative through the Fourier transform. In 1930, Liouville generalized the order of the derivative into an arbitrary order, the reader is referred to [5].
Researchers have been investigating fractional calculus for developing advanced mathematical models which can depict complicated anomalous systems accurately [6]. Under the effect of various force fields, the elementary particles execute complex motion and the particles' trajectories create geometrical objects of complex structure [7]. Since the Gauss' distribution cannot explain the possibility that the particles will be at a specific time at given spatial points, it can no longer be modeled by the diffusion equation dependent on the Fickian equation (classical Fick's law) [8]. For complex situations, it was demonstrated that the density of probability distribution of the migrating particles could be depicted by equations that contain fractional derivatives [9, 10, 11, 12, 13, 14, 15]. The fractured porous medium is considered as fractal due to its complicated structure. The material particles execute complex motion while departing through fractures. Under the effect of various force fields, the equations of anomalous diffusion of the elementary particles motion will be similar to the diffusion equation in the porous medium, see [8]. Anomalous diffusion phenomena are

common in many complex dynamical systems in the natural sciences. These systems consist of a large variety of elementary units with strong interactions between them. Hence, as time advances, the anomalous evolution is non-predictable. Fractional kinetic equations are used as an effective technique to depict these complex systems such as diffusion, diffusive convection, and Fokker-Planck of fractional differential equations [5].

Definition 1.1. *Mean squared displacement* $\left(MSD, \left\langle (\Delta x)^2 \right\rangle\right)$ *is the measure of the deviation of the position of a particle regarding a reference position over time. It is defined as*

$\boldsymbol{MSD} = \left\langle (x - x_0)^2 \right\rangle = \frac{1}{N} \sum_{n=1}^{N} (x_n(t) - x_n(0))^2,$

where N represents the number of particles to be averaged, $x_n(0) = x_0$ *is the reference position of each particle,* $x_n(t)$ *is the position of each particle in determined time t [16].*

Randomness diffusion occurs in a space with the following classification:

$$\left\langle \ (\Delta x)^2 \right\rangle \propto t^{\alpha} = \begin{cases} \alpha < 1, & \text{sub-diffusion,} \\ \alpha = 1, & \text{diffusion,} \\ \alpha > 1, & \text{super-diffusion.} \end{cases}$$

Recently, fractional differential equations have gained a lot of popularity in many applications such as the mathematical modeling of transport processes in the spatially heterogeneous medium. Many researchers have shown that the partial differential equations, including fractional derivatives, are more useful for understanding spatial heterogeneity and non-locality than the corresponding integer-order. The fractional derivatives have been utilized in hydrology [17], image denoising [18], anomalous diffusion [19], turbulence [20], elasticity [21], finance [22, 23, 24, 25], soft matter [26], and numerous applications for problems across disciplines such as physics, biology, and chemistry [15, 27, 28, 29, 30]. For instance, Baeumer *et al.* [30] used the frac-

tional reaction-diffusion equation that captured the realistic spreading behavior of invading species. In finance, Wang *et al.* [25] implemented a circulant preconditioning technique for barrier options pricing using the fully implicit scheme with the shifted Grünwald approximation. In groundwater hydrology, the transport of passive tracers carried by fluid flow in a porous medium was modeled by the fractional advection-dispersion equation [31, 32]. In water resources, the transport of chemical and pollutant through heterogeneous aquifers was described by the fractional models [33, 34, 35].

The fractional generalizations of the model equations have been considered for space-fractional derivatives, for example, in quantum mechanics [36], plasma physics [37], and contaminant dispersion [38]. They also have been considered for time-fractional derivatives, for example, in viscoelasticity [39], porous media [40], and diffusion problems in biological systems [41]. The fractional Laplacian has been intensively considered among different fractional operators in the recent literature. The integer-order Laplacian has been replaced by the fractional Laplacian in many applications of fractional models including reaction-diffusion [42], Schrödinger [43], quasi-geostrophic [44] and porous medium [45]. The fractional Laplacian is defined in many different ways, for example, Riesz potential operator [46], Fourier multiplier [47], and hypersingular integral [48]. These definitions are shown to be equivalent in $\mathbb{R}^d$, where $d = 1, 2, 3$, under certain assumptions. Nevertheless, when a bounded domain $\Omega \subset \mathbb{R}^d$ is considered, the associated boundary conditions produce various operators and the equivalence no longer holds [49].

1.1 Fractional Laplacian

The fractional Laplacian is defined as [49, 50]

$$(-\Delta)^{\frac{\alpha}{2}} u(x) := c_{\alpha,d} \text{ P.V.} \int_{\mathbb{R}^d} \frac{u(x) - u(y)}{|x - y|^{\alpha+d}} dy,$$

where P.V. stands for the Cauchy principal value integration, and

$$c_{\alpha,d} = \frac{2^{\alpha}\Gamma(\frac{d+\alpha}{2})}{\pi^{d/2}|\Gamma(\frac{-\alpha}{2})|}.$$

In this study, we mainly focus on the utilization of the fractional Laplacian on a bounded domain. We discuss three common definitions of the nonlocal operator on the bounded domain.

- **Integral fractional Laplacian**

  The fractional Laplacian of $u(x),\ x \in \Omega$ is defined by extending $u(x)$ to a function in $\mathbb{R}^d$

  $$\tilde{u}(x) = \begin{cases} u(x) & x \in \Omega, \\ 0 & x \in \Omega^c, \end{cases}$$

  then the usual fractional Laplacian definition is used

  $$-(-\Delta)_I^{\frac{\alpha}{2}} u(x) := -(-\Delta)^{\frac{\alpha}{2}} \tilde{u}(x).$$

  It is also defined by the Fourier transform as

  $$-(-\Delta)_I^{\frac{\alpha}{2}} u(x) := \mathcal{F}^{-1}(|u|^{\alpha}\mathcal{F}\tilde{u}).$$

- **Spectral fractional Laplacian**

  The fractional Laplacian is defined by using the spectral definition

  $$-(-\Delta)_S^{\frac{\alpha}{2}} u(x) := \sum_{i \in N} u_i \lambda_i^{\frac{\alpha}{2}} \varphi_i(x),$$

  where λ_i and φ_i are the eigenvalues and eigenfunctions of the standard Laplace operator Δ in Ω with homogeneous Dirichlet boundary data, and u_i is the projection of u in the direction e_i

  $$\begin{cases} -\Delta\varphi_i = \lambda_i\varphi_i \ \text{ in } \Omega, \\ \varphi_i = 0 \quad \text{on } \partial\Omega. \end{cases}$$

- **Regional fractional Laplacian**

  This definition is obtained through restricting the integration domain to Ω

$$-(-\Delta)_R^{\frac{\alpha}{2}} u(x) := c_{\alpha,d} \int_\Omega \frac{u(x)-u(y)}{|x-y|^{\alpha+d}} dy.$$

The non-locality of fractional operators represents an important qualitative feature of the mathematical models, but introduces additional challenges to their numerical implementation. Several discretization schemes have been proposed in the literature to deal with this issue [51, 52, 53, 54, 55]. A thorough review of the finite difference methods, Galerkin finite element methods, and the spectral methods for the fractional partial differential equations can be found in [56]. We discuss in brief some of the second-order spatial discretizations and mention some related critical definitions and lemmas.

1.1.1 Basic definitions and lemmas

Definition 1.1.1.1. *([47, 57]). The Riesz fractional operator for $n-1 < \alpha \leq n$ on a finite interval $0 \leq x \leq L$ is defined as*

$$\frac{\partial^\alpha}{\partial |x|^\alpha} u(x,t) = -C_\alpha ({}_0D_x + \ {}_xD_L) u(x,t),$$

where

$C_\alpha = \frac{1}{2\cos(\pi\alpha/2)}, \quad \alpha \neq 1,$

${}_0D_x u(x,t) = \frac{1}{\Gamma(n-\alpha)} \frac{\partial^n}{\partial x^n} \int_0^x \frac{u(\xi,t)}{(x-\xi)^{\alpha+1-n}} d\xi,$

${}_xD_L u(x,t) = \frac{(-1)^n}{\Gamma(n-\alpha)} \frac{\partial^n}{\partial x^n} \int_x^L \frac{u(\xi,t)}{(\xi-x)^{\alpha+1-n}} d\xi.$

Definition 1.1.1.2. *([58]). Let the Laplacian $(-\Delta)$ have a complete set of orthonormal eigenfunctions φ_n corresponding to eigenvalues λ_n^2 on a bounded region Ω with the homogeneous boundary conditions, then*

$$(-\Delta)^{\frac{\alpha}{2}} f = \begin{cases} (-\Delta)^m f, & \alpha = 2m,\ m = 0, 1, 2, \ldots, \\ (-\Delta)^{\frac{\alpha}{2}-m}(-\Delta)^m f, & m-1 < \frac{\alpha}{2} < m,\ m = 1, 2, \ldots, \\ \sum_{n=1}^{\infty} \lambda_n^{\alpha} \langle f, \varphi_n \rangle \varphi_n, & \alpha < 0. \end{cases}$$

Lemma 1.1.1.3. *[59]. For a function u(x) defined on the infinite domain $-\infty < x < \infty$, the following equality holds*

$$-(-\Delta)^{\alpha/2} u(x) = -\frac{1}{2\cos\left(\frac{\pi\alpha}{2}\right)} \left[{}_{-\infty}D_x^{\alpha} u(x) + {}_x D_{\infty}^{\alpha} u(x) \right] = \frac{\partial^{\alpha}}{\partial |x|^{\alpha}} u(x).$$

1.1.2 Riesz derivative approximation

As discussed in [60], utilizing the fractional centered difference proposed by Ortigueira [61], the symmetric Riesz derivative of fractional-order α is approximated by $H_M^{(\alpha)}$. The left-sided Riemann-Liouville derivative ${}_{-\infty}D_x^{\alpha} u(x,t)$ and the right-sided Riemann-Liouville derivative ${}_x D_{\infty}^{\alpha} u(x,t)$ are approximated by the upper triangular strip matrix $B_M^{(\alpha)}$ and the lower triangular strip matrix $L_M^{(\alpha)}$ [62], respectively, such that

$$\left[u_M^{(\alpha)} u_{M-1}^{(\alpha)} \ldots u_1^{(\alpha)} u_0^{(\alpha)} \right]^T = B_M^{(\alpha)} \left[u_M^{(\alpha)} u_{M-1}^{(\alpha)} \ldots u_1^{(\alpha)} u_0^{(\alpha)} \right]^T,$$

$$\left[u_M^{(\alpha)} u_{M-1}^{(\alpha)} \ldots u_1^{(\alpha)} u_0^{(\alpha)} \right]^T = L_M^{(\alpha)} \left[u_M^{(\alpha)} u_{M-1}^{(\alpha)} \ldots u_1^{(\alpha)} u_0^{(\alpha)} \right]^T,$$

where

$$B_M^{(\alpha)} = \frac{1}{h^\alpha}\begin{bmatrix} \omega_0^{(\alpha)} & \omega_1^{(\alpha)} & \ddots & \ddots & \omega_{M-1}^{(\alpha)} & \omega_M^{(\alpha)} \\ 0 & \omega_0^{(\alpha)} & \omega_1^{(\alpha)} & \ddots & \ddots & \omega_{M-1}^{(\alpha)} \\ 0 & 0 & \omega_0^{(\alpha)} & \omega_1^{(\alpha)} & \ddots & \ddots \\ \dots & \dots & \dots & \ddots & \ddots & \ddots \\ 0 & \dots & 0 & 0 & \omega_0^{(\alpha)} & \omega_1^{(\alpha)} \\ 0 & 0 & \dots & 0 & 0 & \omega_0^{(\alpha)} \end{bmatrix},$$

and

$$L_M^{(\alpha)} = \frac{1}{h^\alpha}\begin{bmatrix} \omega_0^{(\alpha)} & 0 & 0 & 0 & \dots & 0 \\ \omega_1^{(\alpha)} & \omega_0^{(\alpha)} & 0 & 0 & \dots & 0 \\ \omega_2^{(\alpha)} & \omega_1^{(\alpha)} & \omega_0^{(\alpha)} & 0 & \dots & 0 \\ \ddots & \ddots & \ddots & \ddots & \dots & \dots \\ \omega_{M-1}^{(\alpha)} & \ddots & \omega_2^{(\alpha)} & \omega_1^{(\alpha)} & \omega_0^{(\alpha)} & 0 \\ \omega_M^{(\alpha)} & \omega_{M-1}^{(\alpha)} & \ddots & \omega_2^{(\alpha)} & \omega_1^{(\alpha)} & \omega_0^{(\alpha)} \end{bmatrix},$$

$\omega_j^{(\alpha)} = (-1)^j \binom{\alpha}{j}, \quad j = 0, 1, 2, ..., M,$ in which $x = jh$ $(j = 0, 1, 2, ..., M)$ where h is the spatial step size.

$$H_M^{(\alpha)} = \frac{1}{h^\alpha}\begin{bmatrix} \omega_0^{(\alpha)} & \omega_1^{(\alpha)} & \omega_2^{(\alpha)} & \omega_3^{(\alpha)} & \dots & \omega_M^{(\alpha)} \\ \omega_1^{(\alpha)} & \omega_0^{(\alpha)} & \omega_1^{(\alpha)} & \omega_2^{(\alpha)} & \dots & \omega_{M-1}^{(\alpha)} \\ \omega_2^{(\alpha)} & \omega_1^{(\alpha)} & \omega_0^{(\alpha)} & \omega_1^{(\alpha)} & \dots & \omega_{M-2}^{(\alpha)} \\ \ddots & \ddots & \ddots & \ddots & \dots & \dots \\ \omega_{M-1}^{(\alpha)} & \ddots & \omega_2^{(\alpha)} & \omega_1^{(\alpha)} & \omega_0^{(\alpha)} & \omega_1^{(\alpha)} \\ \omega_M^{(\alpha)} & \omega_{M-1}^{(\alpha)} & \ddots & \omega_2^{(\alpha)} & \omega_1^{(\alpha)} & \omega_0^{(\alpha)} \end{bmatrix},$$

where

$$\omega_j^{(\alpha)} = \frac{(-1)^j \Gamma(\alpha+1)\cos(\alpha\pi/2)}{\Gamma(\alpha/2-j+1)\Gamma(\alpha/2+j+1)}, \qquad j = 0, 1, 2, ..., M.$$

1.1.3 Matrix Transfer Technique (MTT)

As mentioned in [55], if the fractional Laplacian $(-\Delta)^{\alpha/2}$ is discretized with a uniform mesh of step size h by using the MTT suggested by Ilic *et al.* [58], then the following

form is obtained

$$(-\Delta)^{\alpha/2}u \approx \frac{A^{\alpha/2}}{h^{\alpha}}u.$$

The matrix $\frac{A^{\alpha/2}}{h^{\alpha}}$ is generated from the matrix representation of the standard Laplace operator using the eigenvalues and eigenvectors, thus $\frac{A^{\alpha/2}}{h^{\alpha}} = \frac{H\Lambda^{\alpha/2}H^{-1}}{h^{\alpha}}$ where Λ and H are the eigenvalues and eigenfunctions of the matrix $\frac{A}{h^2}$.

$A = \text{tridiag}\{-1, 2, -1\}$,

$\Lambda = \text{diag}(\lambda_1, \lambda_2, \lambda_3, \ldots, \lambda_{M-1}), \quad \lambda_j = 4\sin^2\left(\frac{j\pi}{2M}\right), \qquad j = 1, 2, \ldots, M-1,$

and $H = (\xi_1, \xi_2, \xi_3, \ldots, \xi_{M-1}), \;\; \xi_j = \left(\sin\left(\frac{1j\pi}{M}\right), \sin\left(\frac{2j\pi}{M}\right), \sin\left(\frac{3j\pi}{M}\right), \ldots, \sin\left(\frac{(M-1)j\pi}{M}\right)\right)^T.$

We discuss in detail discretizing the fractional Laplacian by using the Fourier spectral approach, second-order MTT for non-homogeneous boundary conditions, and fourth-order MTT in Chapters 2, 4, and 5, respectively.

1.2 Exponential Time Differencing (ETD) Schemes

To develop a better understanding of some phenomena related to the systems of nonlinear time-dependent fractional partial differential equations (FPDEs), accurate and efficient numerical schemes are required. Many efforts have been directed in recent years for developing reliable numerical schemes due to the complexities in evaluating an analytical solution of the nonlinear FPDEs. The method of lines is one of the most common approaches to solve such systems [63, 64]. After the space-fractional derivative of the nonlinear FPDEs is discretized with either finite difference, finite element or any other approximation, a system of ordinary differential equations (ODEs) in time is obtained. Then, the numerical solution to the FPDEs can be obtained by employing any time stepping method. The ETD schemes are well-known efficient time integration schemes which can be combined with any spatial approximation to get a numerical solution for semi-linear FPDEs. These ETD schemes were considered for partial differential equations in the 1960s by Certaine [65]. They have some special features including the exact treatment of the linear part and the explicit treatment

of the integral part by polynomial approximations. They also avoid solving nonlinear systems at each time step which makes them efficient compared to other time stepping methods. For the integer-order derivatives, Cox and Mathews [66] derived Runge-Kutta based ETD schemes utilizing polynomial formulas. When the linear term is a non-diagonal matrix, the implementation of the ETD schemes suffers with some computational challenges such as efficiency and accuracy. Efficient numerical evaluation of functions of the form $\frac{e^z-1}{z}$ and higher order generalizations thereof are computationally challenging where the cancellation errors have to be avoided [67, 68]. Thus developing these schemes is necessary, Kassam and Trefethen [68] modified the ETD schemes by introducing a method based on contour integration to address the computational difficulties. As in [69], the contour in their approach varies from problem to problem which makes it problem dependent. Additionally, it has to encircle the spectrum of the discretization matrix, which is usually unbounded and unknown for more finer discretization. The serious and challenging issue in both schemes is computing the matrix exponential, if a matrix is large. They utilized Matlab's expm function with $\mathcal{O}(n^3)$ complexity which makes their approach computationally impractical and inefficient for large problems with multi-dimensions. These issues were solved by applying Padé approximations that prevented direct computing of the matrix exponential function and utilized partial fraction decomposition, see Khaliq *et al.* [69].

1.2.1 Rational Approximation

Let $R_{r,s}(z)$ denote the (r, s)-Padé approximation, the $(r + s)^{th}$ order rational Padé approximation to e^{-z} is defined as in [70]

$$R_{r,s}(z) = \frac{P_{r,s}(z)}{Q_{r,s}(z)},$$

where

$$P_{r,s}(z) = \sum_{j=0}^{r} \frac{(s+r-j)!r!}{(s+r)!j!(r-j)!}(-z)^j,$$

$$Q_{r,s}(z) = \sum_{j=0}^{s} \frac{(s+r-j)!}{(s+r)!j!(s-j)!}(z)^j.$$

Definition 1.2.1.1. *[71, pp. 233]. A rational approximation $R_{r,s}(z)$ of e^z is said to be A-acceptable if $|R_{r,s}(z)| < 1$, whenever $Re(z) < 0$ and L-acceptable if it is A-acceptable and, in addition, $|R_{r,s}(z)| \to 0$ as $Re(z) \to -\infty$.*

- A-acceptable if $r = s$.
- L-acceptable if $r = s - 1$ or $r = s - 2$.

1.3 Time-Dependent Space-Fractional Reaction-Diffusion Equations

We consider the space-fractional reaction-diffusion equation

$$\frac{\partial u(x,t)}{\partial t} = -\kappa_\alpha(-\Delta)^{\alpha/2}u(x,t) + f(u,t), \quad 0 \le t \le T,\ 1 < \alpha \le 2, \tag{1}$$

subject to the initial condition given by

$$u(x,0) = u_0(x), \quad x \in \Omega \subset \mathbb{R}^d, \quad \text{where} \quad d = 1,2,3. \tag{2}$$

with homogeneous and non-homogeneous Dirichlet or Neumann boundary conditions, Ω is bounded in $\mathbb{R}$, κ_α represents the diffusion coefficient, $(-\Delta)^{\frac{\alpha}{2}}$ is the fractional Laplacian of order α $(1 < \alpha \le 2)$ [59, 72, 73, 74, 75], and f represents the nonlinear reaction term. As in [76], to ensure that (1) with specified initial and boundary conditions possesses a unique solution, we suppose that f is a sufficiently smooth function of u and t, and $f_u \ge -L$, where $L > 0$ is a constant. In order to avoid any blow-up in the solutions, we assume that $f_u \ge -L$. For the blow-up phenomena of

the solutions, see for example [77, 78].

Time-dependent fractional models have also been considered. Contrary to the local partial differential equations, the naïve application of the semi-implicit Euler integration schemes can be inefficient, as the fully dense matrix equations have to be solved at each time step. Several space discretization techniques have been discussed in [72, 79, 80] to tackle this issue. Also, there have been proposed several fast integration techniques based on the effective preconditioning [81], the Krylov scheme [82], and the rational approximation using the Gauss-Jacobi rule [83]. Other schemes such as the Sinc-Legendre collocation method, meshless element-free Galerkin, local discontinuous Galerkin, and variational multiscale element-free Galerkin methods have been considered in [84, 85, 86, 87]. Additionally, the Fourier spectral approach was employed by Bueno-Orovio *et al.* in [52] and Lee in [88]. However, the backward Euler scheme which was used for the temporal discretization in [52] is only first-order accurate and the operator-splitting scheme in [88] is applicable only for two-dimensional equations.

1.4 Reaction-Diffusion System

In this study, we consider systems of nonlinear time-dependent FPDEs for variant applications of mathematical modeling of some physical, biological, and chemical problems. We investigate the performance of the proposed time stepping schemes on several numerical experiments of pattern formations and examine their properties. Reaction-diffusion systems are one of the most common systems that have been the subject of intensive study during the last few decades because of their sophisticated dynamic attitude [89, 90]. They consist of two terms: the diffusion term that is connected with the random motion of each constituent, and the reaction term that depicts the interaction between the physical and biological species [91]. Among others, we discuss the following reaction-diffusion models:

- FitzHugh-Nagumo model

  FitzHugh and Nagumo introduced a model to simulate the signal observed in living organism's excitable cells. The FitzHugh-Nagumo model is a simpler version of the Hodgkin-Huxley model [92], it is used as a generic model for describing the waves propagation in the excitable media. The non-linear reaction term describes the action potential propagation on an axon membrane.

$$\frac{\partial u}{\partial t} = -\kappa_\alpha(-\Delta)^{\alpha/2}u + u(1-u)(u-a) - v,$$
$$\frac{\partial v}{\partial t} = \epsilon(\beta u - \gamma v - \delta),$$

  where κ_α is the diffusion tensor, $\beta,\ a,\ \epsilon,\ \gamma$, and δ are the constant parameters that characterize the model attitude, u is the fast variable that describes the membrane potential of the cell and v is the slow variable that joins by an inverse ratio with the medium conductivity.

  The FitzHugh-Nagumo model has been used a lot in the auto-oscillatory process. For instance, spiral waves in the 2D system and scroll waves in the 3D system, which are used for arrhythmic activities in mammalian hearts [93, 94, 95, 96]. It has also been used as a basis for cardiac electrophysiology models [97], and to illustrate impulse propagation in nerve membranes [98, 99].

- Gray-Scott model

  The Gray-Scott is an irreversible model that rules the two chemical reaction equations in a gel reactor

$$\mathcal{U} + 2\mathcal{V} \to 3\mathcal{V},$$

$$\mathcal{V} \to \mathcal{P},$$

  where $\mathcal{P}$ is the inert product and $\mathcal{V}$ catalyzes its reaction with $\mathcal{U}$, both $\mathcal{U}$ and $\mathcal{V}$ are removed from the feed process [100, 101].

  The Gray-Scott model shows a wide discipline of new patterns such as pulses in one-dimensional self replicate [102], and spots in two-dimensional self replicate

[103], that have been noticed in a ferrocyanide-iodate-sulfite reaction [104]. The diffusivities κ_u and κ_v of $\mathcal{U}$ and $\mathcal{V}$ could be any non-negative numbers. For instance, the pulse splitting, in the 1D simulations, was observed at $\kappa_u = 1$ and $\kappa_v = 0.01$ [105], and the spot replication, in the 2D simulations, was observed at $\kappa_u = 2\kappa_v = 2 \times 10^{-5}$ [106].

Let u and v indicate the concentrations of $\mathcal{U}$ and $\mathcal{V}$, respectively, then the space-fractional reaction-diffusion system is given as:

$$\frac{\partial u}{\partial t} = -\kappa_u(-\Delta)^{\alpha/2}u - uv^2 + F(1-u),$$
$$\frac{\partial u}{\partial t} = -\kappa_v(-\Delta)^{\alpha/2}v + uv^2 - Bv,$$

where F is the rate such that $\mathcal{U}$ is fed to the reactor from the reservoir, the concentration of $\mathcal{V}$ in the reservoir is zero, and B is the sum of F and the constant rate κ that equals the rate when $\mathcal{V}$ is converted to an inert product [102]. This model has important applications in the autocatalytic chemical reaction to investigate the morphogenesis and pattern formation. For example, Lefévre and Mangin [107] proposed using the Gray-Scott model as a phenomenological model that is based on reaction-diffusion mechanisms including Turing morphogens for the differential growth of the sulci and gyri which are the bottom and top of folds.

- Brusselator model

  The Brusselator model has also been referred to the trimolecular model [108]. It is a sophisticated model in the cooperative processes of chemical kinetics study [109], it exhibits the non-linear oscillations of the chemical reaction-diffusion mechanism [90]. It has been used in laser physics between certain modes in multiple couplings, in plasma, in enzymatic reactions, and in a trimolecular reaction step that appears by atomic oxygen in the formation of ozone through

a triple collision [109].

$$\frac{\partial u}{\partial t} = -\kappa_u(-\Delta)^{\alpha/2}u + B + u^2v - (C+1)u,$$
$$\frac{\partial v}{\partial t} = -\kappa_v(-\Delta)^{\alpha/2}v + Cu - u^2v,$$

where κ_u and κ_v are the diffusion coefficients, B and C are the constant concentrations of the input reagents, and u and v are the chemical concentrations of the reaction products.

- Schnakenberg model

  The Schnakenberg model is one of the reaction models that demonstrates Turing pattern formation [110]. Schnakenberg developed his kinematic reaction model [111] to search for a minimal that exhibits so-called limit-cycle behavior. Such an idea came from studies on biological areas including the ecological cycles of population densities and metabolic regulation.

$$\frac{\partial u}{\partial t} = -\kappa_u(-\Delta)^{\alpha/2}u + \gamma(a - u + u^2v),$$
$$\frac{\partial v}{\partial t} = -\kappa_v(-\Delta)^{\alpha/2}v + \gamma(b - u^2v),$$

  κ_u and κ_v are the diffusion coefficients, γ, a, and b are constants.

  The Schnakenberg model has been used to investigate the spatiotemporal pattern formation like oscillatory behavior and spatial patterns because of its algebraic simplicity [112, 113].

The motivation of this study is to formulate second and fourth-order A-stable and L-stable ETD schemes using rational approximations and partial fraction decomposition. The schemes are combined with three different discretizations of the fractional Laplacian which are the Fourier spectral approach, second-order MTT for nonhomogeneous boundary conditions, and MTT based on the compact fourth-order finite difference approximation to solve systems of nonlinear reaction-diffusion equations with smooth and non-smooth initial data. Moreover, one of the most challenging

problems in numerical analysis is the computational challenge of large matrix exponential functions such as in a system that is defined on high dimensional spatial domains [114]. We tackle these difficulties by implementing accurate and efficient second-order and fourth-order ETD schemes for solving multidimensional systems of nonlinear FPDEs.

1.5 Contents of the dissertation

In Chapter 2, we propose two numerical schemes for problems with non-smooth initial data based on using (1,1)-Padé and (0,2)-Padé approximations to the matrix exponential. The schemes are combined with the Fourier spectral approach in space to alleviate the numerical inefficiency caused by the non-locality of the fractional operator. We extend them in Chapter 3 to an ETD scheme with fourth-order accuracy in time. We introduce modified versions of the ETDRK4 scheme combined with MTT for non-homogeneous boundary conditions in Chapter 4, and MTT for homogeneous boundary conditions with non-smooth initial data in Chapter 5. Moreover, a reliability constraint on the choice of the time step is proposed when the A-stable scheme is applied with irregular initial data to avoid the unwanted oscillations due to high frequency components in the solutions. We examine the stability analysis and show the ability of the L-stable schemes to damp the unwanted oscillations in the solutions. We investigate the performance of the developed schemes on several test problems of well-known mathematical models. The numerical experiments and CPU time are based on computations via Matlab R2018a platforms ran on an Intel Core i5 2.5 GHz workstation. Finally, a summary of the dissertation is included in Chapter 6.

CHAPTER 2

FOURIER SPECTRAL SECOND-ORDER ETD SCHEMES

2.1 Introduction

In this chapter, we propose two numerical schemes for solving the space-fractional reaction-diffusion equations, which are based on a Fourier spectral approach in space and ETD schemes in time. The advantages of the approaches are that they attain spectral convergence, produce a full diagonal representation of the fractional operator, and the extension to multiple spatial dimensions is the same as the one-dimensional space. These approaches can overcome the constraints associated with many of the numerical schemes for these equations such as the computational efficiency caused by the non-locality of the fractional operator, which results in full, dense matrices. Moreover, the proposed schemes are second-order convergent in time, unconditionally stable, and highly efficient due to the predictor-corrector feature when comparing them with the existing scheme. It is observed that the scheme based on using (1,1)-Padé approximations to the matrix exponential introduces oscillations with non-smooth initial data due to high frequency components present in the solution for some time steps, which diminish as the fractional-order decreases. However, the scheme based on (0,2)-Padé approximations to the matrix exponential is oscillation-free for any time step. Numerical experiments for well-known models from the literature are performed to show the reliability and effectiveness of the proposed schemes.

The space-fractional reaction-diffusion equation is given as

$$\frac{\partial u(x,t)}{\partial t} = -\kappa_\alpha(-\Delta)^{\alpha/2}u(x,t) + f(u,t), \quad 0 \le t \le T,\ 1 < \alpha \le 2, \tag{3}$$

subject to the initial condition given by

$$u(x,0) = u_0(x), \quad x \in \Omega \subset \mathbb{R}^d, \quad \text{where} \quad d = 1,2,3, \tag{4}$$

with homogeneous Dirichlet or Neumann boundary conditions.

Most approaches for solving space-fractional diffusion problems involve applying the finite volume, finite element, or finite difference discretization of the fractional operator. Several numerical schemes involve some constraints such as the computational efficiency caused by the non-locality of the fractional operator, that leads to full, dense matrices. Meerschaert and Tadjeran [115] proposed numerical approaches for solving the Caputo space-fractional advection-dispersion equation using the finite difference scheme. Ilic *et al.* [58] presented the MTT to solve the space-fractional diffusion equations.

For the Riesz space-fractional derivatives, Yang *et al.* [59] proposed three numerical methods, which are the standard/shifted Grünwald method, L1/L2-approximation method, and the matrix transform method. Ortigueira [61] suggested the fractional centered derivative, Çelik and Duman [116] followed his approach by applying the Crank-Nicolson scheme for solving the fractional diffusion equation in a finite domain. Space and time fractional Bloch-Torrey equations in 2D were considered with both the Riesz derivative form and the fractional Laplacian [117, 118]. Yang *et al.* considered the 2D Riesz space-fractional diffusion equation on irregular convex domain [119].

Aceto and Novati [83] introduced the rational approximation to the integral representation of the fractional Laplacian using the Gauss-Jacobi quadrature rule. Li and Chen [56] gave a comprehensive review of several numerical methods such as the Galerkin finite element methods, finite difference methods, and spectral methods for space-fractional, time-fractional, and space-time-fractional partial differential equations. Some other numerical schemes for non-integer order differential systems based on using Riemann-Liouville and Caputo derivatives with numerical analysis to pattern formations can be found in [120, 121]. A finite volume method with preconditioned Lanczos method was proposed for solving 2D space-fractional reaction-diffusion equations [122], numerical methods related to fractional partial differential equations were

also considered with analysis results in [123].

Bueno-Orovio *et al.* [52] presented the Fourier spectral approach for the integration of the fractional Laplacian which is used to describe the space-fractional reaction-diffusion equations. However, this method is based on the backward Euler for the time discretization, which is just first-order accurate in time. Lee [88] followed their approach and proposed a second-order operator splitting method which is only applicable for 1D and 2D problems.

We introduce the numerical integration of the fractional differential equations using the Fourier transform that yields to a system of fractional ordinary differential equations in Fourier space, which are then solved by the fractional ETD schemes. We apply the second-order unconditionally stable ETD-CN (or ETD-Padé(1,1)) and ETD-Padé(0,2) schemes for the temporal discretization in a predictor-corrector manner which avoids solving nonlinear systems. Although the schemes are unconditionally stable, the ETD-CN scheme produces solutions with unwanted oscillations when the initial data is non-smooth for some time steps due to the high frequency components of the growth factor of the discretized problem. Whereas the ETD-Padé(0,2) scheme produces solutions without the oscillations and achieves the second-order accuracy in time.

2.2 Spatial discretization

Assume the Laplacian $(-\Delta)$ have a complete set of orthonormal eigenfunctions φ_n, $\varphi_{n,m}$ or $\varphi_{n,m,l}$ satisfying standard boundary conditions on a bounded region $\Omega \subset \mathbb{R}^d$, with corresponding eigenvalues λ_n, $\lambda_{n,m}$, or $\lambda_{n,m,l}$ respectively, i.e.,

$$(-\Delta)\varphi_n = \lambda_n \varphi_n, \qquad if \quad d = 1,$$
$$(-\Delta)\varphi_{n,m} = \lambda_{n,m} \varphi_{n,m}, \qquad if \quad d = 2,$$
$$(-\Delta)\varphi_{n,m,l} = \lambda_{n,m,l} \varphi_{n,m,l}, \qquad if \quad d = 3,$$

for $n, m, l = 0, 1, 2, \ldots$, on Ω, and let

$$u_1 = \sum_{n=0}^{\infty} \hat{u}_n \varphi_n, \quad \hat{u}_n = \langle u_1, \varphi_n \rangle, \quad \sum_{n=0}^{\infty} |\hat{u}_n|^2 |\lambda_n|^\alpha < \infty,$$

$$u_2 = \sum_{n=0}^{\infty}\sum_{m=0}^{\infty} \hat{u}_{n,m} \varphi_{n,m}, \quad \hat{u}_{n,m} = \langle u_2, \varphi_{n,m} \rangle, \quad \sum_{n=0}^{\infty}\sum_{m=0}^{\infty} |\hat{u}_{n,m}|^2 |\lambda_{n,m}|^\alpha < \infty,$$

$$u_3 = \sum_{n=0}^{\infty}\sum_{m=0}^{\infty}\sum_{l=0}^{\infty} \hat{u}_{n,m,l} \varphi_{n,m,l}, \quad \hat{u}_{n,m,l} = \langle u_3, \varphi_{n,m,l} \rangle, \quad \sum_{n=0}^{\infty}\sum_{m=0}^{\infty}\sum_{l=0}^{\infty} |\hat{u}_{n,m,l}|^2 |\lambda_{n,m,l}|^\alpha < \infty.$$

Then,

$$(-\Delta)^{\frac{\alpha}{2}} u_1 = \sum_{n=0}^{\infty} \hat{u}_n \lambda_n^{\frac{\alpha}{2}} \varphi_n, \tag{5}$$

$$(-\Delta)^{\frac{\alpha}{2}} u_2 = \sum_{n=0}^{\infty}\sum_{m=0}^{\infty} \hat{u}_{n,m} \lambda_{n,m}^{\frac{\alpha}{2}} \varphi_{n,m}, \tag{6}$$

$$(-\Delta)^{\frac{\alpha}{2}} u_3 = \sum_{n=0}^{\infty}\sum_{m=0}^{\infty}\sum_{l=0}^{\infty} \hat{u}_{n,m,l} \lambda_{n,m,l}^{\frac{\alpha}{2}} \varphi_{n,m,l}. \tag{7}$$

The space-fractional reaction-diffusion equation is obtained by replacing the standard Laplace operator by its fractional correspondent. Hence, the spectral decomposition of the fractional Laplacian $(-\Delta)^{\frac{\alpha}{2}}$ has the same interpretation as the spectral decomposition of the standard Laplace operator. The eigenvalues and eigenvectors of the standard Laplace operator depend on the specified boundary conditions. For the homogeneous Dirichlet boundary conditions with $x \in \Omega = (a, b)^d,\ d = 1, 2, 3$, the eigenvalues and eigenvectors are

$$\lambda_{\eta_1,\ldots,\eta_d} = \sum_{n=\eta_1}^{\eta_d} \left(\frac{(n+1)\pi}{b-a} \right)^2,$$

$$\varphi_{\eta_1,\ldots,\eta_d} = \left(\sqrt{\frac{2}{b-a}} \right)^d \prod_{n=\eta_1}^{\eta_d} \sin\left(\frac{(n+1)\pi(x_n - a)}{b-a} \right),\ \eta_i = 0, 1, 2, \ldots,$$

respectively, whereas for the homogeneous Neumann boundary conditions, the eigenvalues and eigenvectors are

$$\lambda_{\eta_1,\ldots,\eta_d} = \sum_{n=\eta_1}^{\eta_d} \left(\frac{n\pi}{b-a} \right)^2,$$

$$\varphi_{\eta_1,\ldots,\eta_d} = \left(\sqrt{\frac{2}{b-a}}\right)^d \prod_{n=\eta_1}^{\eta_d} \cos\left(\frac{n\pi(x_n - a)}{b-a}\right),\ \eta_i = 0, 1, 2, \ldots,$$

respectively. The reader is referred to [124] for periodic boundary conditions.
If we consider a finite number of the orthonormal trigonometric eigenfunctions φ_n, then the fractional Laplacian is approximated by a truncated series

$$(-\Delta)^{\frac{\alpha}{2}} u \approx \sum_{n=0}^{N_x-1} \hat{u}_n \lambda_n^{\frac{\alpha}{2}} \varphi_n. \tag{8}$$

The following is the representation of (3) in Fourier space when $d = 1$ by using the definition of the fractional Laplacian and applying the Fourier transform [125]

$$\frac{d}{dt}\mathcal{F}[u(x,t)] = -A\mathcal{F}[u(x,t)] + \mathcal{F}[f(u,t)], \tag{9}$$

where $A = \kappa_\alpha(\lambda^2)^{\alpha/2}$, for the homogeneous Dirichlet boundary conditions

$$\lambda_i = \frac{(i)\pi}{b-a}, \tag{10}$$

$$x_i = a + ih, \quad h = (b-a)/(N_x+1),$$

and for the homogeneous Neumann boundary conditions

$$\lambda_i = \frac{(i-1)\pi}{b-a}, \tag{11}$$

$$x_i = a + (i-1)h + \frac{h}{2}, \quad h = (b-a)/N_x,$$

$i \in \{1, N_x\}$, h is the spatial step size and N_x is the number of the internal points [52]. We compute the coefficients $\hat{u}_n$ and the inverse reconstruction of u, in physical space, by using efficient algorithms (Discrete Sine or Cosine transforms and their inverses) based on the specified homogeneous boundary conditions [126, 127].

2.3 Time discretization

The following system of nonlinear differential equations is obtained by approximating the fractional-order spatial derivative in (3) with the Fourier spectral approach

mentioned above

$$\hat{u}_t = -A\hat{u} + \hat{F}(u,t), \tag{12}$$

where $\hat{u} = \mathcal{F}[u]$, $\hat{F}(u,t) = \mathcal{F}[f(u,t)]$ and A as in (9).

Let $t_{n+1} = t_n + k$, k be the temporal step size, then the exact solution of (12) is the following recurrence formula

$$\hat{u}(t_{n+1}) = e^{-kA}\hat{u}(t_n) + k\int_0^1 e^{-kA(1-\tau)}\hat{F}(u(t_n+\tau k), t_n+\tau k)d\tau, \tag{13}$$

Eq. (13) is the basis of the ETD schemes, which can be obtained by using different approximations to the matrix exponential and the integral involving the nonlinear reaction term. The simplest approximation to the integral term in (13) is by approximating $\hat{F}(u(t_n), t_n)$ by $\hat{F}(u_n, t_n)$, which yields the first-order accurate

$$\begin{aligned}\hat{u}_{n+1} &\approx e^{-kA}\hat{u}_n + ke^{-kA}\int_0^1 e^{kA\tau}d\tau\hat{F}(u_n,t_n)\\ &= e^{-kA}\hat{u}_n + A^{-1}(1-e^{-kA})\hat{F}(u_n,t_n).\end{aligned} \tag{14}$$

To get the second-order accurate scheme of Runge-Kutta type, we let (14) to be an intermediate prediction of $\hat{u}(t_{n+1})$

$$\hat{a}_n = e^{-kA}\hat{u}_n + A^{-1}(1-e^{-kA})\hat{F}(u_n,t_n). \tag{15}$$

Now, we approximate the nonlinear term $\hat{F}(u(t_n),t_n)$ in (13) by averaging over two intervals [128]

$$\hat{F}(u(t_n),t_n) \approx \hat{F}(u_n,t_n) + (t-t_n)\frac{\hat{F}(\hat{a}_n,t_n+k) - \hat{F}(u_n,t_n)}{k}, \quad t\in[t_n,t_{n+1}] \tag{16}$$

where $\hat{a}_n$ as in (15), using (16) in (13) yields

$$\begin{aligned}\hat{u}_{n+1} &= e^{-kA}\hat{u}_n + ke^{-kA}\int_0^1 e^{kA\tau}\left(\hat{F}(u_n,t_n) + k\tau\frac{\hat{F}(\hat{a}_n,t_n+k)-\hat{F}(u_n,t_n)}{k}\right)d\tau\\ &= \hat{a}_n + \frac{A^{-2}}{k}(e^{-kA}-1+kA)(\hat{F}(\hat{a}_n,t_n+k) - \hat{F}(u_n,t_n)).\end{aligned} \tag{17}$$

Eq. (17) represents the second-order ETDRK [66]. We want to compute $A^{-1}(1-e^{-kA})$ and $\frac{A^{-2}}{k}(e^{-kA}-1+kA)$ in (15) and (17) efficiently by approximating the matrix exponential by diagonal and sub-diagonal Padé approximations. Here, we employ the second-order ETD-CN (ETD-Padé(1,1)) and ETD-Padé(0,2) schemes, where their derivations for the integer order are given in [128] and [129], respectively.

2.3.1 The second-order ETD schemes

The rational approximations (1,1)-Padé and (0,2)-Padé to e^{-z} are given by

$$R_{1,1}(z) = (2-z)(2+z)^{-1},$$
$$R_{0,2}(z) = 2(2+2z+z^2)^{-1}.$$

In Fig. 1, we show the behavior of the exponential function (e^{-z}) and the Padé approximation $R_{1,1}(z)$, and the behavior of the exponential function (e^{-z}) and the Padé approximation $R_{0,2}(z)$ for real values of z, where $z \in [0, 20]$. In Fig. 2, we show the behavior of the Padé approximations $R_{1,1}(z)$ and $R_{0,2}(z)$ for $z = x + iy$, where $x \in [0, 20]$ and $y \in [-10, 10]$.

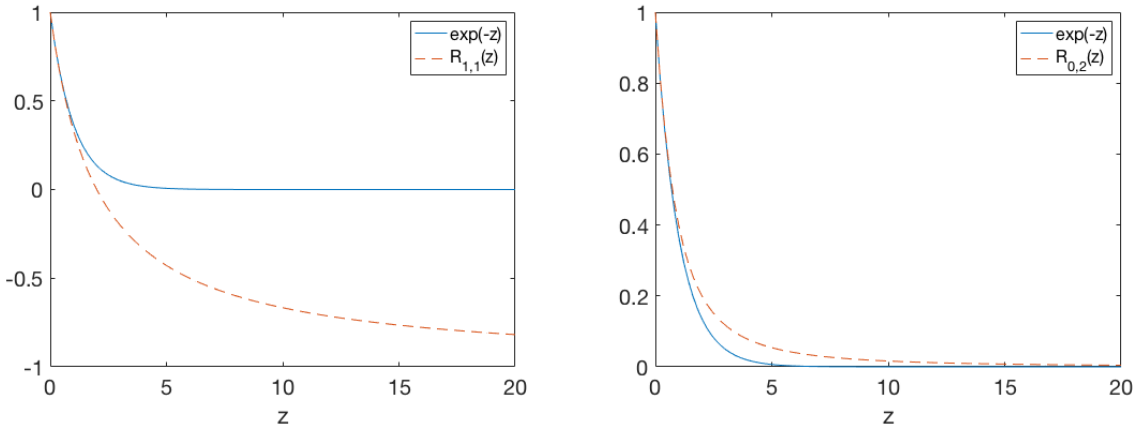

Figure 1: Behavior of e^{-z} and $R_{1,1}(z)$, e^{-z} and $R_{0,2}(z)$ for $z \in [0, 20]$.

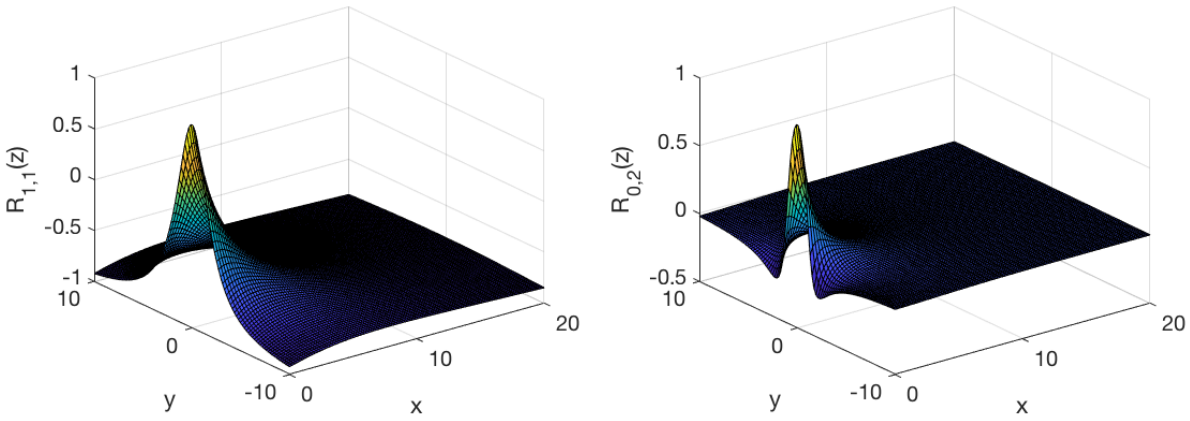

Figure 2: Behavior of $R_{1,1}(z)$ and $R_{0,2}(z)$ for $z \in [0, 20] \times [-10, 10]$.

2.3.1.1 The ETD-CN scheme

By replacing the matrix exponential (e^{-kA}) in (17) with the Padé approximation $R_{1,1}(kA)$, we obtain the ETD-CN scheme [130]

$$\begin{aligned}\hat{v}_{n+1} &= \hat{b}_n + \frac{A^{-2}}{k}(R_{1,1} - 1 + kA)(\hat{F}(\hat{b}_n, t_n + k) - \hat{F}(v_n, t_n)) \\ &= \hat{b}_n + k(2 + kA)^{-1}[\hat{F}(\hat{b}_n, t_n + k) - \hat{F}(v_n, t_n)], \end{aligned} \tag{18}$$

where

$$\begin{aligned}\hat{b}_n &= R_{1,1}(kA)\hat{v}_n + A^{-1}(1 - R_{1,1}(kA))\hat{F}(v_n, t_n) \\ &= R_{1,1}(kA)\hat{v}_n + 2k(2 + kA)^{-1}\hat{F}(v_n, t_n),\end{aligned}$$

with

$$R_{1,1}(kA) = (2 - kA)(2 + kA)^{-1}.$$

2.3.1.2 The ETD-Padé(0,2) scheme

Similarly, replacing the matrix exponential (e^{-kA}) in (17) by the Padé approximation

$R_{0,2}(kA)$, we obtain the ETD-Padé(0,2) scheme [130]

$$\begin{aligned}\hat{v}_{n+1} &= \hat{b}_n + \frac{(-A)^{-2}}{k}(R_{0,2}(kA) - 1 + kA)(\hat{F}(\hat{b}_n, t_n + k) - \hat{F}(v_n, t_n)) \\ &= \hat{b}_n + k(2 + 2kA + (kA)^2)^{-1}(1 + kA)[\hat{F}(\hat{b}_n, t_n + k) - \hat{F}(v_n, t_n)] \\ &= \hat{b}_n + kP_1(kA)[\hat{F}(\hat{b}_n, t_n + k) - \hat{F}(v_n, t_n)], \end{aligned} \tag{19}$$

where

$$\begin{aligned}\hat{b}_n &= R_{0,2}(kA)\hat{v}_n + A^{-1}(1 - R_{0,2}(kA))\hat{F}(v_n, t_n) \\ &= R_{0,2}(kA)\hat{v}_n + k(2 + 2kA + (kA)^2)^{-1}(2 + kA)\hat{F}(v_n, t_n) \\ &= R_{0,2}(kA)\hat{v}_n + kP_2(kA)\hat{F}(v_n, t_n),\end{aligned}$$

with

$$\begin{aligned}R_{0,2}(kA) &= 2(2 + 2kA + (kA)^2)^{-1}, \\ P_1(kA) &= (2 + 2kA + (kA)^2)^{-1}(1 + kA), \\ P_2(kA) &= (2 + 2kA + (kA)^2)^{-1}(2 + kA).\end{aligned}$$

2.4 Stability analysis

We study the linear stability of the ETD-CN and ETD-Padé(0,2) schemes by plotting their stability regions. We consider the following nonlinear ODE

$$\hat{u}_t = -c\hat{u} + \hat{F}(u). \tag{20}$$

Assume that there exists a fixed point $\hat{u}_0$ such that $-c\hat{u}_0 + \hat{F}(\hat{u}_0) = 0$, after linearizing we obtain

$$\hat{u}_t = -c\hat{u} + \lambda\hat{u}, \tag{21}$$

where $\hat{u}$ is the perturbation of $\hat{u_0}$ and $\lambda = \hat{F}'(\hat{u}_0)$, cf. [66].

For all λ, the fixed point $\hat{u_0}$ is stable if $Re(\lambda - c) < 0$. Let $y = -ck$ and $x = \lambda k$, where k is the time step. We introduce the amplification factor by applying the ETD-CN scheme to (21)

$$r(x, y) = \frac{\hat{u}_{n+1}}{\hat{u}_n} = c_0 + c_1 x + c_2 x^2, \tag{22}$$

where

$$\begin{aligned} c_0 &= \frac{2+y}{(2-y)}, \\ c_1 &= \frac{2+y}{(2-y)^2} + \frac{1}{(2-y)}, \\ c_2 &= \frac{2}{(2-y)^2}. \end{aligned}$$

Similarly, by applying the ETD-Padé(0,2) scheme to (21), we get the following amplification factor

$$r(x, y) = \frac{\hat{u}_{n+1}}{\hat{u}_n} = c_0 + c_1 x + c_2 x^2, \tag{23}$$

where

$$\begin{aligned} c_0 &= \frac{2}{(2+2y+y^2)}, \\ c_1 &= \frac{4+4y+y^2}{(2+2y+y^2)^2}, \\ c_2 &= \frac{2+3y+y^2}{(2+2y+y^2)^2}. \end{aligned}$$

If $y = 0$, then the amplification factors in (22) and (23) become

$$r(x, 0) = 1 + x + \frac{1}{2}x^2,$$

which represents the amplification factor of the second-order Runge-Kutta scheme. In order to get the stability regions, we assume that $r(x, y) < 1$. By choosing x to be a complex number with some fixed negative values of y, the stability regions can be seen in Figs. 3a and 3b for the ETD-CN and ETD-Padé(0,2) schemes, respectively.

According to Beylkin et al. [131], for the method to be useful, it is important that the stability regions grow as $|y|$ becomes larger. Figs. 3a and 3b indicate the stability of the ETD-CN and ETD-Padé(0,2) schemes since the stability regions become larger as $y \to -\infty$ [66].

2.5 The ETD-CN algorithm

Algorithm 1 ETD-CN three-dimensional algorithm with Neumann boundary conditions

1: Given: $L = (b-a), \quad \alpha, \quad N_x, \quad k, \quad \kappa_\alpha, \quad u, \quad \text{and} \quad T.$

2: Compute $\lambda = (((0 : N_x - 1)\pi/L)^2 + ((0 : N_y - 1)\pi/L)^2 + ((0 : N_z - 1)\pi/L)^2)^{\frac{\alpha}{2}}$. ▷ $N_x = N_y = N_z$.

3: Let $h = \frac{L}{N_x}$, compute $x,\ y,$ and z such that $x = y = z = a + (0 : N_x - 1)h + \frac{h}{2}$.

4: Set $a_1 = (2 + k\kappa_\alpha\lambda)$ and $a_2 = (2 - k\kappa_\alpha\lambda)$. ▷ ETD-CN coefficients.

5: **for** $n = 1, 2, \ldots,$ round(T/dt), **do**

6: $u_{dct} = dctn(u)$.

7: $t = nk$.

8: Compute $f(u_n, t_n)$ as f_n using the given u. ▷ reaction term.

9: $b_n = idctn((a_2 u_{dct} + 2k\ dctn(f_n))/a_1)$.

10: Compute $f(b_n, t_n + k)$ as f_{n+1} using b_n.

11: $u = idctn(dctn(b_n) + (k\ dctn(f_{n+1} - f_n))/a_1)$.

12: **end for**

2.6 The ETD-Padé(0,2) algorithm

Algorithm 2 ETD-Padé(0,2) three-dimensional algorithm with Neumann boundary conditions

1: Given: $L = (b - a)$, α, N_x, k, κ_α, u, and T.

2: Compute $\lambda = (((0 : N_x - 1)\pi/L)^2 + ((0 : N_y - 1)\pi/L)^2 + ((0 : N_z - 1)\pi/L)^2)^{\frac{\alpha}{2}}$. ▷ $N_x = N_y = N_z$.

3: Let $h = \frac{L}{N_x}$, compute x, y, and z such that $x = y = z = a + (0 : N_x - 1)h + \frac{h}{2}$.

4: Set $a_1 = (2 + 2k\kappa_\alpha\lambda + (k\kappa_\alpha\lambda)^2)$ and $a_2 = (1 + k\kappa_\alpha\lambda)$. ▷ ETD-Padé(0,2) coefficients.

5: **for** $n = 1, 2, \ldots,$ round(T/dt), **do**

6: $u_{dct} = dctn(u)$.

7: $t = nk$.

8: Compute $f(u_n, t_n)$ as f_n using the given u. ▷ reaction term.

9: $b_n = idctn((2u_{dct} + k(2 + k\kappa_\alpha\lambda)dctn(f_n))/a_1)$.

10: Compute $f(b_n, t_n + k)$ as f_{n+1} using b_n.

11: $u = idctn(dctn(b_n) + (k\ a_2\ dctn(f_{n+1} - f_n))/a_1)$.

12: **end for**

Remark. *In the case of using the homogeneous Dirichlet boundary conditions,* $\lambda = (((1 : N_x)\pi/L)^2 + ((1 : N_y)\pi/L)^2 + ((1 : N_z)\pi/L)^2)^{\frac{\alpha}{2}}$, $h = \frac{L}{N_x+1}$, *dctn and idctn are replaced by dstn and idstn*[1], *respectively. 1D and 2D (Discrete Sine/Cosine*

[1]dstn/dctn represent the Discrete Sine/Cosine Transforms for n arbitrary deminsions, and idstn/idctn are their inverses.

Transforms and their inverses) are also discussed in details for the scheme proposed by Bueno-Orovio et al. *[52].*

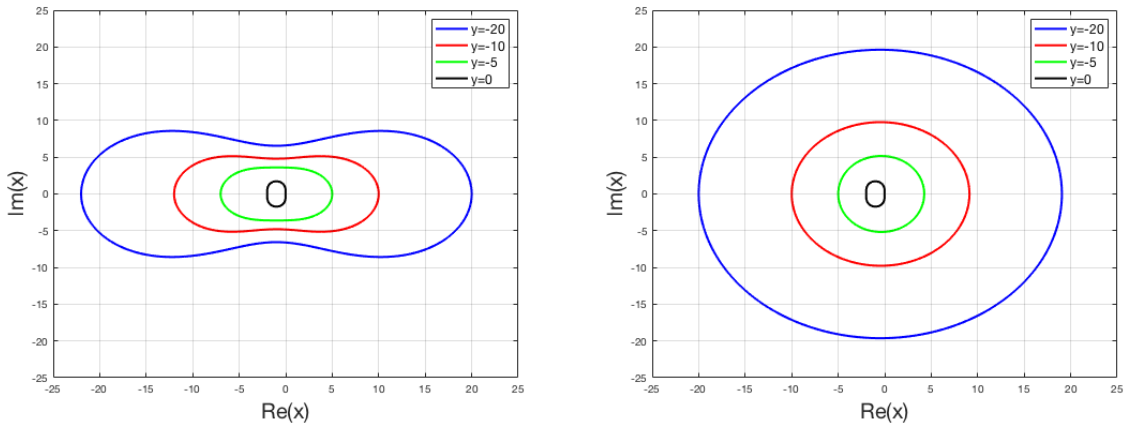

(a) ETD-CN

(b) ETD-Padé (0,2)

Figure 3: Stability regions at some fixed negative values of y.

2.7 Numerical experiments

This section discusses the results obtained by applying our schemes to different widely used space-fractional reaction-diffusion models. Numerical experiments include a 2D heat equation with a source term, the FitzHugh Nagumo model which arises in the excitable media study [98, 99], the Schnakenberg model that includes oscillatory behavior and depicts an auto-catalytic chemical reaction [111], the Brusselator model which appears in the study of the formation of ozone by atomic oxygen via a triple collision [109], a 3D enzyme kinetics reaction-diffusion problem of the Michaelis-Menten type [132], and finally, the 2D Allen-Cahn equation with non-smooth initial condition, that describes the domain coarsening kinetics in alloys, and other systems developing formation and motion of phase boundaries [81, 133].

2.7.1 Test Problem 1: a 2D heat equation

We consider the 2D space-fractional heat equation with a source term [52]

$$\frac{\partial u}{\partial t} = -\kappa_\alpha(-\Delta)^{\alpha/2}u + f(u,t), \tag{24}$$

where

$$f(u,t) = t^\alpha \frac{\kappa_\alpha}{16}\sum_{i=1}^{4}\left(1+\lambda_i^{\alpha/2}\right)v_i + \alpha t^{\alpha-1}\sin^3(\pi x)\sin^3(\pi y) - \kappa_\alpha u,$$

and

$$\begin{aligned}
v_1 &= 9\sin(\pi x)\sin(\pi y), && \lambda_1 = 2\pi^2,\\
v_2 &= -3\sin(\pi x)\sin(3\pi y), && \lambda_2 = 10\pi^2,\\
v_3 &= -3\sin(3\pi x)\sin(\pi y), && \lambda_3 = 10\pi^2,\\
v_4 &= \sin(3\pi x)\sin(3\pi y), && \lambda_4 = 18\pi^2,
\end{aligned}$$

subject to the initial condition $u(x,y,0) = 0$ and homogeneous Dirichlet boundary conditions, $(x,y) \in [0,1]^2$. The exact solution is

$$u(x,y,t) = t^\alpha \sin(3\pi x)\sin(3\pi y).$$

We selected this problem as a benchmark test problem with an exact solution to verify that the proposed schemes achieve the second-order accuracy in time as expected. The numerical and exact solutions of (24) are demonstrated in Fig. 4 at $\kappa_\alpha = 10$, $N_x = 128$, and $k = 0.0025$ for $\alpha = 2$ and $\alpha = 1.5$, the simulations run up to $T = 1.0$.

The L_∞ error, and order of convergence for the proposed schemes and for the Bueno-Orovio *et al.* scheme (using the fixed point iteration $M = 1$ for treating the nonlinear term) are listed in Tables 1 and 2 at $T = 1$, and $N_x = 128$ with the fractional power $\alpha = 2$ and 1.5. The computed rates of convergence agree with the expected rates of the proposed schemes which are second-order accurate in time, while the

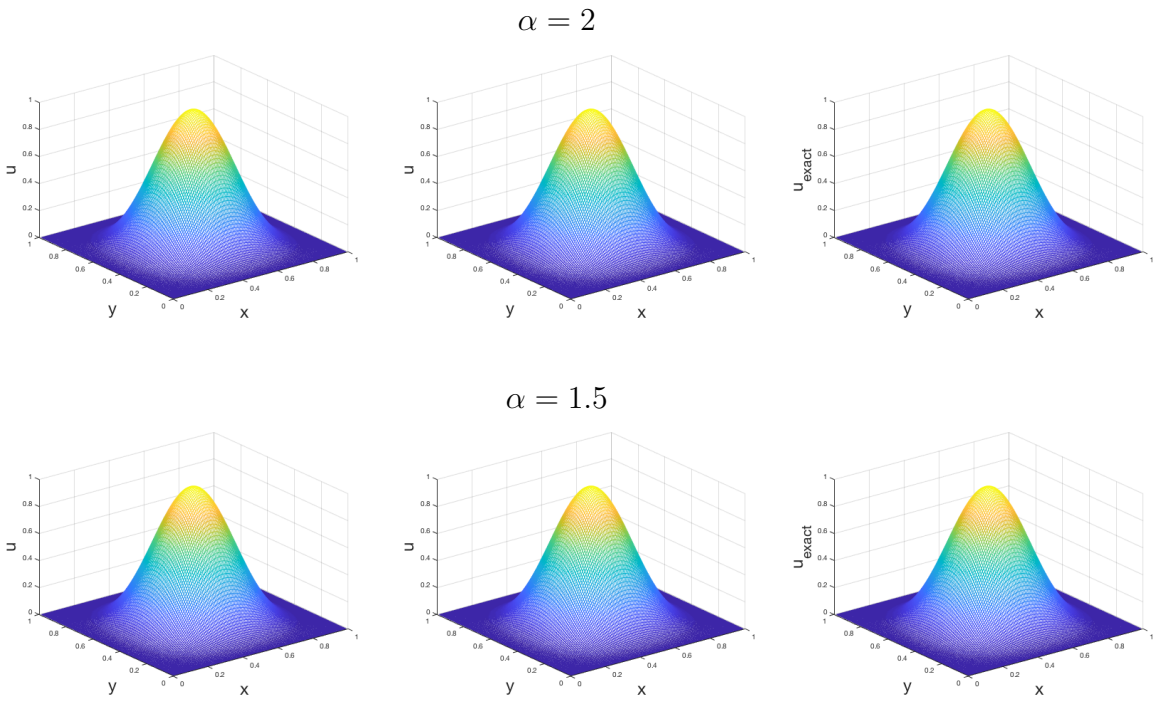

(a) ETD-CN (b) ETD-Padé(0,2) (c) Exact solution

Figure 4: Numerical and exact solutions of (24).

Bueno-Orovio *et al.* scheme is just a first-order accurate in time. When the exact solution is known, the order of convergence in time is computed by

$$\text{order of convergence} = \frac{\log_{10}\left(\left\|u - u_{k_j}\right\|_\infty / \left\|u - u_{k_{j+1}}\right\|_\infty\right)}{\log_{10}(k_j/k_{j+1})},$$

where u is the exact solution, u_{k_j} and $u_{k_{j+1}}$ are the numerical solutions with the time step size k_j and k_{j+1}, respectively. Fig. 5 visualizes the time rates of convergence of the schemes with Log-Log scale graph.

$\alpha = 2$

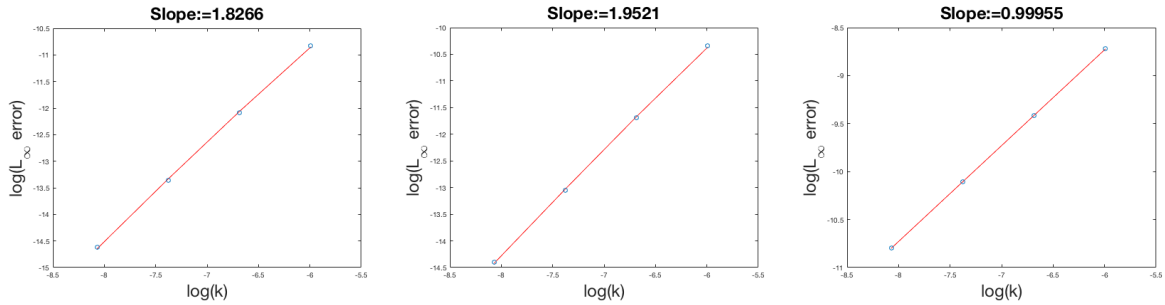

$\alpha = 1.5$

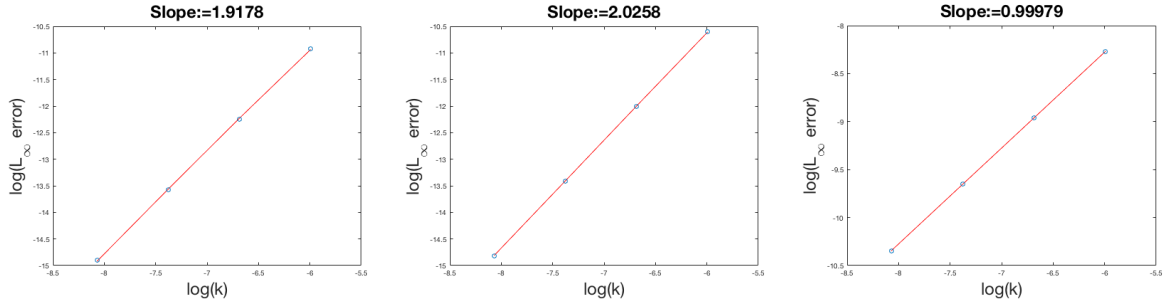

(a) ETD-CN (b) ETD-Padé(0,2) (c) Bueno-Orovio scheme

Figure 5: Time rates of convergence.

2.7.2 Test Problem 2: the FitzHugh-Nagumo model (FHN)

We consider the 2D FitzHugh-Nagumo model, which exhibits excitability [98, 99], with homogeneous Neumann boundary conditions

$$\begin{aligned} \frac{\partial u}{\partial t} &= -\kappa_\alpha(-\Delta)^{\frac{\alpha}{2}}u + u(1-u)(u-a) - v, \\ \frac{\partial v}{\partial t} &= \epsilon(\beta u - \gamma v - \delta), \end{aligned} \tag{25}$$

where $a = 0.1$, $\epsilon = 0.01$, $\beta = 0.5$, $\gamma = 1$, and $\delta = 0$. The domain of interest is $[0, 2.5]^2$ and the diffusion coefficient $\kappa_\alpha = 10^{-4}$. The initial state $(u, v) = (0, 0)$ was perturbed

Table 1: $\alpha = 2$.

	ETD-CN		ETD-Padé(0,2)		Bueno-Orovio *et al.* scheme	
k	L_∞ error	order	L_∞ error	order	L_∞ error	order
0.00250	1.9380e-05	-	3.1475e-05	-	1.6309e-04	-
0.00125	5.7744e-06	1.7469	8.5540e-06	1.8796	8.1588e-05	0.9992
0.00063	1.6211e-06	1.8327	2.1950e-06	1.9624	4.0805e-05	0.9996
0.00031	4.3490e-07	1.8982	5.4466e-07	2.0108	2.0405e-05	0.9998

Table 2: $\alpha = 1.5$.

	ETD-CN		ETD-Padé(0,2)		Bueno-Orovio *et al.* scheme	
k	L_∞ error	order	L_∞ error	order	L_∞ error	order
0.00250	1.7857e-05	-	2.4822e-05	-	2.5681e-04	-
0.00125	4.8957e-06	1.8669	6.1472e-06	2.0136	1.2844e-04	0.9996
0.00063	1.2896e-06	1.9246	1.5017e-06	2.0333	6.4228e-05	0.9998
0.00031	3.3158e-07	1.9595	3.6825e-07	2.0278	3.2116e-05	0.9999

by setting the lower-left quarter of the spatial domain to $u = 1$ and the upper half part to $v = 0.1$, causing the initial data to curve and rotate clockwise creating the spiral waves. Fig. 6 shows the spiral waves of this model at the choice of $T = 2000$, $k = 1$, and $N_x = 256$. It can be observed from Figs. 6b, 6c, 6e, and 6f that the width of the wavefront is reduced as α decreases and also the same to the wavelength, which allows the domain to accommodate a larger number of wavefronts for a small value of α.

Fig. 7 shows the effect of decreasing the diffusion coefficient in the solution profiles of the model. In Figs. 7a - 7f we have the same choice of the parameters as those for Fig. 6a except for the diffusion coefficient κ_α, and we notice that the width of the wavefront in Figs. 7b, 7c, 7e, and 7f are approximately the same as that in Figs. 6b, 6c, 6e, and 6f, respectively, but with a larger wavelength of the system in the fractional diffusion case, see [52, 134]. Table 3 shows the efficiency of the ETD-CN and ETD-Padé(0,2) schemes compared with the scheme introduced by Bueno-Orovio *et al.* [52].

ETD-CN

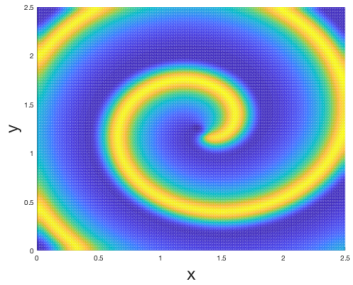

(a) $\alpha = 2$

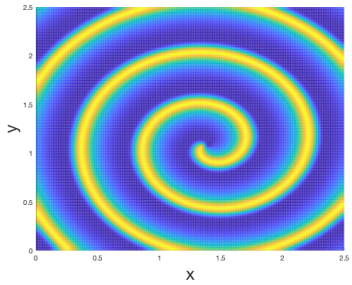

(b) $\alpha = 1.7$

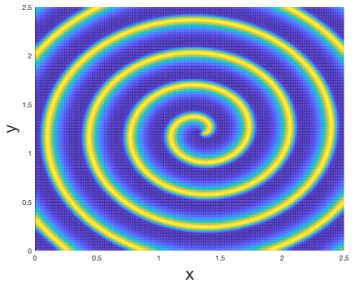

(c) $\alpha = 1.5$

ETD-Padé(0,2)

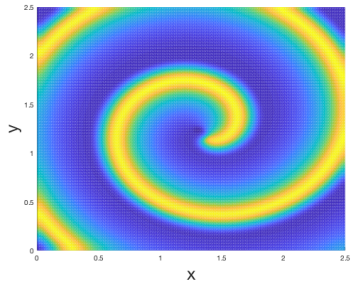

(d) $\alpha = 2$

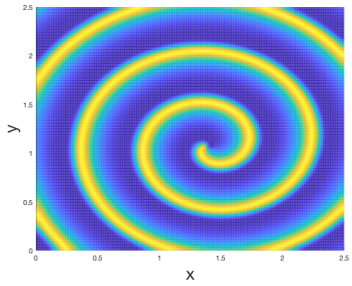

(e) $\alpha = 1.7$

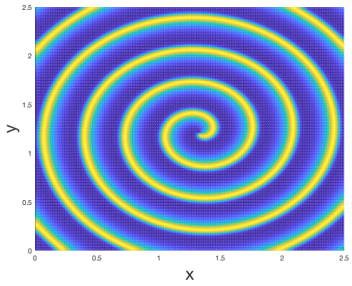

(f) $\alpha = 1.5$

Figure 6: Spiral waves of the FHN (25) at different values of α.

Table 3: Time in seconds for solving (25) at $\alpha = 1.8$ and $T = 100$.

N_x	ETD-CN	ETD-Padé(0,2)	Bueno-Orovio *et al.* scheme
64	0.4224	0.7583	0.8528
128	1.1236	1.3261	2.1251
256	5.4989	6.0402	8.8458
512	25.1288	25.9283	36.2416

ETD-CN

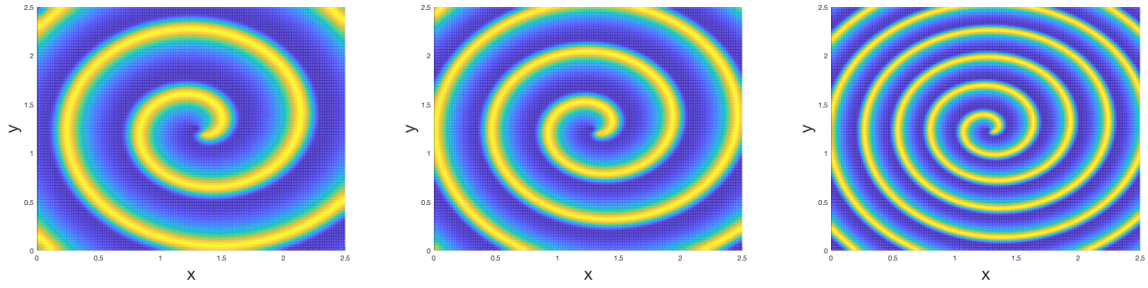

(a) $\kappa_\alpha = 5 \times 10^{-5}$ (b) $\kappa_\alpha = 3 \times 10^{-5}$ (c) $\kappa_\alpha = 10^{-5}$

ETD-Padé(0,2)

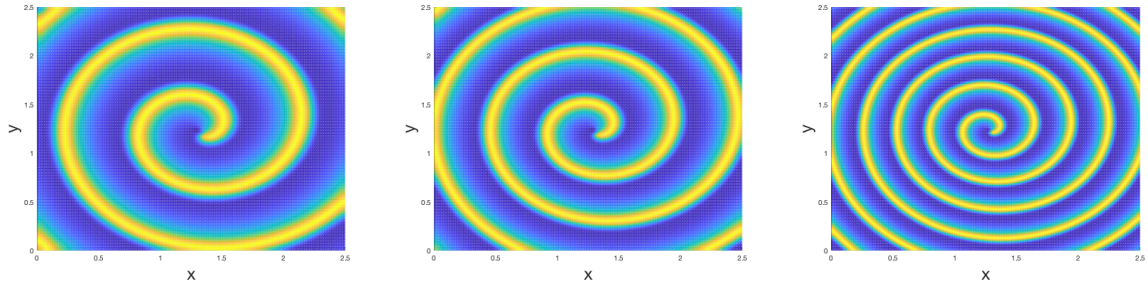

(d) $\kappa_\alpha = 5 \times 10^{-5}$ (e) $\kappa_\alpha = 3 \times 10^{-5}$ (f) $\kappa_\alpha = 10^{-5}$

Figure 7: Spiral waves of the FHN (25) at different values of κ_α.

2.7.3 Test Problem 3: the 2D Schnakenberg model

We consider the 2D space-fractional Schnakenberg model [111] with homogeneous Neumann boundary conditions on $0 < x, y < 1$. The model is considered as a simplified version of the Brusselator model [90]

$$\begin{aligned} \frac{\partial u}{\partial t} &= -\kappa_u(-\Delta)^{\frac{\alpha}{2}} u + \gamma(a - u + u^2 v), \\ \frac{\partial v}{\partial t} &= -\kappa_v(-\Delta)^{\frac{\alpha}{2}} v + \gamma(b - u^2 v), \end{aligned} \tag{26}$$

the initial conditions are given as

$$u(x,y,0) = 0.919145 + 0.0016\cos(2\pi(x+y)) + 0.01\sum_{j=1}^{8}\cos(2\pi jx),$$

$$v(x,y,0) = 0.937903 + 0.0016\cos(2\pi(x+y)) + 0.01\sum_{j=1}^{8}\cos(2\pi jx),$$

where u and v represent the chemical products concentrations. The parameters are constants and are selected similar to that in [135] as follows: $\kappa_u = 1$, $\kappa_v = 10$, $a = 0.126779$, $b = 0.792366$, and $\gamma = 1000$.

The concentrations of u and v are depicted in Figs. 8 and 9 at $T = 1$ for both of the derived schemes. As shown in the figures, when the fractional-order decreases, the observed peaks are thinner and greater in number. Table 4 shows the comparison of the ETD-CN, ETD-Padé(0,2) schemes, and the scheme introduced by Bueno-Orovio *et al.* [52] regarding the CPU(s).

Table 4: Time in seconds for solving (26) at $\alpha = 1.9$ and $T = 0.02$ using the time step $k = 0.0001$.

N_x	ETD-CN	ETD-Padé(0,2)	Bueno-Orovio *et al.* scheme
64	0.8723	0.8702	1.7735
128	2.3072	2.3856	4.4085
256	10.5086	11.0750	19.8865
512	52.8898	55.2367	95.3377

2.7.4 Test Problem 4: the 3D Brusselator model

The 3D space-fractional Brusselator model [136] is considered with homogeneous Neumann boundary conditions

$$\begin{aligned}\frac{\partial u}{\partial t} &= -\kappa_u(-\Delta)^{\frac{\alpha}{2}}u + B + u^2v - (C+1)u,\\ \frac{\partial v}{\partial t} &= -\kappa_v(-\Delta)^{\frac{\alpha}{2}}v + Cu - u^2v,\end{aligned} \tag{27}$$

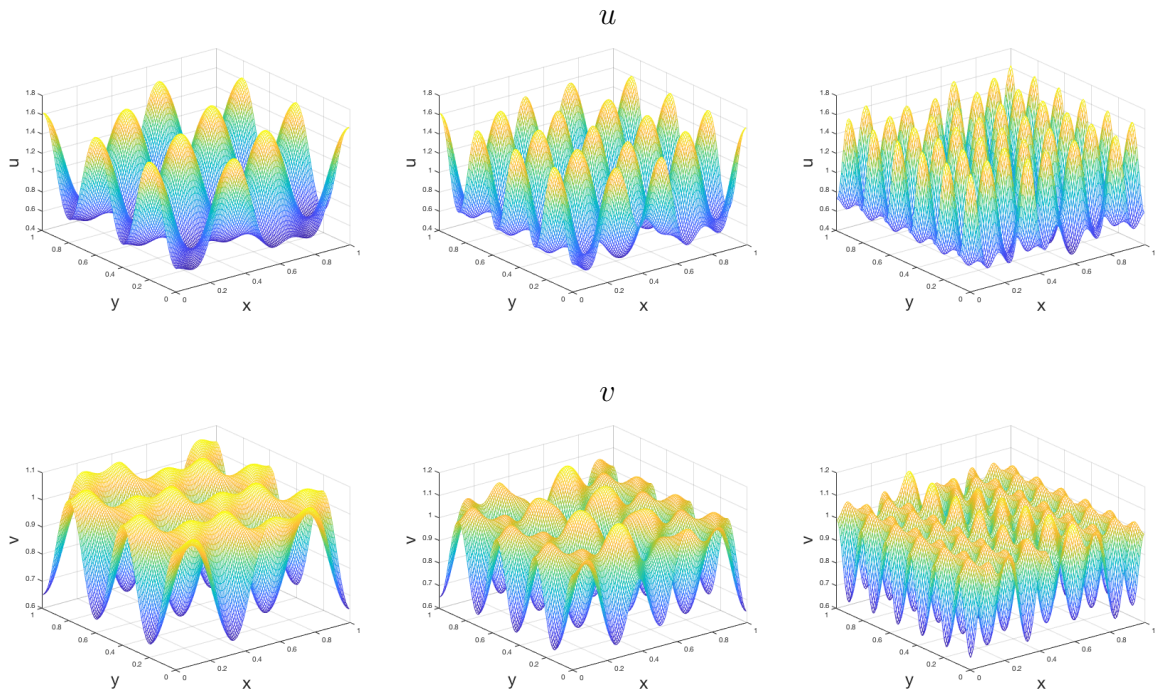

(a) $\alpha = 2$ (b) $\alpha = 1.8$ (c) $\alpha = 1.6$

Figure 8: The concentration profiles of (26) as obtained by the ETD-CN scheme at $k = 0.001$ and $N_x = 128$.

the initial conditions for u and v are

$$u(x, y, z, 0) = B + \cos(2\pi x)\cos(2\pi y)\cos(2\pi z),$$
$$v(x, y, z, 0) = \frac{C}{B} + \cos(2\pi x)\cos(2\pi y)\cos(2\pi z),$$

$0 \leq x, y, z \leq 10$, $\kappa_u = 2$, $\kappa_v = 10$, $B = 5$, and $C = 12$.

In Figs. 10 and 11 interesting isosurfaces of $u = B$ are shown at different values of α and T, similar isosurfaces of $v = C/B$ can be obtained. In Table 5, we observe a much better performance for the ETD-CN and ETD-Padé(0,2) schemes than the scheme employed by Bueno-Orovio *et al.* in [52] for a large N_x in particular.

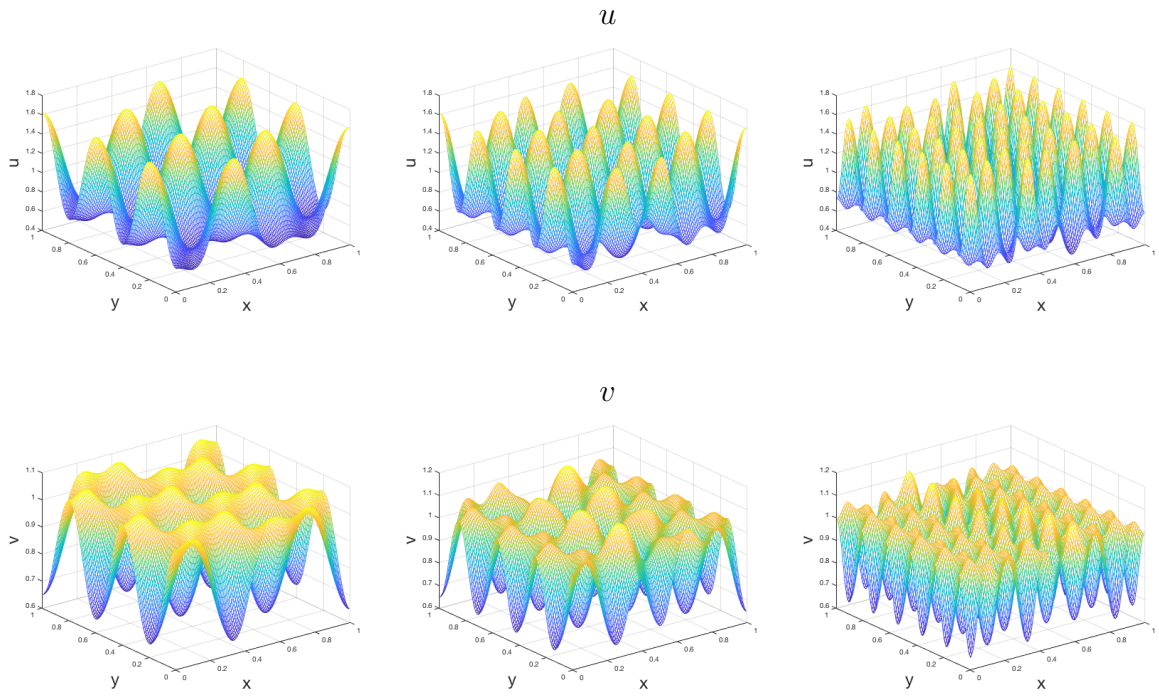

(a) $\alpha = 2$ (b) $\alpha = 1.8$ (c) $\alpha = 1.6$

Figure 9: The concentration profiles of (26) as obtained by the ETD-Padé(0,2) scheme at $k = 0.001$ and $N_x = 128$.

Table 5: Time in seconds for solving (27) at $\alpha = 1.8$ and $T = 1$ using the time step $k = 0.01$.

N_x	ETD-CN	ETD-Padé(0,2)	Bueno-Orovio *et al.* scheme
20	1.8560	1.8617	3.6178
64	37.0119	36.7273	69.1401
100	144.6593	144.7999	264.9958
128	279.4489	285.5881	519.6427

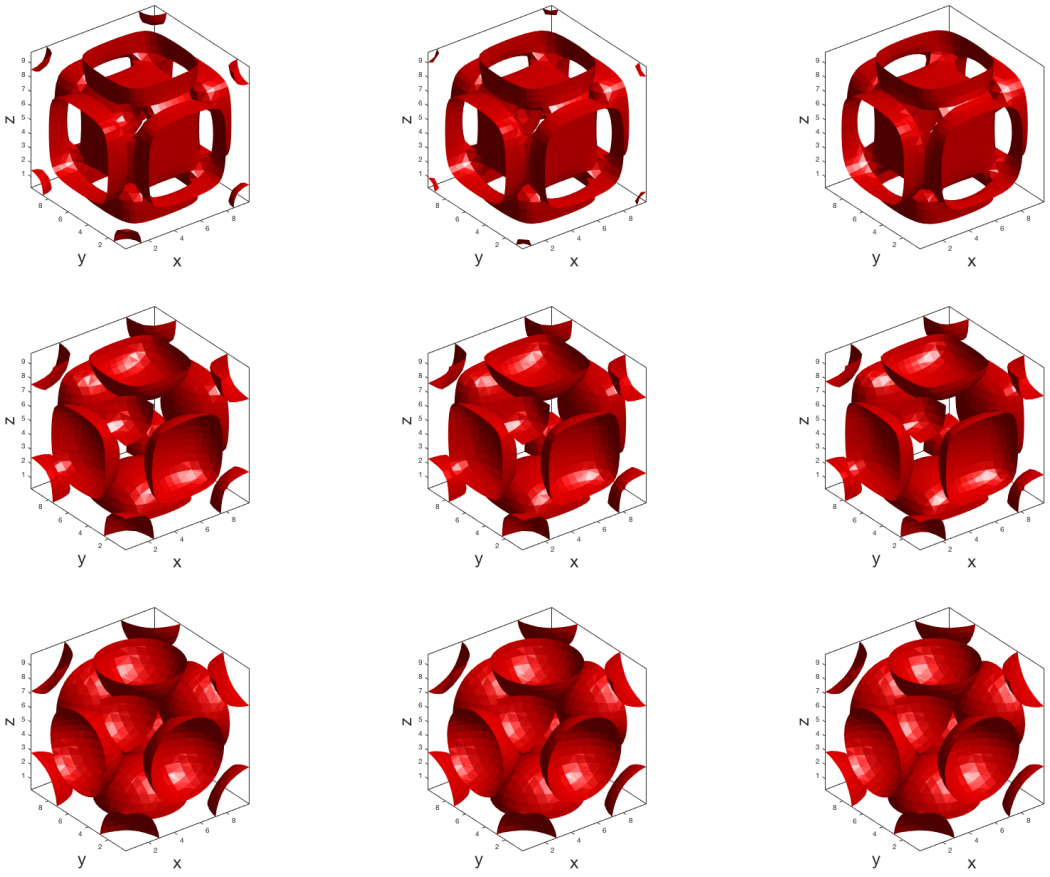

(a) $\alpha = 2$ (b) $\alpha = 1.8$ (c) $\alpha = 1.6$

Figure 10: Isosurfaces of $u = B$ with the ETD-CN at $T = 5, 10$, and 100 (first, second, and third row, respectively), $k = 0.01$ and $N_x = 21$.

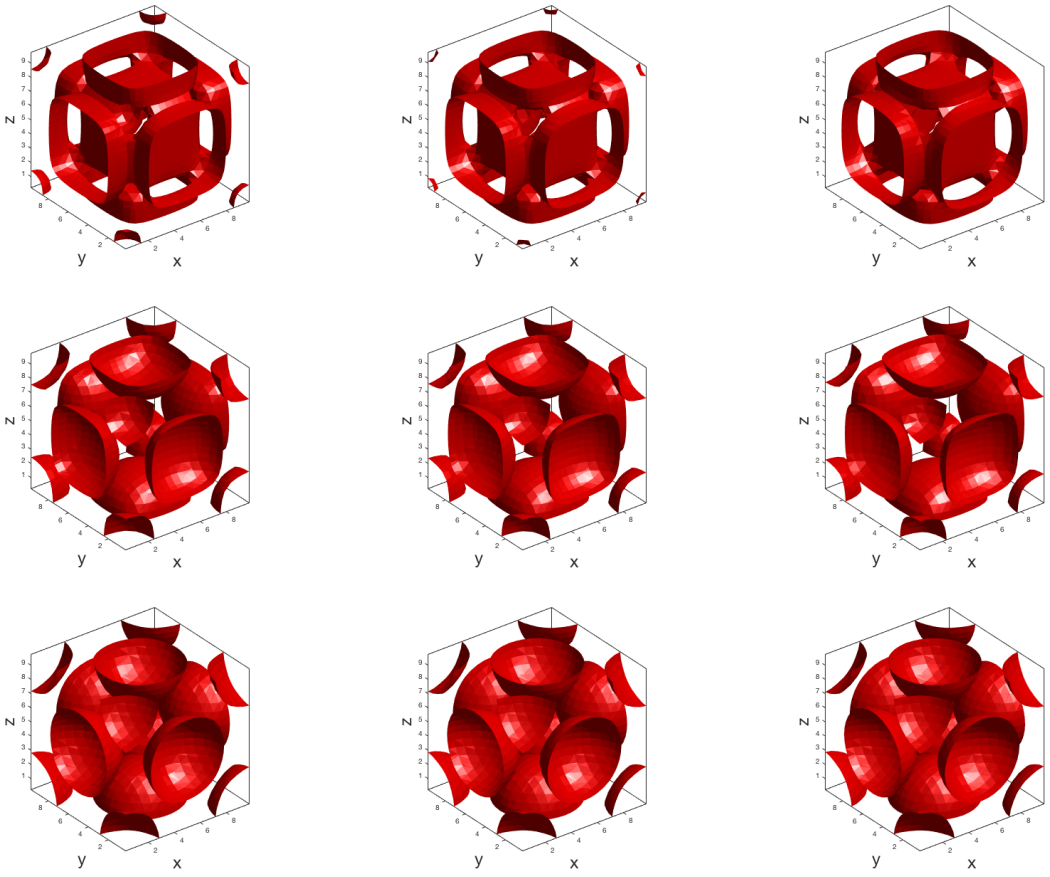

(a) $\alpha = 2$ (b) $\alpha = 1.8$ (c) $\alpha = 1.6$

Figure 11: Isosurfaces of $u = B$ with the ETD-Padé(0,2) at $T = 5, 10$, and 100 (first, second, and third row, respectively), $k = 0.01$ and $N_x = 21$.

2.7.5 Test Problem 5: a 3D scalar problem

We consider the 3D analogue of a 1D enzyme kinetics reaction-diffusion problem of the Michaelis-Menten type [132] with the homogeneous Dirichlet boundary conditions

$$\frac{\partial u}{\partial t} = -\kappa_\alpha(-\Delta)^{\frac{\alpha}{2}}u - \left(\frac{u}{1+u}\right), \tag{28}$$

the initial condition is given as follows

$$u(x, y, z, 0) = 1,$$

and the domain is $[0, 1]^3$.

ETD-CN

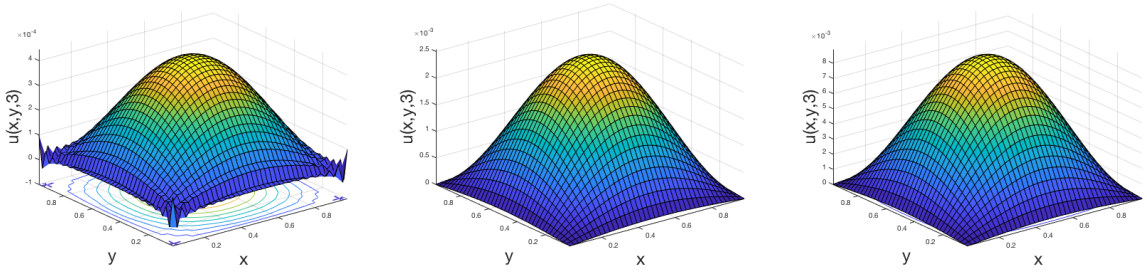

(a) $\alpha = 2$ (b) $\alpha = 1.8$ (c) $\alpha = 1.6$

ETD-Padé(0,2)

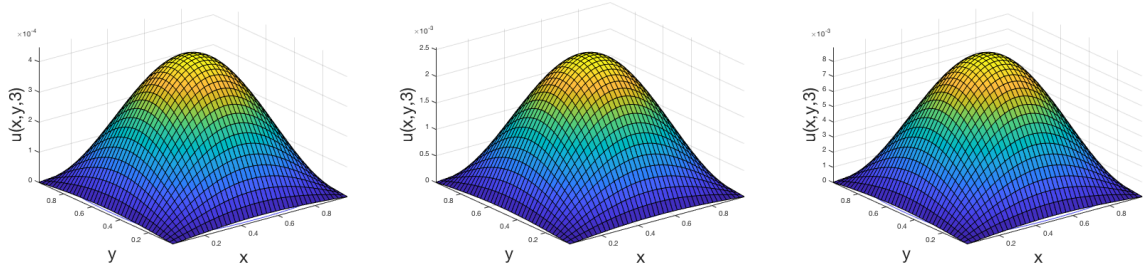

(d) $\alpha = 2$ (e) $\alpha = 1.8$ (f) $\alpha = 1.6$

Figure 12: The solution profiles of $u(:, :, 3)$ at $T = 1$, $k = 0.01$, $\kappa_\alpha = 0.2$, and $N_x = 40$.

A discontinuity in the biochemistry problem in (28) between the initial and boundary conditions introduces spurious oscillations in the solution. It is observed that in Fig. 12a the solution obtained by the A-stable scheme (ETD-CN) has oscillations near the boundary when $\alpha = 2$ while the solution obtained by the damping L-stable

scheme (ETD-Padé(0,2)) in Fig. 12d at the same value of α is oscillations-free. As the fractional-order decreases in Figs. 12b and 12c the oscillations in the solutions obtained by the ETD-CN scheme diminish at $\alpha = 1.8$, and 1.6, respectively. Also Figs. 13a, 13b, and 13c use several values of α to show that the oscillations in the solutions produced by the ETD-CN scheme increase as κ_α and α increase and that the solutions produced by the ETD-Padé(0,2) scheme remain oscillations-free even though κ_α increases as in Figs. 13d, 13f, and 13e at different values of α.

ETD-CN

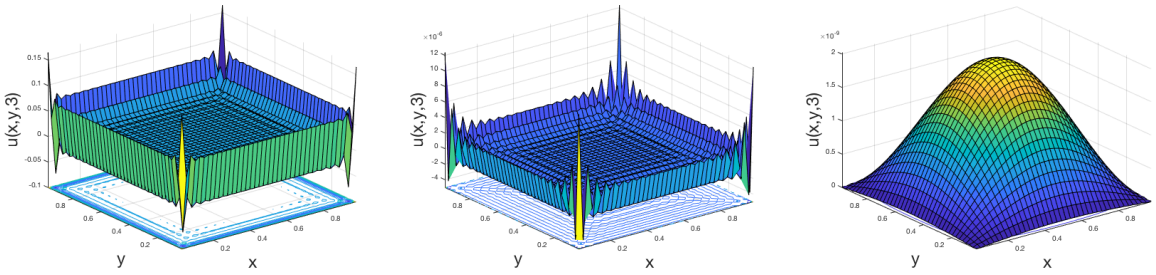

(a) $\alpha = 2$ (b) $\alpha = 1.5$ (c) $\alpha = 1.3$

ETD-Padé(0,2)

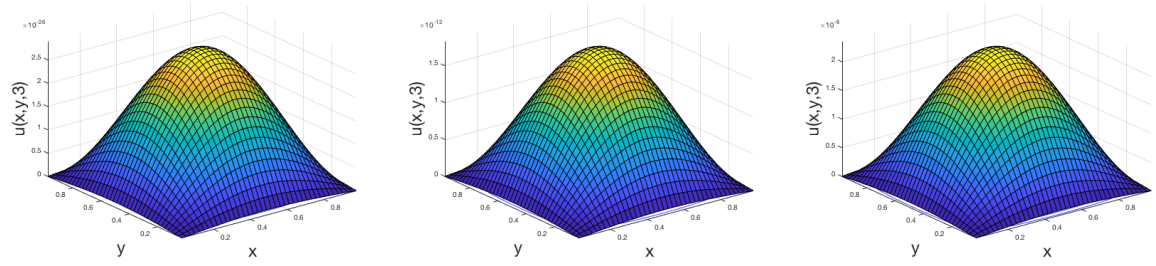

(d) $\alpha = 2$ (e) $\alpha = 1.5$ (f) $\alpha = 1.3$

Figure 13: The solution profiles of $u(:,:,3)$ at $T = 1$, $k = 0.01$, $\kappa_\alpha = 2$, and $N_x = 40$.

The L_2, L_∞ errors, and the order of convergence of the ETD-CN and ETD-

Padé(0,2) schemes with $T = 1$, $N_x = 20$, $k = 0.01$ and $\kappa_\alpha = 0.2$ are reported in Tables 6 and 7 at $\alpha = 2$ and $\alpha = 1.6$, respectively. Since the exact solution of the problem is unknown, the order of convergence in time is computed as

$$\text{order of convergence} = \frac{\log_{10}\left(E_k/E_{k/2}\right)}{\log_{10}(2)},$$

where $E_k = \|u_k - u_{2k}\|$ and $E_{k/2} = \left\|u_{k/2} - u_k\right\|$, and $\|.\|$ represents the L_2 and L_∞ norms.

In Figs. 14 and 15, we compare the efficiency of the ETD-CN, ETD-Padé(0,2) schemes and the scheme introduced by Bueno-Orovio *et al.* [52] utilizing the Log-Log graph of CPU time and L_2 errors, and the Log-Log graph of CPU time and L_∞ errors at $\alpha = 2$ and $\alpha = 1.6$, respectively. With the same CPU time, the ETD-CN and ETD-Padé(0,2) schemes produce small errors, which indicates better efficiency.

Table 6: $\alpha = 2$.

	ETD-CN				ETD-Padé(0,2)			
k	L_2 error	order	L_∞ error	order	L_2 error	order	L_∞ error	order
0.01000	-	-	-	-	-	-	-	-
0.00500	2.8401e-05	-	4.0789e-06	-	4.9699e-05	-	7.1379e-06	-
0.00250	7.1379e-06	1.9924	1.0251e-06	1.9924	1.2703e-05	1.9680	1.8245e-06	1.9680
0.00125	1.7867e-06	1.9982	2.5660e-07	1.9982	3.2098e-06	1.9846	4.6101e-07	1.9846
0.00063	4.4675e-07	1.9997	6.4161e-08	1.9997	8.0631e-07	1.9931	1.1581e-07	1.9931

Table 7: $\alpha = 1.6$.

	ETD-CN				ETD-Padé(0,2)			
k	L_2 error	order	L_∞ error	order	L_2 error	order	L_∞ error	order
0.01000	-	-	-	-	-	-	-	-
0.00500	8.6494e-05	-	1.1722e-05	-	1.6268e-04	-	2.2222e-05	-
0.00250	2.1620e-05	2.0002	2.9300e-06	2.0003	4.1046e-05	1.9867	5.5996e-06	1.9886
0.00125	5.4040e-06	2.0003	7.3236e-07	2.0003	1.0305e-05	1.9939	1.4047e-06	1.9950
0.00063	1.3508e-06	2.0002	1.8307e-07	2.0002	2.5813e-06	1.9972	3.5172e-07	1.9978

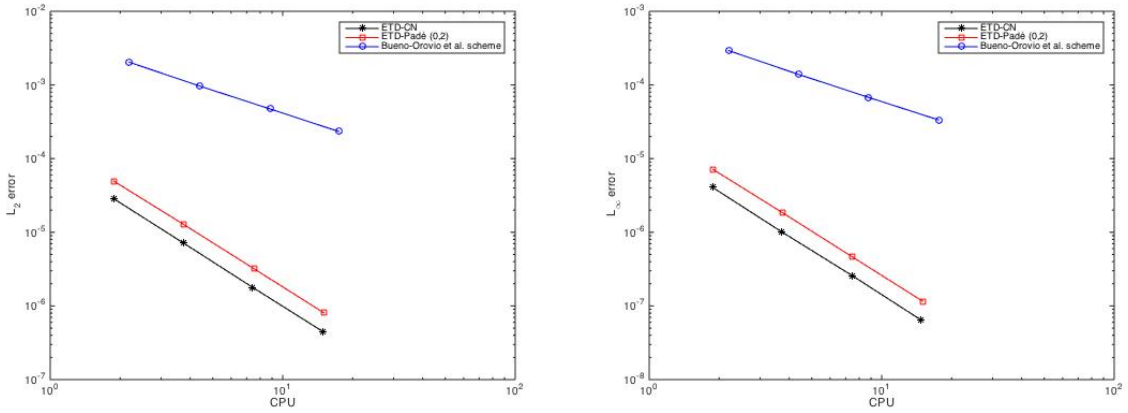

Figure 14: A comparison of the errors vs CPU time at $\alpha = 2$, $T = 1$, $k = 0.01$, $\kappa_\alpha = 0.2$, and $N_x = 20$.

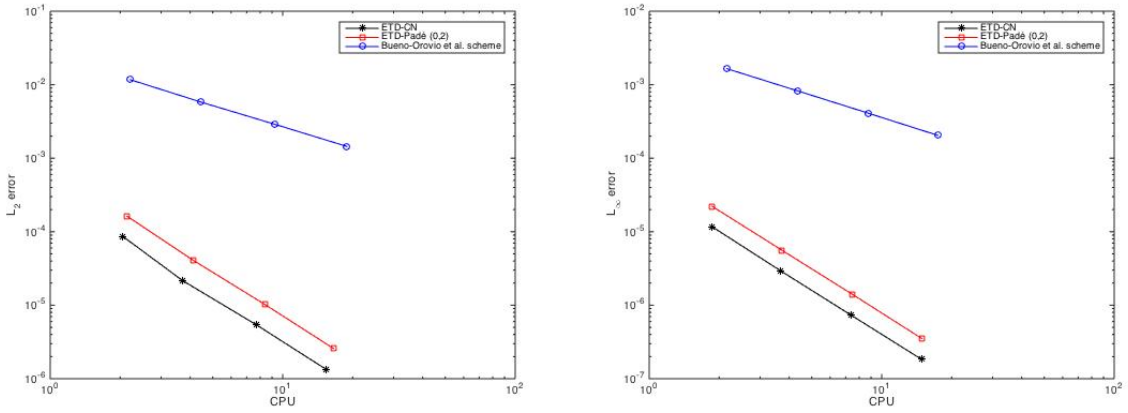

Figure 15: A comparison of the errors vs CPU time at $\alpha = 1.6$, $T = 1$, $k = 0.01$, $\kappa_\alpha = 0.2$, and $N_x = 20$.

2.7.6 Test Problem 6: the 2D Allen-Cahn equation with non-smooth data

Finally, we consider the 2D Allen-Cahn equation with the homogeneous Dirichlet boundary conditions and non-smooth initial data

$$\frac{\partial u}{\partial t} = -\kappa_\alpha(-\Delta)^{\frac{\alpha}{2}}u + \big(u^3 - u\big),\ (x,y) \in [0,1]^2, \tag{29}$$

subject to the following initial condition [137], see Fig. 16,

$$u(x,y,0) = \begin{cases} x^3\big(1-x^3\big)y(1-y), & x \in [0,0.5], \\ \\ \frac{7}{16}x(1-x)y(1-y), & x \in (0.5,1]. \end{cases} \tag{30}$$

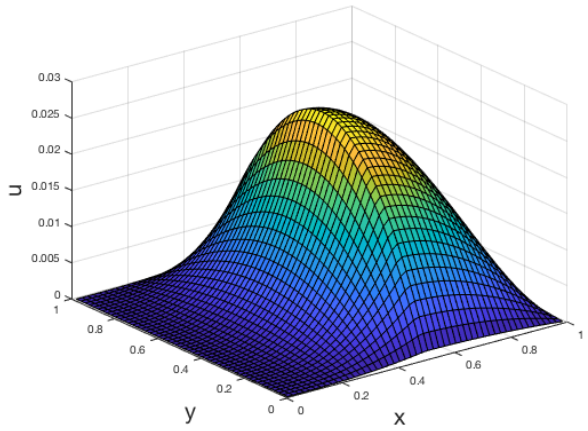

Figure 16: The non-smooth initial condition (30).

Fig. 17 shows the solutions of (29) with non-smooth initial condition (30) for $N_x = 30$ and $k = 1/5$. It is observed that the ETD-CN scheme produces solutions with unwanted oscillations, these oscillations diminish as the fractional-order decreases. The ETD-Padé(0,2) scheme is oscillation-free for any value of the fractional-order and with any time step.

ETD-CN

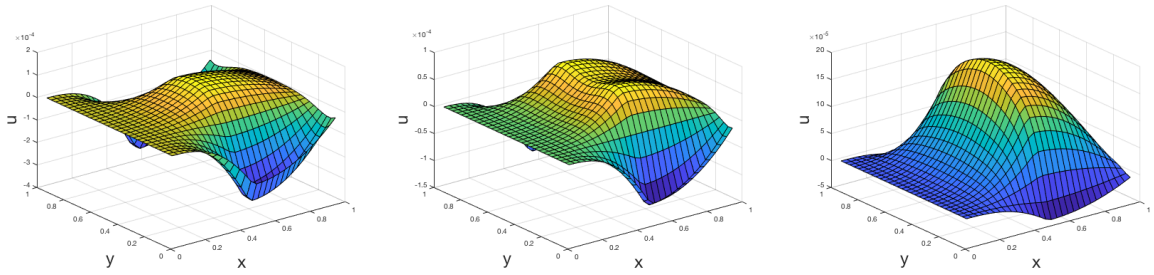

(a) $\alpha = 2$ (b) $\alpha = 1.7$ (c) $\alpha = 1.5$

ETD-Padé(0,2)

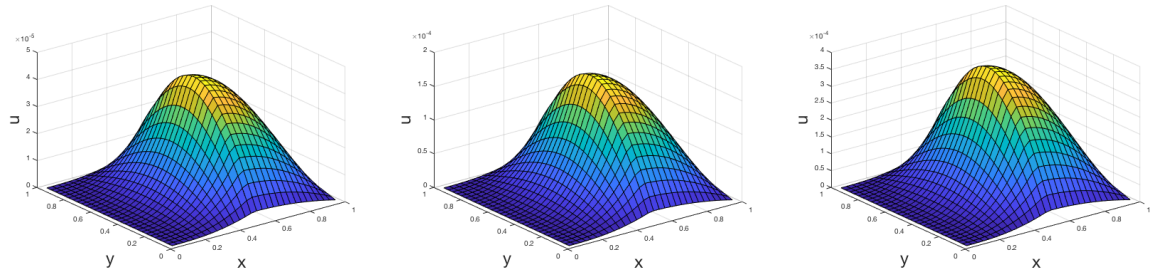

(d) $\alpha = 2$ (e) $\alpha = 1.7$ (f) $\alpha = 1.5$

Figure 17: The solution profiles of (29) using the initial condition (30) at $T = 1$ and $\kappa_\alpha = 0.65$.

2.8 Conclusion

In this chapter, two numerical schemes of the space-fractional reaction-diffusion equations have been introduced. We have used the Fourier spectral approach in space, that can remove the stiffness related to the higher order of the spatial derivative, and second-order ETD schemes in time. The linear stability analysis was discussed. Numerical experiments were performed on multidimensional space-fractional reaction-

diffusion systems for problems of practical interest to validate the effectiveness and reliability of the derived schemes. Their orders of convergence were demonstrated computationally. It was shown that the ETD-CN scheme produced spurious oscillations on problems with non-smooth data, whereas the ETD-Padé(0,2) scheme has been found to produce reliable results without unwanted oscillations.

CHAPTER 3

FOURIER SPECTRAL HIGH-ORDER ETD SCHEME

3.1 Introduction

This chapter introduces a high-order time stepping scheme, which is based on using the Fourier spectral in space and a fourth-order diagonal Padé approximation to the matrix exponential function for solving multidimensional space-fractional reaction-diffusion equations. The resulting time stepping scheme is developed based on an ETD approach which alleviates solving a large non-linear system at each time step while maintaining the stability of the scheme. The non-locality of the fractional operator in some other numerical schemes for these equations leads to full and dense matrices. This scheme is able to overcome such computational inefficiency due to the full diagonal representation of the fractional operator. It also attains spectral convergence for multiple spatial dimensions. The stability of the scheme is discussed through the investigation of the amplification symbol and plotting stability regions, which provides an indication of the stability of the scheme. The convergence analysis is performed empirically to show that the scheme is fourth-order accurate in time, as expected. Numerical experiments on reaction-diffusion systems with application to pattern formation are discussed to show the effect of the fractional-order in space-fractional reaction-diffusion equations and to validate the effectiveness of the scheme. We employ a high-order ETD Runge-Kutta scheme for multidimensional systems of space-fractional reaction-diffusion equations. The original ETDRK4 scheme was developed by Cox and Matthews in [66] for the integer-order reaction-diffusion equations. It requires inversion of the matrix polynomial which can be computationally inefficient and inaccurate. These issues were avoided for integer-order equations by employing rational Padé approximations (see for example, Khaliq *et al.* [69]). In this work, we extend this approach to fractional partial differential equations. For the

spatial discretization, we use the Fourier approximation, which provides the spectral convergence and allows the non-local fractional operator to be diagonalized.

3.2 Fourth-order time stepping scheme

The fractional Laplacian is discretized by using the Fourier spectral approach discussed in Chapter 2. Eq. (9) can be rewritten by multiplying it with the integrating factor e^{At} and integrating the equation from t_n to t_{n+1}

$$\hat{u}(t_{n+1}) = e^{-Ak}\hat{u}(t_n) + e^{-Ak}\int_0^k e^{A\tau}\hat{F}(u(t_n+\tau), t_n+\tau)d\tau, \tag{31}$$

where k is the time step, $\hat{u}(t_{n+1}) = \mathcal{F}[u(t_{n+1})]$, $\hat{u}(t_n) = \mathcal{F}[u(t_n)]$, and $\hat{F}(u(t_n+\tau), t_n+\tau) = \mathcal{F}[f(u(t_n+\tau), t_n+\tau)]$.

We let $\hat{u}_n$, $\hat{u}_{n+1}$, and $\hat{F}_n$ denote the numerical solutions of $\hat{u}(t_n)$, $\hat{u}(t_n+1)$, and $\hat{F}(u_n, t_n)$, respectively. Eq. (31) is exact and considered as the basis of the ETD schemes. Depending on the approximations to the matrix exponential functions and the integral term, different ETD schemes are obtained. If $\hat{F}$ is supposed to have the constant value $\hat{F}_n$ between t_n and t_{n+1}, i.e., $\hat{F} = \hat{F}_n + O(k)$, then (31) is given by

$$\hat{u}_{n+1} = e^{-Ak}\hat{u}_n - \frac{\hat{F}_n}{A}(e^{-Ak} - 1). \tag{32}$$

The above equation is considered as the simplest approximation to the integral in (31), with a local truncation error $k^2\hat{F}'/2$. Rather, if we assume a higher-order approximation then

$$\hat{F}(t) = \hat{F}_n + (t - t_n)\frac{\hat{F}_n - \hat{F}_{n-1}}{k}, \quad t \in [t_n, t_{n+1}] \tag{33}$$

and (31) becomes

$$\hat{u}_{n+1} = e^{-Ak}\hat{u}_n + \frac{\hat{F}_n((1-Ak)e^{-Ak} - 1 + 2Ak) - \hat{F}_{n-1}(e^{-Ak} - 1 + Ak)}{A^2k}, \tag{34}$$

which has a local truncation error $5k^3\hat{F}''/12$ [66].

We utilize a fourth-order time stepping scheme as proposed by Khaliq *et al.* [69], which is based on the (2,2)-Padé approximation by replacing the matrix exponential functions in the ETDRK4 given below [66]. In [138], it was noticed that Khaliq *et al.* [69] alleviated the numerical instabilities of the ETDRK4 which appear from issues such as having $A = 0$ for some modes, or having kA too small.

$$\begin{aligned}\hat{u}_{n+1} = \; & e^{-Ak}\hat{u}_n + \frac{1}{k^2}(-A)^{-3}\Big(\hat{F}(u_n, t_n)[-4 + kA + e^{-Ak}(4 + 3kA + (kA)^2)] \\ & + 2(\hat{F}(\hat{a}_n, t_n + (k/2)) + \hat{F}(\hat{b}_n, t_n + (k/2)))[2 - kA + e^{-Ak}(-2 - kA)] \\ & + \hat{F}(\hat{c}_n, t_n + k)[-4 + 3kA - (kA)^2 + e^{-Ak}(4 + kA)]\Big),\end{aligned} \tag{35}$$

where

$$\hat{a}_n = e^{-Ak/2}\hat{u}_n - A^{-1}(e^{-Ak/2} - 1)\hat{F}(u_n, t_n),$$

$$\hat{b}_n = e^{-Ak/2}\hat{u}_n - A^{-1}(e^{-Ak/2} - 1)\hat{F}(\hat{a}_n, t_n + (k/2)),$$

$$\hat{c}_n = e^{-Ak/2}\hat{a}_n - A^{-1}(e^{-Ak/2} - 1)[2\hat{F}(\hat{b}_n, t_n + (k/2)) - \hat{F}(u_n, t_n)].$$

The Padé approximations are known rational approximations. In particular, the (2,2)-Padé approximation to e^{-z} is given by

$$R_{2,2}(z) = (12 - 6z + z^2)/(12 + 6z + z^2). \tag{36}$$

Fig. 18 (left) shows the behavior of the exponential function (e^{-z}) and $R_{2,2}(z)$ for real values of z, where $z \in [0, 20]$. Fig. 18 (right) shows the behavior of $R_{2,2}(z)$ for $z = x + iy \in [0, 20] \times [-10, 10]$.

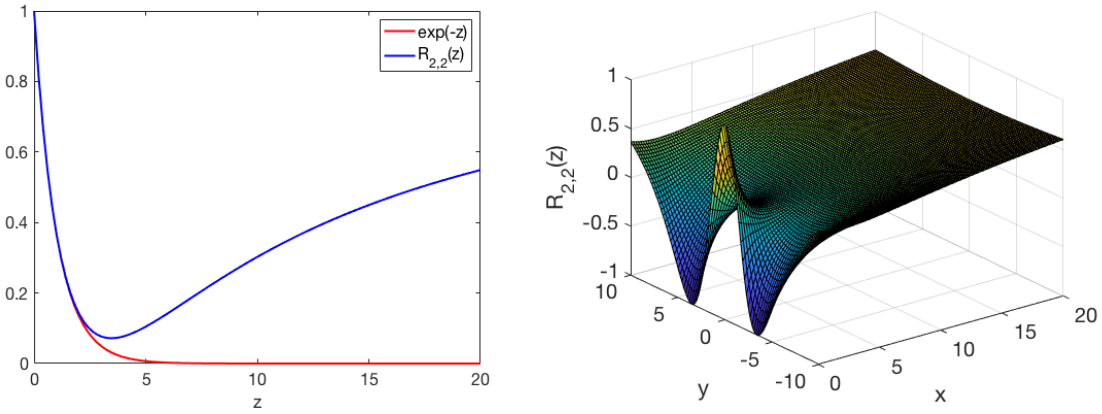

Figure 18: Behavior of e^{-z} and $R_{2,2}(z)$ for $z \in [0, 20]$, and $R_{2,2}(z)$ for $z \in [0, 20] \times [-10, 10]$.

We plug (36) in (35) to obtain the ETD-Padé(2,2) scheme [139]

$$\begin{aligned}\hat{u}_{n+1} = \; & R_{2,2}(kA)\hat{u}_n + P_1(kA)\hat{F}(u_n, t_n) \\ & + P_2(kA)[\hat{F}(\hat{a}_n, t_n + (k/2)) + \hat{F}(\hat{b}_n, t_n + (k/2))] + P_3(kA)\hat{F}(\hat{c}_n, t_n + k),\end{aligned} \tag{37}$$

where

$$\hat{a}_n = R_{2,2}(kA/2)\hat{u}_n + P(kA)\hat{F}(u_n, t_n),$$

$$\hat{b}_n = R_{2,2}(kA/2)\hat{u}_n + P(kA)\hat{F}(\hat{a}_n, t_n + (k/2)),$$

$$\hat{c}_n = R_{2,2}(kA/2)\hat{a}_n + P(kA)[2\hat{F}(\hat{b}_n, t_n + (k/2)) - \hat{F}(u_n, t_n)],$$

with

$$R_{2,2}(kA) = (12 - 6kA + (kA)^2)/(12 + 6kA + (kA)^2),$$

$$R_{2,2}(kA/2) = (48 - 12kA + (kA)^2)/(48 + 12kA + (kA)^2),$$

$$P(kA) = 24k/(48 + 12kA + (kA)^2),$$

$$P_1(kA) = k(2 - kA)/(12 + 6kA + (kA)^2),$$

$$P_2(kA) = 4k/(12 + 6kA + (kA)^2),$$

$$P_3(kA) = k(2 + kA)/(12 + 6kA + (kA)^2).$$

Now, Eq. (37) is fully diagonal, which alleviates related numerical difficulties for the treatment of singular Laplacians such as in the case of the homogeneous Neumann boundary conditions [52, 140].

3.3 Stability regions

This section demonstrates the linear stability of the scheme, by using the general approach for stability analysis of a numerical method that uses different methods for the linear and nonlinear parts of the equation, which was suggested by Cox and Matthews in [66]. We consider the following nonlinear autonomous ODE

$$\hat{u}_t = -c\hat{u} + \hat{F}(u). \tag{38}$$

We assume that there exists a fixed point $\hat{u}(t_0) = \hat{u}_0$, such that $-c\hat{u}_0 + \hat{F}(\hat{u}_0) = 0$. Linearizing about the fixed point $\hat{u}_0$, we obtain

$$\hat{u}_t = -c\hat{u} + \lambda\hat{u}, \tag{39}$$

where $\hat{u}$ is the perturbation of $\hat{u}_0$, and $\lambda = \hat{F}'(u)$. The fixed point $\hat{u}_0$ is stable if $Re(\lambda - c) < 0$ for all λ. Both c and λ are allowed to be complex-valid. The stability region of the ETD-Padé(2,2) scheme is four-dimensional and hence hard to represent [66]. However, the two-dimensional stability region can be obtained if both of the parameters c and λ are purely real or purely imaginary [141], or if c is fixed and real and λ is complex [131].

To get the stability region of our scheme, we apply the ETD-Padé(2,2) scheme in (37) to (39). If we let $r = \hat{u}_{n+1}/\hat{u}_n$, $y = -ck$ and $x = \lambda k$, then we have the following amplification symbol

$$r(x, y) = c_0 + c_1 x + c_2 x^2 + c_3 x^3 + c_4 x^4, \tag{40}$$

where

$$c_0 = \frac{(12 + 6y + y^2)}{(12 - 6y + y^2)},$$

$$c_1 = \frac{(2 + y)}{(12 - 6y + y^2)} + \frac{8(48 + 12y + y^2)}{(48 - 12y + y^2)(12 - 6y + y^2)} + \frac{(2 - y)(48 + 12y + y^2)^2}{(48 - 12y + y^2)^2(12 - 6y + y^2)},$$

$$c_2 = \frac{96}{(48 - 12y + y^2)(12 - 6y + y^2)} + \frac{96(48 + 12y + y^2)}{(48 - 12y + y^2)^2(12 - 6y + y^2)}$$
$$+ \frac{72(2 - y)(48 + 12y + y^2)}{(48 - 12y + y^2)^2(12 - 6y + y^2)} - \frac{24(2 - y)}{(48 - 12y + y^2)(12 - 6y + y^2)},$$

$$c_3 = \frac{2304}{(48 - 12y + y^2)^2(12 - 6y + y^2)} + \frac{1152(2 - y)(48 + 12y + y^2)}{(48 - 12y + y^2)^3(12 - 6y + y^2)},$$

$$c_4 = \frac{27648(2 - y)}{(48 - 12y + y^2)^3(12 - 6y + y^2)}.$$

Fig. 19 shows the stability regions of the ETD-Padé(2,2) scheme where $|r(x, y)| = 1$ in the complex x-plane, which represents the case when c is fixed and real and λ is complex. We select several real non-positive values of y where the axes are imaginary and real parts of x. It is observed that as $y \to 0$, the stability region tends to the stability region of the scheme of the fourth-order Rung-Kutta. According to Beylkin et al. [131], for the method to be useful, it is important that stability regions grow as $y \to -\infty$. The stability regions as shown in Fig. 19 indicate the stability of the ETD-Padé(2,2) scheme since they grow larger as $y \to -\infty$.

3.4 The ETD-Padé(2,2) algorithm

Algorithm 3 ETD-Padé(2,2) three-dimensional algorithm with Neumann boundary conditions

Given: $L = (b - a)$, α, N_x, k, κ_α, u, and T.

Compute $\lambda = (((0 : N_x - 1)\pi/L)^2 + ((0 : N_y - 1)\pi/L)^2 + ((0 : N_z - 1)\pi/L)^2)^{\frac{\alpha}{2}}$. ▷

$N_x = N_y = N_z$.

Let $h = \frac{L}{N_x}$, compute $x,\ y,$ and z such that $x = y = z = a + (0 : N_x - 1)h + \frac{h}{2}$.

Set the coefficients:

$r_1 = (48 + 12\ k\ \kappa_\alpha\ \lambda + (k\ \kappa_\alpha\ \lambda)^2)$, $r_2 = (48 - 12\ k\ \kappa_\alpha\ \lambda + (k\ \kappa_\alpha\ \lambda)^2)$.

$r_3 = (12 + 6\ k\ \kappa_\alpha\ \lambda + (k\ \kappa_\alpha\ \lambda)^2)$, $r_{(2,2)} = (12 - 6\ k\ \kappa_\alpha\ \lambda + (k\ \kappa_\alpha\ \lambda)^2)$.

$p = (24\ k)$, $p_1 = k(2 - k\ \kappa_\alpha\ \lambda)$.

$p_2 = (4\ k)$, $p_3 = k\ (2 + k\ \kappa_\alpha\ \lambda)$.

for $n = 1, 2, \ldots,$ round(T/dt), **do**

$u_{dct} = dctn(u)$.

$t = nk$.

Compute $f(u_n, t_n)$ as f_{u_n} using the given u.

$a_n = idctn((r_2\ u_{dct} + p\ dctn(f_{u_n}))/r_1)$.

Compute $f(a_n, t_n + k)$ as f_{a_n} using a_n.

$b_n = idctn((r_2\ u_{dct} + p\ dctn(f_{a_n}))/r_1)$.

Compute $f(b_n, t_n + k)$ as f_{b_n} using b_n.

$c_n = idctn((r_2\ dctn(a_n) + p\ dctn(2\ f_{b_n}\ -\ f_{u_n}))/r_1)$.

Compute $f(c_n, t_n + k)$ as f_{c_n} using c_n.

$u = idctn((r_{(2,2)}\ u_{dct} + p_1\ dctn(f_{u_n}) + p_2\ dctn(f_{a_n} + f_{b_n}) + p_3\ dctn(f_{c_n}))/r_3)$.

end for

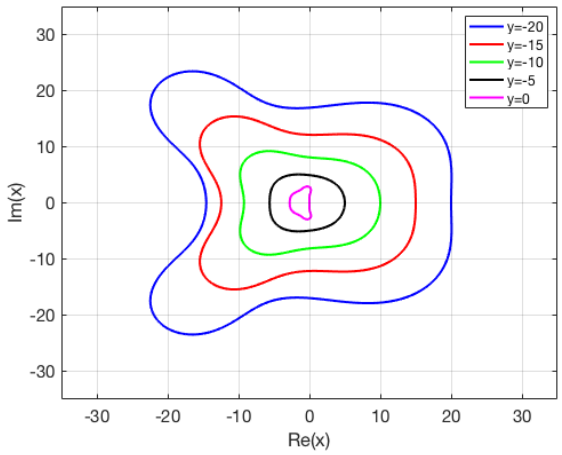

Figure 19: Stability regions of the ETD-Padé(2,2) scheme in the complex x-plane.

3.5 Numerical experiments

This section includes several numerical problems to demonstrate the effectiveness of the proposed scheme. We consider a 2D heat equation with a source term, the Gray-Scott model and the Brusselator problem (both of which are 2D systems), and finally the 3D Schnakenberg system. In these test problems, we consider both homogeneous Dirichlet and Neumann boundary conditions. In the numerical tests, we perform some computational convergence analysis. The accuracy of the approach is measured using the discrete L_2 norm error and the maximum norm error L_∞ defined as

$$L_2 = \sqrt{h\langle e_j, e_j\rangle},$$

$$L_\infty = \max_j |e_j|,$$

where $e_j = u_j - U_j$, u_j and U_j are the jth exact and numerical solutions, respectively. The rate of convergence in time can be computed as

$$\text{rate of convergence} = \frac{\log_{10}\left(\left\|(u-u_{k_j})\right\| / \left\|(u-u_{k_{j+1}})\right\|\right)}{\log_{10}(k_j/k_{j+1})}, \tag{41}$$

where u is the exact solution, u_{k_j} and $u_{k_{j+1}}$ are the numerical solutions with the time step size k_j and k_{j+1}, respectively.

3.5.1 Test Problem 1: a 2D benchmark problem

The following problem is the space-fractional heat equation in two space dimensions with a source term [52]

$$\frac{\partial u}{\partial t} = -\kappa_\alpha(-\Delta)^{\alpha/2}u + f(u,t), \tag{42}$$

where

$$f(u,t) = t^\alpha \frac{\kappa_\alpha}{16}\sum_{i=1}^{4}(1+\lambda_i^{\alpha/2})v_i + \alpha t^{\alpha-1}\sin^3(\pi x)\sin^3(\pi y) - \kappa_\alpha u,$$

and

$$\begin{aligned}
v_1 &= 9\sin(\pi x)\sin(\pi y), & \lambda_1 &= 2\pi^2,\\
v_2 &= -3\sin(\pi x)\sin(3\pi y), & \lambda_2 &= 10\pi^2,\\
v_3 &= -3\sin(3\pi x)\sin(\pi y), & \lambda_3 &= 10\pi^2,\\
v_4 &= \sin(3\pi x)\sin(3\pi y), & \lambda_4 &= 18\pi^2,
\end{aligned}$$

with the initial condition $u(x,y,0) = 0$ and homogeneous Dirichlet boundary conditions, $(x,y) \in [0,1]^2$. The exact solution is given by

$$u(x,y,t) = t^\alpha \sin(3\pi x)\sin(3\pi y).$$

We selected this problem as a benchmark test problem with an exact solution to verify that the proposed scheme achieves the fourth-order accuracy in time, as expected. The numerical and exact solutions of (42) are demonstrated in Fig. 20 for $\kappa_\alpha = 10,\ N_x = 51,\ k = 0.01,\ \alpha = 1.6$ and the simulations run up to $T = 1.0$. To present the performance of the derived scheme, the numerical experiment was carried out up to $T = 1.0$ with $\alpha = 1.5$. We also used temporal step sizes starting with $k = 0.01$ and

a large space step with $N_x = 60$, whereas the step size is given by using $N_x = 150$ for the scheme proposed by Bueno-Orovio *et al.* [52]. The results such as the maximum error, rates of convergence, and CPU time are listed in Table 8. Despite the higher-order of the ETD-Padé(2,2) scheme, it achieves better performance in terms of the computational efficiency. The L_2 norm error, maximum error (L_∞ norm error), rate of convergence, and CPU time for the ETD-Padé(2,2) scheme are listed in Table 9 at $T = 1,\ N_x = 40,$ and $k = 0.001$ for various fractional powers α. The computed rates of convergence agree with the expected rate of the proposed scheme. Fig. 21 shows the log-log graphs of the L_2 and L_∞ errors vs. the time step to visualize the rate of convergence of the scheme using different values of α at $N_x = 40$ and $k = 0.001$.

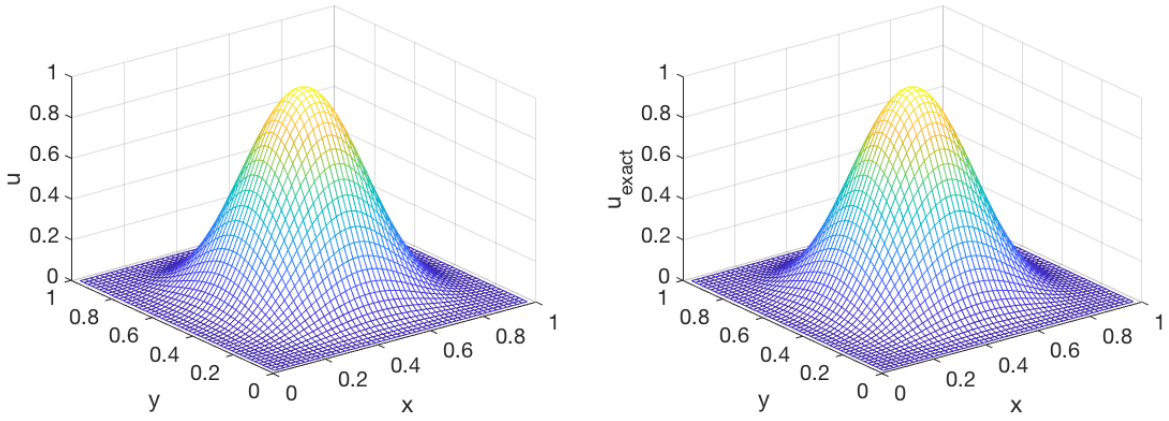

Figure 20: The solution obtained by the ETD-Padé(2,2) (left) and the exact solution of (42) (right).

Table 8: A comparison in terms of the errors, rate of convergence, and CPU(s).

k	ETD-Padé$(2,2)$			Bueno-Orovio *et al.*		
	L_∞ error	order	CPU(s)	L_∞ error	order	CPU(s)
0.00100	2.08×10^{-9}	-	7.50	2.53×10^{-6}	-	53.37
0.00050	1.45×10^{-10}	3.84	15.40	1.26×10^{-6}	1.00	154.00
0.00025	9.59×10^{-12}	3.92	29.24	6.32×10^{-7}	1.00	352.83
0.00013	6.17×10^{-13}	3.96	59.76	3.16×10^{-7}	1.00	763.02
0.00006	4.98×10^{-14}	3.63	121.24	1.58×10^{-7}	1.00	1547.45

Table 9: Errors, convergence rates in time and CPU(s).

α	k	L_2 error	order	L_∞error	order	CPU(s)
2	0.00100	1.6022e-08	-	8.8929e-09	-	2.9496
	0.00050	1.4611e-09	3.4549	8.1198e-10	3.4531	5.6273
	0.00025	1.1078e-10	3.7213	6.1363e-11	3.7260	11.0524
	0.00013	7.6334e-12	3.8592	4.2086e-12	3.8659	21.9122
1.8	0.00100	7.2614e-09	-	4.0632e-09	-	3.0059
	0.00050	5.7213e-10	3.6658	3.1943e-10	3.6691	5.5985
	0.00025	4.0195e-11	3.8313	2.2390e-11	3.8346	11.1008
	0.00013	2.6602e-12	3.9174	1.4752e-12	3.9239	22.1343
1.6	0.00100	2.8492e-09	-	1.5990e-09	-	2.9363
	0.00050	2.0506e-10	3.7965	1.1488e-10	3.7990	5.8309
	0.00025	1.3752e-11	3.8983	7.6905e-12	3.9009	11.4474
	0.00013	8.8223e-13	3.9624	4.8650e-13	3.9826	22.3631
1.4	0.00100	9.9190e-10	-	5.5513e-10	-	2.8237
	0.00050	6.7557e-11	3.8760	3.7778e-11	3.8772	5.6050
	0.00025	4.4027e-12	3.9397	2.4575e-12	3.9423	11.0941
	0.00013	2.7373e-13	4.0076	1.3223e-13	4.2161	21.9620

$\alpha = 2.0$

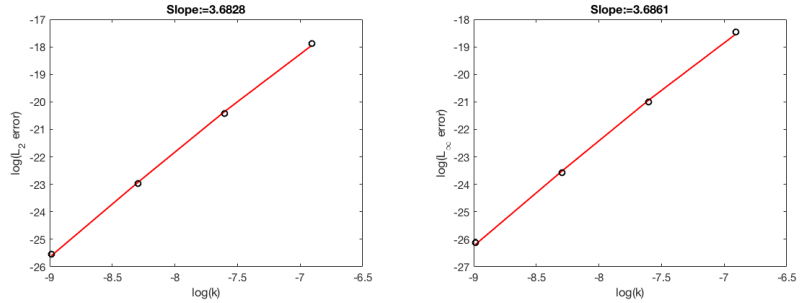

$\alpha = 1.8$

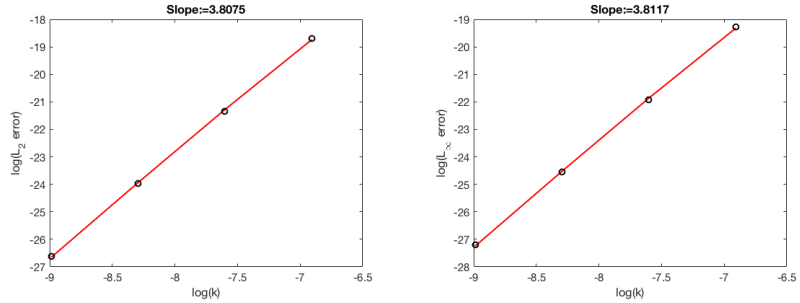

$\alpha = 1.6$

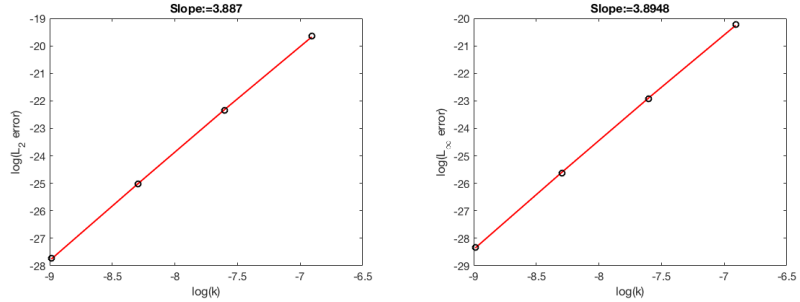

$\alpha = 1.4$

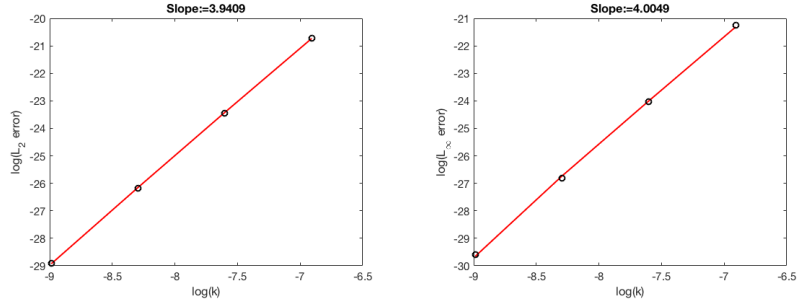

Figure 21: Time rates of convergence of the scheme.

3.5.2 Test Problem 2: the Gray-Scott model

We consider the space-fractional version of the Gray-Scott model with homogeneous Neumann boundary conditions [142, 143]

$$\begin{aligned}\frac{\partial u}{\partial t} &= -\kappa_u(-\Delta)^{\frac{\alpha}{2}}u - uv^2 + F(1-u),\\ \frac{\partial v}{\partial t} &= -\kappa_v(-\Delta)^{\frac{\alpha}{2}}v + uv^2 - (F+\kappa)v,\end{aligned} \tag{43}$$

which corresponds to the two reactions [106]

$$U + 2V \to 3V,$$

$$V \to P.$$

The diffusion coefficients (κ_u and κ_v), dimensionless feed rate F, and dimensionless depletion rate κ are all positive constants, with $\frac{\kappa_u}{\kappa_v} > 1$. Depending on the values of F and κ, different patterns can be obtained. The domain is taken to be $[0,1]^2$. We chose $\kappa_u = 2\times 10^{-5}$, $\frac{\kappa_u}{\kappa_v} = 2, F = 0.03$ and $\kappa = 0.055$ based on that in [52]. The system was placed in the initial state $(u,v) = (1,0)$, and then, (32×32) mesh points from the center of the grid were perturbed to $(u,v) = (0.5, 0.25)$. The initial disturbance propagates from the center outward until the entire grid is influenced by the initial perturbation.

Fig. 22 shows the pattern formations of the Gray-Scott model that are obtained by applying the ETD-Padé(2,2) scheme for different values of α using $N_x = 400$ and $k = 1$ at $T = 1000,\ 2000,\ 6000,$ and 8000, corresponding to the first, second, third, and fourth columns, respectively.

When $\alpha = 2$, the model represents the negative solutions in the steady-state field. As the fractional power decreases to $\alpha = 1.7$, the velocity of propagation of the initial perturbation reduces. A finer granulation can be observed as α decreases and T grows to reach the final steady-state field [52].

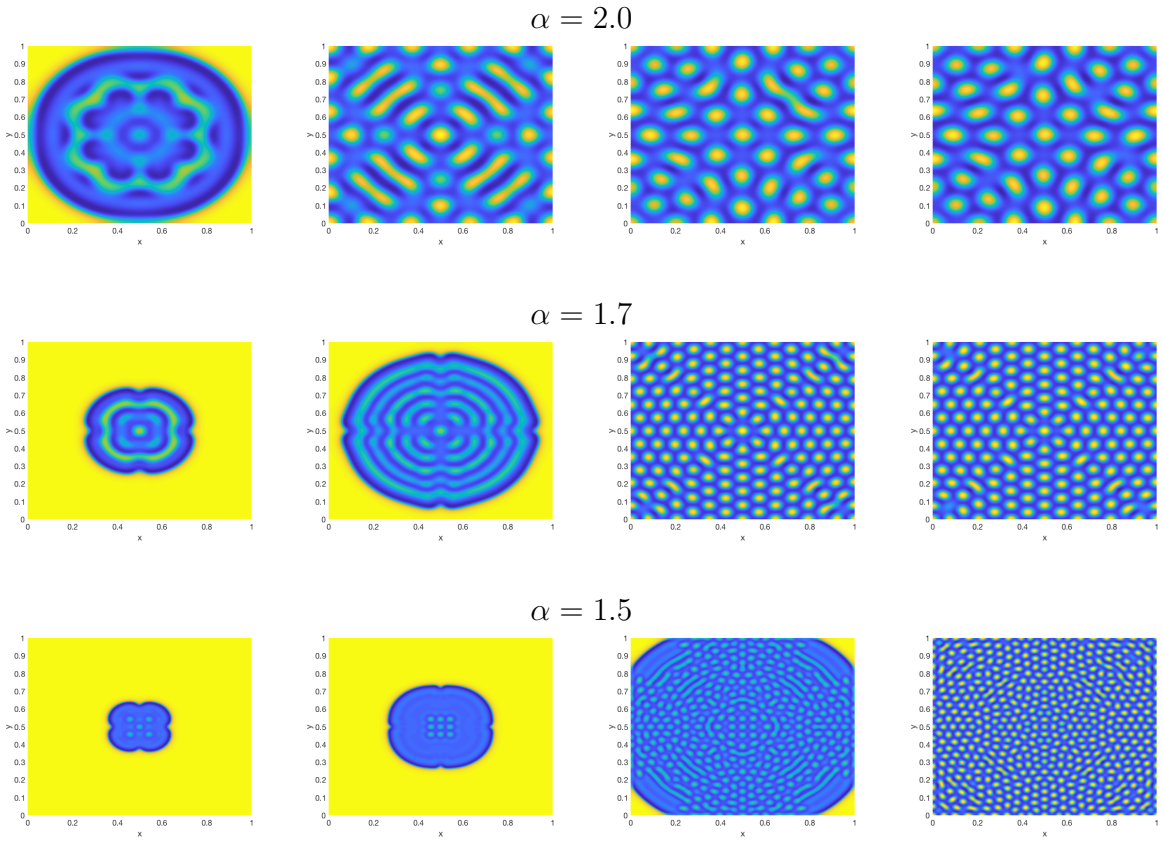

Figure 22: Solution profiles of the Gray-Scott model (43) at different values of α.

3.5.3 Test Problem 3: the 2D Brusselator model

We consider the 2D space-fractional Brusselator system of two equations, on $[0,1]^2$ [144, pp. 248-252]

$$\begin{aligned}\frac{\partial u}{\partial t} &= -\kappa_\alpha(-\Delta)^{\frac{\alpha}{2}}u + B + u^2v - (C+1)u,\\ \frac{\partial v}{\partial t} &= -\kappa_\alpha(-\Delta)^{\frac{\alpha}{2}}v + Cu - u^2v,\end{aligned} \tag{44}$$

subject to homogeneous Neumann boundary conditions and the following initial conditions

$$u(x, y, 0) = 0.5 + y,$$

$$v(x, y, 0) = 1 + 5x.$$

Computations are performed using $\kappa_\alpha = 2 \times 10^{-3}$, $B = 1$, $C = 3.4$, and carried out up to $T = 10$. The solution profiles of the concentrations u and v for $\alpha = 2,\ 1.8,\ \text{and } 1.6$, $N_x = 100,\ \text{and } k = 0.1$ are shown in Fig. 23.

In Tables 10 and 11, the L_2, L_∞ errors, rates of convergence and CPU(s) for both the u and v components are computed based on (45) for a sequence of temporal steps starting with $k = 0.05$. We also set $N_x = 64$, $T = 5$, and $\alpha = 2,\ \text{and } 1.7$. Since the exact solution is unknown for this nonlinear problem, then the error is calculated between the consecutive solutions as the time step k is halved, and the rate of convergence in time can be computed as

$$\text{rate of convergence} = \frac{\log_{10}(E_k/E_{k/2})}{\log_{10}(2)}, \tag{45}$$

where $E_k = \|u_k - u_{2k}\|$ and $E_{k/2} = \left\|u_{k/2} - u_k\right\|$ are the L_2 or L_∞ norm errors at k and $k/2$.

Table 10: Errors, convergence rates in time and CPU(s) for u.

α	k	L_2 error	order	L_∞error	order	CPU(s)
2	0.05000	-	-	-	-	0.6297
	0.02500	3.4140e-04	-	4.8167e-04	-	1.1647
	0.01250	2.4525e-05	3.7991	3.4662e-05	3.7966	2.4769
	0.00625	1.6482e-06	3.8952	2.3277e-06	3.8964	4.4538
	0.00313	1.0689e-07	3.9467	1.5077e-07	3.9485	8.6909
1.7	0.05000	-	-	-	-	0.7571
	0.02500	5.2202e-04	-	8.0601e-04	-	1.1982
	0.01250	3.5260e-05	3.8880	5.6652e-05	3.8306	2.3498
	0.00625	2.2985e-06	3.9392	3.7449e-06	3.9191	4.4212
	0.00313	1.4676e-07	3.9692	2.4098e-07	3.9579	8.7474

Table 11: Errors, convergence rates in time and CPU(s) for v.

α	k	L_2 error	order	L_∞error	order	CPU(s)
2	0.05000	-	-	-	-	0.6046
	0.02500	5.2376e-04	-	6.0522e-04	-	1.1618
	0.01250	3.5881e-05	3.8676	4.3577e-05	3.7958	2.2414
	0.00625	2.3790e-06	3.9148	2.9271e-06	3.8960	4.5707
	0.00313	1.5341e-07	3.9549	1.8963e-07	3.9482	9.3587
1.7	0.05000	-	-	-	-	0.7382
	0.02500	7.1002e-04	-	9.3479e-04	-	1.2476
	0.01250	4.7016e-05	3.9166	6.5755e-05	3.8295	2.3908
	0.00625	3.0492e-06	3.9466	4.3579e-06	3.9154	4.4764
	0.00313	1.9427e-07	3.9723	2.8023e-07	3.9590	8.7510

3.5.4 Test Problem 4: the Schnakenberg model

We consider the system of 3D space-fractional Schnakenberg model [112, 145]

$$\begin{aligned}\frac{\partial u}{\partial t} &= -\kappa_u(-\Delta)^{\frac{\alpha}{2}}u + \gamma(a - u + u^2 v),\\ \frac{\partial v}{\partial t} &= -\kappa_v(-\Delta)^{\frac{\alpha}{2}}v + \gamma(b - u^2 v),\end{aligned} \tag{46}$$

with homogeneous Neumann boundary conditions, and the initial conditions are given by

$$u(x, y, z, 0) = 1 - \exp(-10((x - 0.5)^2 + (y - 0.5)^2 + (z - 0.5)^2)),$$

$$v(x, y, z, 0) = \exp(-10((x - 0.5)^2 + 2(y - 0.5)^2 + (z - 0.5)^2)).$$

The parameters used in the numerical experiments are: $\kappa_u = 1$, $\kappa_v = 12$, $a = 0.1$, $b = 0.9$ and $\gamma = 10$. The numerical simulation of this model results in interesting isosurfaces which illustrate the emergence of pattern formations dependent on the values of T and the fractional power α as can be seen in Figs. 24 and 25.

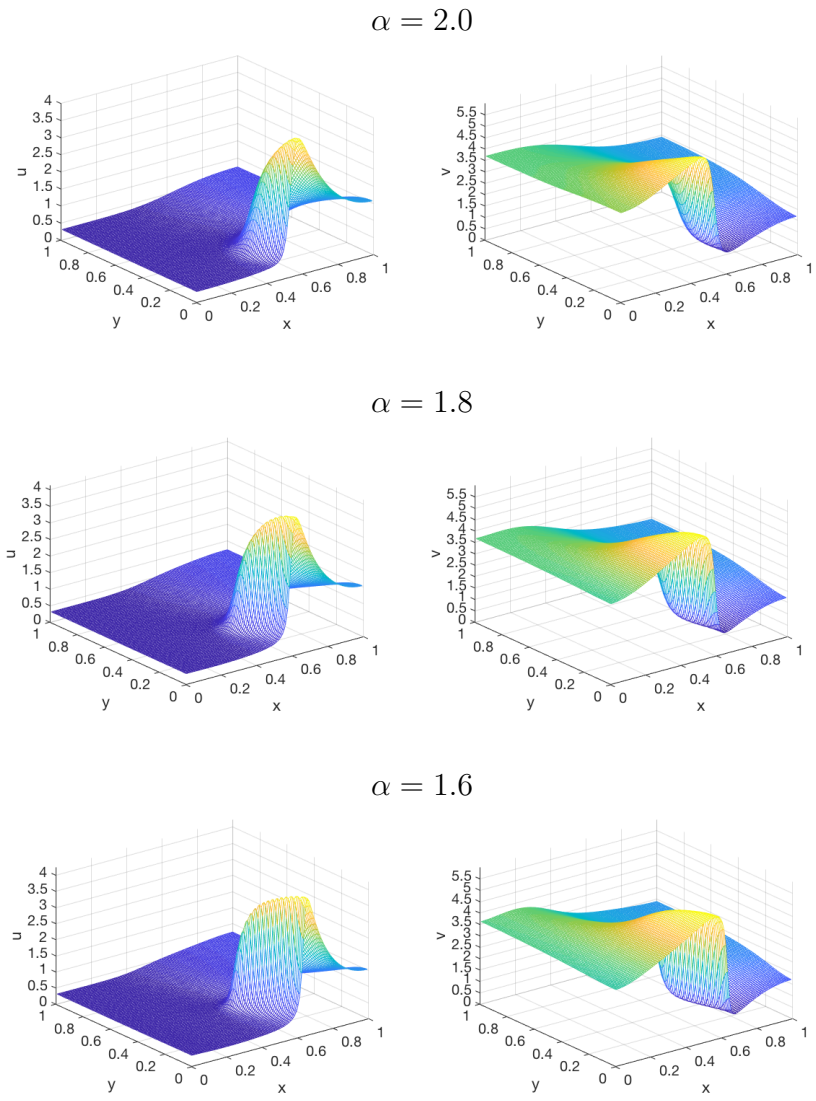

Figure 23: Solution profiles of the Brusselator model (44) (u (left column) and v (right column)).

$\alpha = 2.0$

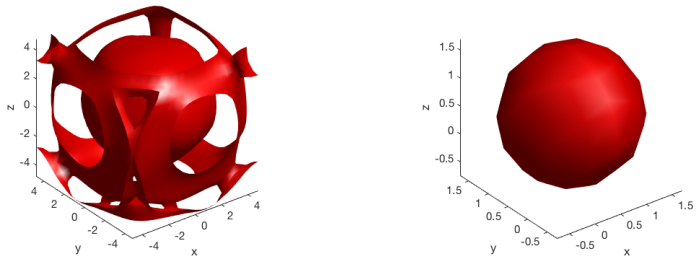

$T = 2$

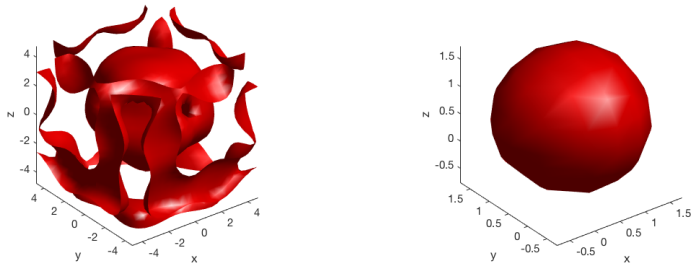

$T = 5$

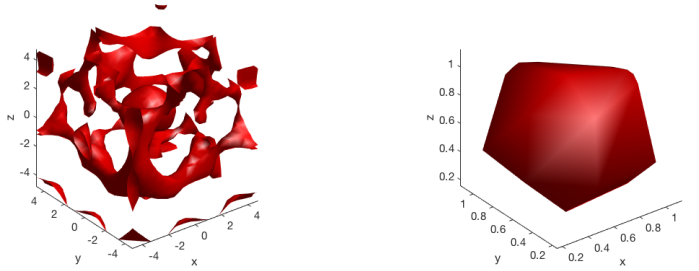

$T = 10$

Figure 24: Isosurfaces of u (left column) and v (right column) for the 3D Schnakenberg model (46) with $\alpha = 2,\ N_x = 21,$ and $k = 0.1$ at different values of the final time.

$\alpha = 1.5$

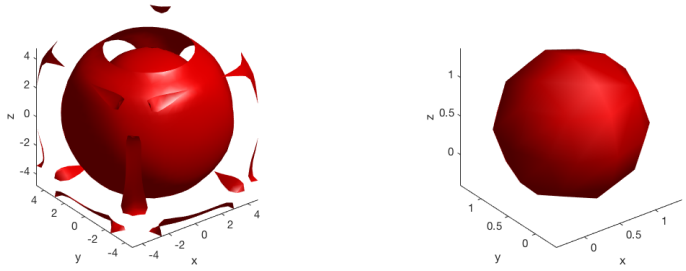

$T = 2$

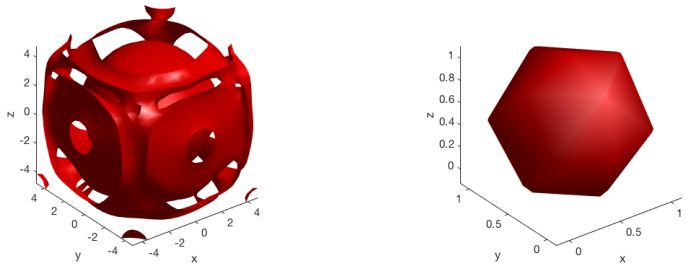

$T = 5$

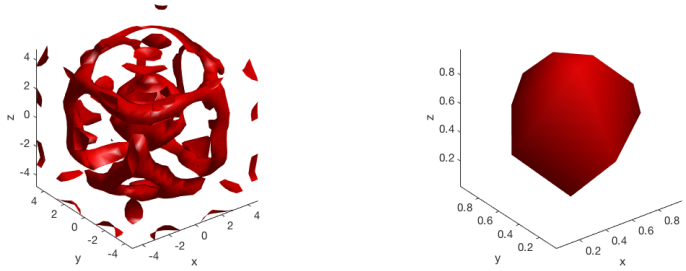

$T = 10$

Figure 25: Isosurfaces of u (left column) and v (right column) for the 3D Schnakenberg model (46) with $\alpha = 1.5,\ N_x = 21,$ and $k = 0.1$ at different values of the final time.

3.6 Conclusion

We have developed a high-order time stepping scheme in combination with the Fourier spectral approach. The scheme was able to remove the stiffness related to the high-order spatial derivative of the space-fractional reaction-diffusion equations. Moreover, the scheme was implemented efficiently on large systems of multidimensional space-fractional reaction-diffusion equations. The stability of the scheme was investigated by plotting its stability regions, which gave an explanation of its behavior. Numerical experiments were performed on multidimensional systems, and the results showed the reliability and stability of the scheme. The rate of convergence of the scheme was examined computationally and shown to be fourth-order accurate in time.

CHAPTER 4

FOURTH-ORDER ETD SCHEME WITH NON-HOMOGENEOUS BOUNDARY CONDITIONS

4.1 Introduction

In this chapter, we develop a fourth-order scheme for space-fractional reaction-diffusion equations with non-homogeneous boundary conditions. For the spatial discretization, a modified MTT is used to handle the non-homogeneous boundary conditions and is combined with a fourth-order time integration based on the ETD approximation. The partial fraction splitting technique is applied to reduce the computational complexity of the scheme to be the same as that for the backward Euler. Numerical experiments are performed to illustrate the reliability and accuracy of the scheme.

Developing numerical solutions for the fractional equations is essential since there is no effective technique to obtain the exact solution of these equations. Ilic *et al.* [72] proposed numerical solution of the space-fractional diffusion equation based on the MTT with homogeneous boundary conditions, Yang *et al.* [82] followed this approach to solve the 2D time-space fractional diffusion equation. Most of the numerical schemes were considered with homogeneous boundary conditions for solving nonlinear space-fractional equations, see for instance [146, 147]. Ilic *et al.* [58] extended the MTT with non-homogeneous boundary conditions for the fractional diffusion equation.

We develop a fourth-order scheme in time using (2,2)-Padé approximations to the matrix exponential combined with the MTT for non-homogeneous boundary conditions. The scheme avoids solving nonlinear systems at each time step. Moreover, it is computationally efficient for solving systems of space-fractional reaction-diffusion equations due to the utilization of the partial fraction decomposition which only requires Euler-type solvers.

4.2 MTT with non-homogeneous boundary conditions

We consider the space-fractional reaction-diffusion equation

$$\begin{aligned} \frac{\partial u(x,t)}{\partial t} &= -\kappa_\alpha(-\Delta)^{\frac{\alpha}{2}}u(x,t) + f(u,t),\ 1<\alpha\leq 2,\ t>0, \\ u(x,0) &= u_0(x),\quad x\in\Omega=(a,b)\subset\mathbb{R}, \\ u(a,t) &= g_1(t)\ \text{ and }\ u(b,t)=g_2(t), \end{aligned} \tag{47}$$

the fractional Laplacian $(-\Delta)^{\frac{\alpha}{2}}$ is defined via the spectral decomposition of the standard Laplacian $(-\Delta)$.

Ilić et al. [72] introduced the MTT for approximating the fractional Laplacian with homogeneous boundary conditions on a uniform mesh of step size h as

$$(-\Delta)^{\frac{\alpha}{2}}u \approx h^{-\alpha}M^{\frac{\alpha}{2}}u,$$

the matrix representation of the fractional Laplacian is generated from the matrix representation of the standard Laplace operator using the eigenvalues and eigenvectors, thus

$$M^{\frac{\alpha}{2}} = P\Lambda^{\frac{\alpha}{2}}P^{-1},$$

where Λ is the eigenvalues matrix and P is the eigenvectors matrix,

$\Lambda = \operatorname{diag}(\lambda_1,\lambda_2,\lambda_3,\ldots,\lambda_{m-1})$, $\lambda_i = 4\sin^2\left(\frac{i\pi}{2m}\right)$, $\quad i=1,2,\ldots,m-1$,

and $P=(\xi_1,\xi_2,\xi_3,\ldots,\xi_{m-1})$, $\quad \xi_i=\left(\sin\left(\frac{1i\pi}{m}\right),\sin\left(\frac{2i\pi}{m}\right),\sin\left(\frac{3i\pi}{m}\right),\ldots,\sin\left(\frac{(m-1)i\pi}{m}\right)\right)^T$.

The matrix representation of the standard Laplace operator utilizing the finite difference method with imposed non-homogeneous boundary conditions becomes

$$(-\Delta)u \approx h^{-2}(Mu + e_1g_1(t) + e_{m-1}g_2(t)),$$

where e_1 and e_{m-1} are the 1^{st} and $(m-1)^{th}$ canonical basis vectors in $\mathbb{R}^{m-1}$, then

$$\begin{aligned} (-\Delta)^{\frac{\alpha}{2}}u &= (-\Delta)^{\frac{\alpha}{2}-1}(-\Delta)u \\ &\approx (h^{-2}M)^{\frac{\alpha}{2}-1}(h^{-2}(Mu+e_1g_1(t)+e_{m-1}g_2(t))) \\ &= h^{-\alpha}M^{\frac{\alpha}{2}}u + h^{-\alpha}M^{\frac{\alpha}{2}-1}(e_1g_1(t)+e_{m-1}g_2(t)). \end{aligned}$$

If we consider the standard space reaction-diffusion equation

$$\begin{aligned} \frac{\partial u(x,t)}{\partial t} &= -\kappa_\alpha \left(-\frac{\partial^2}{\partial x^2}\right) u(x,t) + f(u,t),\ t>0, \\ u(x,0) &= u_0(x), \quad x \in \Omega = (a,b) \subset \mathbb{R}, \\ u(a,t) &= g_1(t) \ \text{ and } \ u(b,t) = g_2(t), \end{aligned} \tag{48}$$

and the space derivative is approximated by utilizing the finite difference method, then we obtain

$$\begin{aligned} \frac{du(x_i,t)}{dt} &= -\frac{\kappa_\alpha}{h^2}(-u(x_{i-1},t) + 2u(x_i,t) - u(x_{i+1},t)) + f(u(x_i,t),t),\ i = 1,2,\ldots,m-1, \\ u(x_i,0) &= u_0(x_i),\ i = 1,2,\ldots,m-1, \\ u(x_0,t) &= g_1(t) \ \text{ and } \ u(x_m,t) = g_2(t). \end{aligned}$$

We rewrite the above equation in a matrix form as

$$\begin{aligned} \frac{du}{dt} &= -\frac{\kappa_\alpha}{h^2} Mu + \frac{\kappa_\alpha}{h^2}(e_1 g_1(t) + e_{m-1} g_2(t)) + f(u,t), \\ u(x,0) &= u_0(x), \end{aligned}$$

where $M = \text{tridiag}\{-1, 2, -1\}$. Utilizing the MTT as in [58], the space-fractional reaction-diffusion equation is approximated as

$$\begin{aligned} \frac{du}{dt} &= -\frac{\kappa_\alpha}{h^\alpha} M^{\frac{\alpha}{2}} u + \frac{\kappa_\alpha}{h^\alpha} M^{\frac{\alpha}{2}-1}(e_1 g_1(t) + e_{m-1} g_2(t)) + f(u,t), \\ u(x,0) &= u_0(x). \end{aligned}$$

4.3 ETD with non-homogeneous boundary conditions

The following system of ODEs is obtained by using the above mentioned MTT with non-homogeneous boundary conditions

$$\frac{du}{dt} = -A^{\frac{\alpha}{2}} u + F(u,t), \tag{49}$$

where $u(0) = u_0$, $A^{\frac{\alpha}{2}} = \frac{\kappa_\alpha}{h^\alpha} M^{\frac{\alpha}{2}}$, $F(u,t) = \frac{\kappa_\alpha}{h^\alpha} M^{\frac{\alpha}{2}-1}(e_1 g_1(t) + e_{m-1} g_2(t)) + f(u,t)$,
$u(t) = [u_1(t), u_2(t), u_2(t), \ldots, u_{m-1}(t)]^T$,
and $f(u,t) = [f(u_1(t),t), f(u_2(t),t), f(u_3(t),t), \ldots, f(u_{m-1}(t),t)]^T$.
Let $k = t_{n+1} - t_n$ be the time step size such that $t_n = nk$, $n = 0, 1, 2, \ldots$ and $u_n =: u(t_n)$. Then the exact solution of (49) is obtained by the recurrence formula as

$$u(t_{n+1}) = e^{-kA^{\frac{\alpha}{2}}} u(t_n) + k \int_0^1 e^{-kA^{\frac{\alpha}{2}}(1-\tau)} F(u(t_n + \tau k), t_n + \tau k) d\tau. \tag{50}$$

Cox and Mathews [66] developed the higher-order approximation ETDRK4 scheme of Runge-Kutta type

$$\begin{aligned} u_{n+1} = \; & e^{-kA^{\frac{\alpha}{2}}} u_n + \frac{1}{k^2}\big(-A^{\frac{\alpha}{2}}\big)^{-3} \Bigg(F(u_n, t_n)\big[-4I + kA^{\frac{\alpha}{2}} + e^{-kA^{\frac{\alpha}{2}}}\big(4I + 3kA^{\frac{\alpha}{2}} + \big(kA^{\frac{\alpha}{2}}\big)^2\big)\big] \\ & + 2\left(F\left(a_n, t_n + \frac{k}{2}\right) + F\left(b_n, t_n + \frac{k}{2}\right)\right)\big[2I - kA^{\frac{\alpha}{2}} + e^{-kA^{\frac{\alpha}{2}}}\big(-2I - kA^{\frac{\alpha}{2}}\big)\big] \\ & + F(c_n, t_n + k)\big[-4I + 3kA^{\frac{\alpha}{2}} - \big(kA^{\frac{\alpha}{2}}\big)^2 + e^{-kA^{\frac{\alpha}{2}}}\big(4I + kA^{\frac{\alpha}{2}}\big)\big]\Bigg), \end{aligned} \tag{51}$$

where

$$\begin{aligned} a_n &= e^{-\frac{kA^{\frac{\alpha}{2}}}{2}} u_n - A^{-\frac{\alpha}{2}}\left(e^{-\frac{kA^{\frac{\alpha}{2}}}{2}} - I\right) F(u_n, t_n), \\ b_n &= e^{-\frac{kA^{\frac{\alpha}{2}}}{2}} u_n - A^{-\frac{\alpha}{2}}\left(e^{-\frac{kA^{\frac{\alpha}{2}}}{2}} - I\right) F\left(a_n, t_n + \frac{k}{2}\right), \\ c_n &= e^{-\frac{kA^{\frac{\alpha}{2}}}{2}} a_n - A^{-\frac{\alpha}{2}}\left(e^{-\frac{kA^{\frac{\alpha}{2}}}{2}} - I\right)\left[2F\left(b_n, t_n + \frac{k}{2}\right) - F(u_n, t_n)\right]. \end{aligned}$$

The matrix $A^{\frac{\alpha}{2}}$ is non-diagonal, hence implementing the matrix exponential directly may experience numerical instability since it is necessary to compute the inverses and powers.

We propose a modified version of (51) by using the fourth-order (2,2)-Padé approximation to the matrix exponential $e^{-kA^{\frac{\alpha}{2}}}$, which is given as

$$R_{2,2}\big(kA^{\frac{\alpha}{2}}\big) = \frac{12 - 6\big(kA^{\frac{\alpha}{2}}\big) + \big(kA^{\frac{\alpha}{2}}\big)^2}{12 + 6\big(kA^{\frac{\alpha}{2}}\big) + \big(kA^{\frac{\alpha}{2}}\big)^2}. \tag{52}$$

4.3.1 The ETD-Padé(2,2) scheme

By plugging (52) in (51), we get the following scheme

$$\begin{aligned} u_{n+1} = \; & R_{2,2}\big(kA^{\alpha/2}\big)u_n + P_1\big(kA^{\alpha/2}\big)F(u_n, t_n) \\ & + P_2\big(kA^{\alpha/2}\big)\left[F\left(a_n, t_n + \frac{k}{2}\right) + F\left(b_n, t_n + \frac{k}{2}\right)\right] \\ & + P_3\big(kA^{\alpha/2}\big)F(c_n, t_n + k), \end{aligned} \tag{53}$$

where

$$\begin{aligned} R_{2,2}\big(kA^{\alpha/2}\big) &= \big(12I - 6kA^{\alpha/2} + \big(kA^{\alpha/2}\big)^2\big)\big(12I + 6kA^{\alpha/2} + \big(kA^{\alpha/2}\big)^2\big)^{-1}, \\ P_1\big(kA^{\alpha/2}\big) &= k\big(2I - kA^{\alpha/2}\big)\big(12I + 6kA^{\alpha/2} + \big(kA^{\alpha/2}\big)^2\big)^{-1}, \\ P_2\big(kA^{\alpha/2}\big) &= 4k\big(12I + 6kA^{\alpha/2} + \big(kA^{\alpha/2}\big)^2\big)^{-1}, \\ P_3\big(kA^{\alpha/2}\big) &= k\big(2I + kA^{\alpha/2}\big)\big(12I + 6kA^{\alpha/2} + \big(kA^{\alpha/2}\big)^2\big)^{-1}, \end{aligned}$$

and

$$\begin{aligned} a_n &= \tilde{R}_{2,2}\big(kA^{\alpha/2}\big)u_n + \tilde{P}\big(kA^{\alpha/2}\big)F(u_n, t_n), \\ b_n &= \tilde{R}_{2,2}\big(kA^{\alpha/2}\big)u_n + \tilde{P}\big(kA^{\alpha/2}\big)F\left(a_n, t_n + \frac{k}{2}\right), \\ c_n &= \tilde{R}_{2,2}\big(kA^{\alpha/2}\big)a_n + \tilde{P}\big(kA^{\alpha/2}\big)\left[2F\left(b_n, t_n + \frac{k}{2}\right) - F(u_n, t_n)\right], \end{aligned}$$

with

$$\begin{aligned} \tilde{R}_{2,2}\big(kA^{\alpha/2}\big) &= \big(48I - 12kA^{\alpha/2} + \big(kA^{\alpha/2}\big)^2\big)\big(48I + 12kA^{\alpha/2} + \big(kA^{\alpha/2}\big)^2\big)^{-1}, \\ \tilde{P}\big(kA^{\alpha/2}\big) &= 24k\big(48I + 12kA^{\alpha/2} + \big(kA^{\alpha/2}\big)^2\big)^{-1}. \end{aligned}$$

4.3.2 The partial fraction splitting technique of the scheme

The scheme considered above contains inverses of higher-order matrix polynomials, which would produce computational inaccuracies as a result of high condition numbers and roundoff error while computing the power of the matrices. To avoid these difficulties, we employ the partial fraction decomposition proposed by Gallopoulos and Saad [148], and Khaliq *et al.* [149]. This approach is able to alleviate ill-conditioning issues since only implicit Euler-type solvers are needed. It is a parallel algorithm which can use four different implicit Euler-type linear solvers concurrently at each time step on a computer with at least two processors.

To compute u_{n+1} in (53), we consider the following partial fraction forms of $R_{2,2}$ and P_i

$$R_{2,2}(z) = (-1)^2 + \sum_{j=1}^{q_1} \frac{w_j}{z - c_j} + 2 \sum_{j=1+q_1}^{q_1+q_2} \Re\left(\frac{w_j}{z - c_j} \right),$$

$$P_i(z) = k \sum_{j=1}^{q_1} \frac{w_{ij}}{z - c_j} + 2k \sum_{j=1+q_1}^{q_1+q_2} \Re\left(\frac{w_{ij}}{z - c_j} \right), \quad i = 1, 2, 3,$$

where $\{c_j\}$ is the complex pole of $R_{2,2}$ with $q_1 + 2q_2 = 2$, and w_j and w_{ij} are the corresponding weights.

To compute a_n, b_n, and c_n, we apply

$$\tilde{R}_{2,2}(z) = (-1)^2 + \sum_{j=1}^{q_1} \frac{\tilde{w}_j}{z - \tilde{c}_j} + 2 \sum_{j=1+q_1}^{q_1+q_2} \Re\left(\frac{\tilde{w}_j}{z - \tilde{c}_j} \right),$$

$$\tilde{P}(z) = k \sum_{j=1}^{q_1} \frac{\tilde{\Omega}_j}{z - \tilde{c}_j} + 2k \sum_{j=1+q_1}^{q_1+q_2} \Re\left(\frac{\tilde{\Omega}_j}{z - \tilde{c}_j} \right),$$

where $\{\tilde{c}_j\}$ is the complex pole of $\tilde{R}_{2,2}$ with $q_1 + 2q_2 = 2$, and $\tilde{w}_j$ and $\tilde{\Omega}_j$ are the corresponding weights.

To implement the partial fraction form of the fourth-order scheme, poles and corresponding weights were computed as

$c_1 = -3.0 + i1.73205080756887729352,$

$w_1 = -6.0 - i10.3923048454132637611,$

$w_{11} = -0.5 - i1.44337567297406441127,$

$w_{21} = -i1.15470053837925152901,$

$w_{31} = 0.5 + i0.28867513459481288225,$

$\tilde{c}_1 = -6.0 + i3.4641016151377545870548,$

$\tilde{w}_1 = -12.0 - i20.78460969082652752232935,$

$\tilde{\Omega}_1 = -i3.4641016151377458705.$

4.3.3 The ETD-Padé(2,2) algorithm

For $i = 1, \ldots, q_1 + q_2$, where $q_1 = 0$, and $q_2 = 1$.

Algorithm 4 ETD-Padé(2,2) algorithm with non-homogeneous boundary conditions

1: Efficiently precompute $B_1 = \left(kA^{\alpha/2} - \tilde{c}_i I\right)^{-1}$, and $B_2 = \left(kA^{\alpha/2} - c_i I\right)^{-1}$.

2: **for** $m = 1, 2, \ldots, M = T/k$, **do**

3: Step 1: solve $R_{a_i} = B_1(\tilde{w}_i u_n + k\tilde{\Omega}_i F(u_n, t_n))$, and compute a_n as $a_n = u_n + \sum_{i=1}^{q_1} R_{a_i} + 2\sum_{i=1+q_1}^{q_1+q_2} Re(R_{a_i})$.

4: Step 2: solve $R_{b_i} = B_1(\tilde{w}_i u_n + k\tilde{\Omega}_i F(a_n, t_n + k/2))$, and compute b_n as $b_n = u_n + \sum_{i=1}^{q_1} R_{b_i} + 2\sum_{i=1+q_1}^{q_1+q_2} Re(R_{b_i})$.

5: Step 3: solve $R_{c_i} = B_1(\tilde{w}_i a_n + k\tilde{\Omega}_i(2F(b_n, t_n + k/2) - F(u_n, t_n)))$, and compute c_n as $c_n = a_n + \sum_{i=1}^{q_1} R_{c_i} + 2\sum_{i=1+q_1}^{q_1+q_2} Re(R_{c_i})$.

6: Step 4: solve $R_{u_i} = B_2(w_i u_n + k w_{1i} F(u_n, t_n) + k w_{2i}(F(a_n, t_n + k/2) + F(b_n, t_n + k/2)) + k w_{3i} F(c_n, t_n + k))$, and compute u_{n+1} as $u_{n+1} = u_n + \sum_{i=1}^{q_1} R_{u_i} + 2\sum_{i=1+q_1}^{q_1+q_2} Re(R_{u_i})$.

7: **end for**

4.4 Numerical experiments

We consider two test problems with non-homogeneous boundary conditions to demonstrate the effectiveness of the developed scheme. The convergence analysis of the scheme is shown via calculating the order of convergence. When the analytical solution is unknown, the errors and order of convergence in time are computed as

$$\text{order of convergence } = \frac{\log_{10}(E_k/E_{k/2})}{\log_{10}(2)},$$

where $E_k = \|u_k - u_{2k}\|$ and $E_{\frac{k}{2}} = \left\|u_{\frac{k}{2}} - u_k\right\|$ are the L_2 or L_∞ norm errors at k and $k/2$.

4.4.1 Test Problem 1: the Allen-Cahn equation

We consider the 1D space-fractional Allen-Cahn equation with non-homogeneous Dirichlet boundary conditions

$$\begin{aligned} \frac{\partial u}{\partial t} &= -\kappa_\alpha(-\Delta)^{\frac{\alpha}{2}}u + u - u^3, \\ u(x,0) &= 0.53x + 0.47\sin(-1.5\pi x), \\ u(-1,t) &= -1, \qquad u(1,t) = 1, \end{aligned} \tag{54}$$

$-1 \le x \le 1$, $0 \le t \le 100$ and $\kappa_\alpha = 0.01$. The solutions around steady states $u = \pm 1$ display flat areas separated by interfaces of increasing sharpness as κ_α decreases to zero, and the solutions around the unstable state $u = 0$ coalesce over a long period of time. This phenomenon is known as metastability [125]. Fig. 26a shows that the initial data develops to unstable equilibrium, which is followed by a quick evolution to a one interface of the solution up to the final time. The unstable interface's lifetime is largely prolonged as in Fig. 26b when α decreases, and a stable solution can be observed in Fig. 26c because of the long-tailed impact of the process of the fractional diffusion [52]. Table 12 reported the results obtained by applying our scheme at

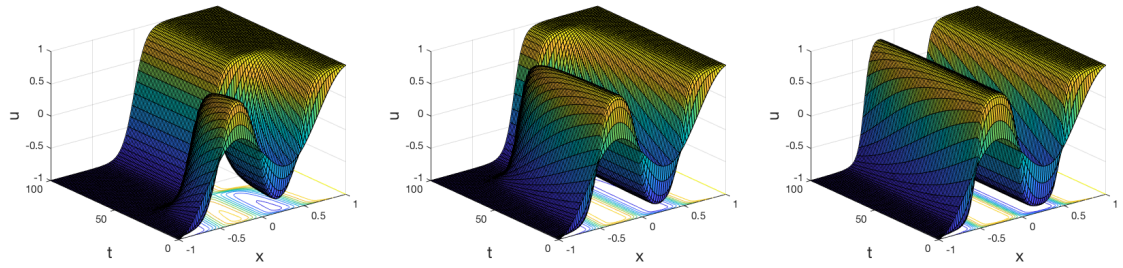

(a) $\alpha = 2$ (b) $\alpha = 1.8$ (c) $\alpha = 1.6$

Figure 26: Numerical solutions of (54) with $h = 0.025$ and $k = 1$ at different values of α.

$h = 0.1$ including the L_2, L_∞ errors, rate of convergence and CPU(s). The scheme achieves the expected fourth-order accuracy in time.

Table 12: Errors, convergence rates in time and CPU(s).

α	k	L_2	order	L_∞	order	CPU(s)
2	0.10000	-	-	-	-	0.0227
	0.05000	1.50e-07	-	2.03e-07	-	0.0245
	0.02500	9.19e-09	4.03	1.22e-08	4.06	0.0281
	0.01250	5.70e-10	4.01	7.52e-10	4.02	0.0328
	0.00625	3.55e-11	4.01	4.68e-11	4.01	0.0485
1.8	0.10000	-	-	-	-	0.0243
	0.05000	1.87e-07	-	2.59e-07	-	0.0263
	0.02500	1.14e-08	4.04	1.56e-08	4.05	0.0295
	0.01250	7.04e-10	4.02	9.60e-10	4.03	0.0342
	0.00625	4.37e-11	4.01	5.95e-11	4.01	0.0498
1.6	0.10000	-	-	-	-	0.0305
	0.05000	2.23e-07	-	3.14e-07	-	0.0325
	0.02500	1.36e-08	4.04	1.88e-08	4.06	0.0365
	0.01250	8.36e-10	4.02	1.15e-09	4.03	0.0414
	0.00625	5.19e-11	4.01	7.12e-11	4.02	0.0570

4.4.2 Test Problem 2: the 1D Brusselator system

We consider the 1D space-fractional Brusselator system of two equations with non-homogeneous Dirichlet boundary conditions

$$\begin{aligned} \frac{\partial u}{\partial t} &= -\kappa_\alpha(-\Delta)^{\frac{\alpha}{2}}u + B + u^2v - (C+1)u, \\ \frac{\partial v}{\partial t} &= -\kappa_\alpha(-\Delta)^{\frac{\alpha}{2}}v + Cu - u^2v, \end{aligned} \tag{55}$$

with the following initial and boundary conditions

$$u(x,0) = 1 + \sin(2\pi x),\ v(x,0) = 3,$$

$$u(0,t) = u(1,t) = 1,\ v(0,t) = v(1,t) = 3,$$

$0 \le x \le 1$ and $0 \le t \le 10$.

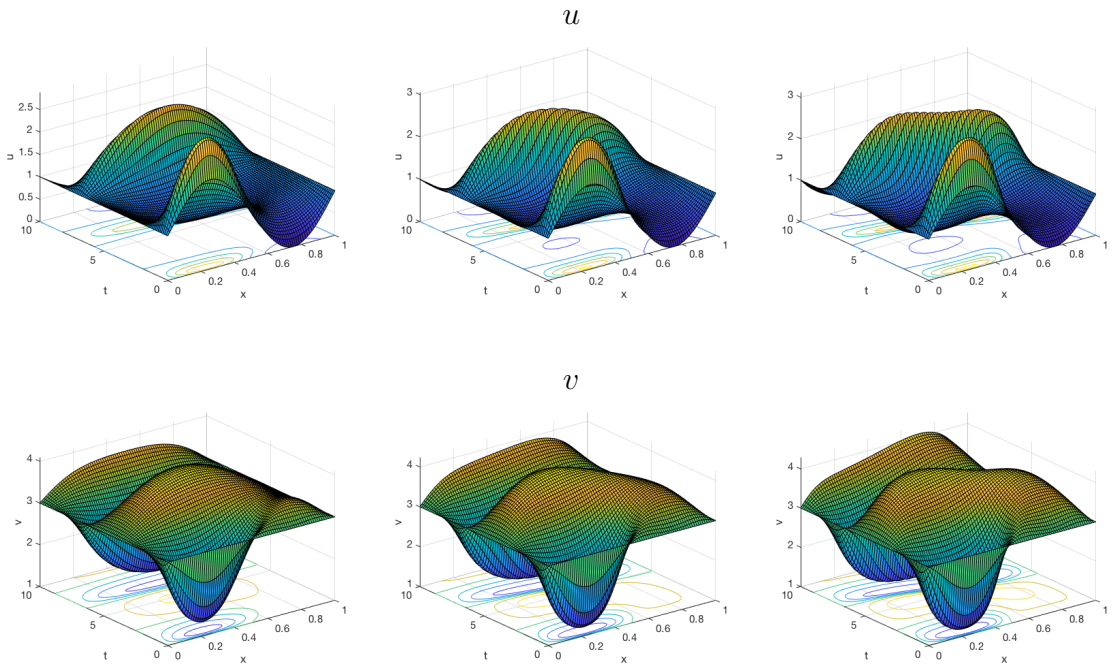

(a) $\alpha = 2$ (b) $\alpha = 1.7$ (c) $\alpha = 1.5$

Figure 27: The concentration profiles of (55) at $h = 0.025$ and $k = 0.125$.

Fig. (27) illustrates the solution profiles of the system at $\kappa_\alpha = 1/50$, $B = 1$, and $C = 3$, which are chosen similar to that in [136], using different values of α.

4.5 Conclusion

In this chapter, we introduced an efficient numerical solution for the space-fractional reaction-diffusion equation with non-homogeneous boundary conditions. The scheme is obtained by using the MTT for the spatial discretization and the (2,2)-Padé approximation for integrating in time. The order of convergence is performed computationally in some mathematical models. The scheme achieved the expected fourth-order accuracy in time.

CHAPTER 5

FOURTH-ORDER MTT-ETD SCHEMES

5.1 Introduction

In this chapter, we propose two high-order schemes for space-fractional reaction-diffusion equations. The schemes are based on a fourth-order MTT for the spatial discretization and a fourth-order ETD Runge-Kutta (ETDRK) for the temporal discretization. The ETDRK schemes are based on diagonal and sub-diagonal Padé approximations to the matrix exponential functions. It is observed that the A-stable scheme incurs unwanted oscillations due to high-frequency components present in the solution. These oscillations diminish as the order of the space-fractional derivative decreases. We propose a reliability constraint, which is dependent on the order of the space-fractional derivative, to avoid these oscillations. However, the L-stable scheme is oscillation-free for any time step. The partial fraction splitting technique is used to compose computationally efficient versions of the schemes. The amplification factor of the schemes is investigated by plotting their stability regions. The convergence analysis is performed on numerical experiments to demonstrate the fourth-order accuracy of the developed schemes in space and time. Numerical experiments were made on multidimensional space-fractional reaction-diffusion equations to demonstrate the reliability, efficiency and stability of the schemes.

We consider the space-fractional reaction-diffusion equation

$$\begin{aligned} \frac{\partial u(x,t)}{\partial t} &= -\kappa_\alpha(-\Delta)^{\frac{\alpha}{2}}u(x,t) + f(u,t),\ 1<\alpha\leq 2,\ t>0, \\ u(x,0) &= u_0(x),\quad x\in\Omega\subset\mathbb{R}^d,\ d=1,2,3, \end{aligned} \tag{56}$$

with either homogeneous Dirichlet or homogeneous Neumann boundary conditions. The solutions of the nonlinear equations for fractional Laplacians are discussed in [150, 151, 152, 153] in terms of existence and uniqueness.

Several numerical approximations for the fractional diffusion and advection-diffusion equations have been proposed, where solving a system of equations which involves a matrix with fractional powers is required at each time step. Different methods have been employed including finite difference [115, 154], finite element [146, 155], and finite volume methods [156]. The Fourier spectral approach [52, 157, 158], Krylov methods [82], and fast numerical integrations in conjunction with effective preconditioners [81] also have been used for fractional equations. Farquhar *et al.* [159] presented an efficient algorithm on GPU using the contour integration method for the spatial discretization and the exponential Euler method for the time discretization to compute the matrix function vector products.

ETD schemes have been utilized with integer-order reaction-diffusion equations in [160, 161]. These schemes handle the non-smooth initial data, optimize the computational time due to the parallel implementation, and achieve higher-order accuracy while maintaining the stability. Moreover, they avoid the iteration treatment for the nonlinear part by using constants integral formula. Utilizing ETDRK schemes, developed by Cox and Matthews [66], requires inverting the matrix polynomials, which cause some computational difficulties such as inefficiency and instability. These issues were solved by employing the Padé approximations and partial fraction decomposition.

We develop two fourth-order schemes for solving space-fractional reaction-diffusion equations. The schemes are A-stable and L-stable, which are obtained by applying (2,2)-Padé and (1,3)-Padé approximations, respectively. For some time steps, the solutions of the A-stable scheme suffer from unwanted oscillations when the initial data are non-smooth. To avoid these oscillations, we propose a reliability constraint to estimate the choice of the time step. However, for any time step the L-stable scheme is oscillation-free and maintains the fourth-order accuracy even though the initial data are non-smooth. The schemes are discretized spatially by utilizing the fourth-order compact scheme MTT developed by Ding and Zhang [162].

5.2 MTT with homogeneous boundary conditions

Definition 5.2.1. *Assume the Laplacian* $(-\Delta)$ *have a complete set of orthonormal eigenfunctions* φ_l *corresponding to the eigenvalues* λ_l *on a bounded region* Ω*, i.e., for* $l = 0, 1, 2, \ldots,$

$$(-\Delta)\varphi_l = \lambda_l \varphi_l,$$

in $\Omega; \mathcal{B}(\varphi) = 0$ *on* $\partial\Omega$*, where* $\mathcal{B}(\varphi)$ *is the homogeneous Dirichlet or Neumann boundary conditions. Let*

$$u = \sum_{l=0}^{\infty} c_l \varphi_l \quad \textit{such that} \quad \sum_{l=0}^{\infty} |c_l|^2 |\lambda_l|^{\alpha} < \infty,$$

then

$$(-\Delta)^{\frac{\alpha}{2}} u = \sum_{l=0}^{\infty} c_l \lambda_l^{\frac{\alpha}{2}} \varphi_l.$$

As mentioned in Chapter 2, for homogeneous Dirichlet boundary conditions with $x \in \Omega = (a, b)^d,\ i,\ d = 1, 2, 3$, the eigenvalues and eigenvectors are

$$\begin{aligned} \lambda_{\eta_1,\ldots,\eta_d} &= \sum_{j=\eta_1}^{\eta_d} \left(\frac{(j+1)\pi}{b-a} \right)^2, \\ \varphi_{\eta_1,\ldots,\eta_d} &= \left(\sqrt{\frac{2}{b-a}} \right)^d \prod_{j=\eta_1}^{\eta_d} \sin\left(\frac{(j+1)\pi(x_m - a)}{b-a} \right),\ \eta_i = 0, 1, 2, \ldots, \end{aligned} \tag{57}$$

respectively, whereas for homogeneous Neumann boundary conditions the eigenvalues and eigenvectors are

$$\begin{aligned} \lambda_{\eta_1,\ldots,\eta_d} &= \sum_{j=\eta_1}^{\eta_d} \left(\frac{j\pi}{b-a} \right)^2, \\ \varphi_{\eta_1,\ldots,\eta_d} &= \left(\sqrt{\frac{2}{b-a}} \right)^d \prod_{j=\eta_1}^{\eta_d} \cos\left(\frac{j\pi(x_m - a)}{b-a} \right),\ \eta_i = 0, 1, 2, \ldots, \end{aligned} \tag{58}$$

respectively. For other definitions of the fractional Laplacian, see for example [6, 48, 163].

By using the MTT developed by Ding and Zhang [162] for discretizing the fractional Laplacian $(-\Delta)^{\frac{\alpha}{2}}$ with a uniform mesh of step size h, we get

$$(-\Delta)^{\frac{\alpha}{2}} u(t) \approx h^{-\alpha} M^{\frac{\alpha}{2}} u(t). \tag{59}$$

The matrix $(h^{-\alpha} M^{\frac{\alpha}{2}})$ is generated from the matrix representation of the standard Laplace operator $(h^{-2}M)$ using the eigenvalues and eigenvectors.

For 1D problems, we use the fourth-order approximation

$$\partial_{xx} \approx -\frac{1}{h^2}\left(1 + \frac{1}{12}\delta_x^2\right)^{-1} (\delta_x^2) + \mathcal{O}(h^4), \tag{60}$$

where δ_x^2 is the second-order central difference operator. For m grid points, the matrix representation of the second-order operator in (60) is $M = A^{-1}B$, where A and B are tridiagonal matrices

$$A = \begin{bmatrix} \frac{5}{6} & \frac{1}{12} & 0 & \dots & 0 & 0 \\ \frac{1}{12} & \frac{5}{6} & \frac{1}{12} & 0 & \dots & 0 \\ 0 & \frac{1}{12} & \frac{5}{6} & \frac{1}{12} & 0 & \dots \\ \vdots & \ddots & \ddots & \ddots & & \vdots \\ \dots & 0 & \frac{1}{12} & \frac{5}{6} & \frac{1}{12} & 0 \\ 0 & \dots & 0 & \frac{1}{12} & \frac{5}{6} & \frac{1}{12} \\ 0 & 0 & \dots & 0 & \frac{1}{12} & \frac{5}{6} \end{bmatrix},$$

and

$$B = \begin{bmatrix} 2 & -1 & 0 & \dots & 0 & 0 \\ -1 & 2 & -1 & 0 & \dots & 0 \\ 0 & -1 & 2 & -1 & 0 & \dots \\ \vdots & \ddots & \ddots & \ddots & & \vdots \\ \dots & 0 & -1 & 2 & -1 & 0 \\ 0 & \dots & 0 & -1 & 2 & -1 \\ 0 & 0 & \dots & 0 & -1 & 2 \end{bmatrix}.$$

The MTT approximates the fractional Laplacian by

$$(-\Delta)^{\alpha/2} \approx h^{-\alpha} M^{\alpha/2} = h^{-\alpha}\big(P \Lambda^{\alpha/2} P^{-1}\big), \tag{61}$$

where Λ is the eigenvalues matrix and P is the eigenvectors matrix. For the homogeneous Dirichlet boundary conditions

$$\begin{aligned} \Lambda &= \operatorname{diag}(\sigma_1, \sigma_2, \ldots, \sigma_{m-1}), \\ P &= (\xi_1, \xi_2, \ldots, \xi_{m-1}), \end{aligned} \tag{62}$$

where

$$\begin{aligned} \sigma_i &= \frac{4\sin^2\left(\frac{i\pi}{2m}\right)}{1-\frac{1}{3}\sin^2\left(\frac{i\pi}{2m}\right)}, \\ \xi_i &= \left(\sin\left(\frac{1i\pi}{m}\right), \sin\left(\frac{2i\pi}{m}\right), \ldots, \sin\left(\frac{(m-1)i\pi}{m}\right)\right)^T, \quad i = 1, 2, \ldots, m-1. \end{aligned}$$

For the homogeneous Neumann boundary conditions

$$\begin{aligned} \Lambda &= \operatorname{diag}(\sigma_0, \sigma_1, \ldots, \sigma_m), \\ P &= (\xi_0, \xi_1, \ldots, \xi_m), \end{aligned} \tag{63}$$

where

$$\begin{aligned} \sigma_i &= \frac{4\cos^2\left(\frac{i\pi}{2m}\right)}{1-\frac{1}{3}\cos^2\left(\frac{i\pi}{2m}\right)}, \\ \xi_i &= \left(\cos\left(\frac{0i\pi}{m}\right), \cos\left(\frac{1i\pi}{m}\right), \ldots, \cos\left(\frac{mi\pi}{m}\right)\right)^T, \quad i = 0, 1, \ldots, m. \end{aligned}$$

For more details about the approach in the diffusion equation, the reader is referred to [162].

Lemma 5.2.2. *The eigenvalues for multidimensional problems with homogeneous Dirichlet boundary conditions:*

$$\sigma_{i,j} = \frac{4\sin^2\left(\frac{i\pi}{2m}\right)}{1-\frac{1}{3}\sin^2\left(\frac{i\pi}{2m}\right)} + \frac{4\sin^2\left(\frac{j\pi}{2m}\right)}{1-\frac{1}{3}\sin^2\left(\frac{j\pi}{2m}\right)}, \quad i, j = 1, 2, \ldots, m-1 \text{ if } d = 2,$$

$$\sigma_{i,j,l} = \frac{4\sin^2\left(\frac{i\pi}{2m}\right)}{1-\frac{1}{3}\sin^2\left(\frac{i\pi}{2m}\right)} + \frac{4\sin^2\left(\frac{j\pi}{2m}\right)}{1-\frac{1}{3}\sin^2\left(\frac{j\pi}{2m}\right)} + \frac{4\sin^2\left(\frac{l\pi}{2m}\right)}{1-\frac{1}{3}\sin^2\left(\frac{l\pi}{2m}\right)}, \quad i, j, l = 1, 2, \ldots, m-1,$$

$$\text{if } d = 3,$$

and with homogeneous Neumann boundary conditions

$$\sigma_{i,j} = \frac{4\cos^2\left(\frac{i\pi}{2m}\right)}{1-\frac{1}{3}\cos^2\left(\frac{i\pi}{2m}\right)} + \frac{4\cos^2\left(\frac{j\pi}{2m}\right)}{1-\frac{1}{3}\cos^2\left(\frac{j\pi}{2m}\right)}, \quad i,j = 0,1,\ldots,m \text{ if } d=2,$$

$$\sigma_{i,j,l} = \frac{4\cos^2\left(\frac{i\pi}{2m}\right)}{1-\frac{1}{3}\cos^2\left(\frac{i\pi}{2m}\right)} + \frac{4\cos^2\left(\frac{j\pi}{2m}\right)}{1-\frac{1}{3}\cos^2\left(\frac{j\pi}{2m}\right)} + \frac{4\cos^2\left(\frac{l\pi}{2m}\right)}{1-\frac{1}{3}\cos^2\left(\frac{l\pi}{2m}\right)}, \quad i,j,l = 0,1,\ldots,m,$$

if $d=3$.

5.3 Fourth-order ETD schemes

By using the above mentioned fourth-order (MTT) to approximate the fractional Laplacian $(-\Delta)^{\frac{\alpha}{2}}$ in (56), we get the system of ODEs

$$\frac{du}{dt} = -A^{\frac{\alpha}{2}}u + f(u,t), \quad u(0) = u_0, \tag{64}$$

where $A^{\frac{\alpha}{2}} = \frac{\kappa_\alpha}{h^\alpha}M^{\frac{\alpha}{2}}$. For the homogeneous Dirichlet boundary conditions,
$u(t) = [u_1(t), u_2(t), u_2(t), \ldots, u_{m-1}(t)]^T$,
and
$f(u,t) = [f(u_1(t),t), f(u_2(t),t), f(u_3(t),t), \ldots, f(u_{m-1}(t),t)]^T$.

We let $u_n =: u(t_n)$ and $t_n = nk$, $n = 0,1,2,\ldots$ where k is the temporal step size. Then, the following formula is the exact solution of (64) using a variation of the constant formula

$$u(t_{n+1}) = e^{-kA^{\frac{\alpha}{2}}}u(t_n) + k\int_0^1 e^{-kA^{\frac{\alpha}{2}}(1-\tau)}f(u(t_n+\tau k), t_n+\tau k)d\tau. \tag{65}$$

Cox and Mathews derived time stepping schemes which give Runge-Kutta type higher-order approximations [66]. Here, we consider the ETDRK4 scheme

$$
\begin{aligned}
u_{n+1} = \; & e^{-kA^{\frac{\alpha}{2}}}u_n + \frac{1}{k^2}\big(-A^{\frac{\alpha}{2}}\big)^{-3}\Bigg(f(u_n,t_n)\big[-4I + kA^{\frac{\alpha}{2}} + e^{-kA^{\frac{\alpha}{2}}}\big(4I + 3kA^{\frac{\alpha}{2}} + \big(kA^{\frac{\alpha}{2}}\big)^2\big)\big] \\
& + 2\left(f\left(a_n, t_n + \frac{k}{2}\right) + f\left(b_n, t_n + \frac{k}{2}\right)\right)\big[2I - kA^{\frac{\alpha}{2}} + e^{-kA^{\frac{\alpha}{2}}}\big(-2I - kA^{\frac{\alpha}{2}}\big)\big] \\
& + f(c_n, t_n + k)\big[-4I + 3kA^{\frac{\alpha}{2}} - \big(kA^{\frac{\alpha}{2}}\big)^2 + e^{-kA^{\frac{\alpha}{2}}}\big(4I + kA^{\frac{\alpha}{2}}\big)\big]\Bigg),
\end{aligned} \tag{66}
$$

where

$$
\begin{aligned}
a_n &= e^{-\frac{kA^{\frac{\alpha}{2}}}{2}}u_n - A^{-\frac{\alpha}{2}}\left(e^{-\frac{kA^{\frac{\alpha}{2}}}{2}} - I\right)f(u_n,t_n), \\
b_n &= e^{-\frac{kA^{\frac{\alpha}{2}}}{2}}u_n - A^{-\frac{\alpha}{2}}\left(e^{-\frac{kA^{\frac{\alpha}{2}}}{2}} - I\right)f\left(a_n, t_n + \frac{k}{2}\right), \\
c_n &= e^{-\frac{kA^{\frac{\alpha}{2}}}{2}}a_n - A^{-\frac{\alpha}{2}}\left(e^{-\frac{kA^{\frac{\alpha}{2}}}{2}} - I\right)\left[2f\left(b_n, t_n + \frac{k}{2}\right) - f\left(u_n, t_n\right)\right].
\end{aligned}
$$

The computation of the matrix exponential is costly. Even if a matrix itself is sparse, its exponential may not be. When the linear operator is a non-diagonal matrix, implementing this scheme directly may experience numerical instability if $A^{\frac{\alpha}{2}}$ has eigenvalues that are close to zero since computing $(-A^{\frac{\alpha}{2}})^{-1}$, $(-A^{\frac{\alpha}{2}})^{-3}$, $e^{-kA^{\frac{\alpha}{2}}}$, and $e^{-kA^{\frac{\alpha}{2}}/2}$ are needed.

In this chapter, we propose a modified version of (66) by using fourth-order (2,2)-Padé and (1,3)-Padé approximations to the matrix exponential e^{-z}. We consider the rational (2,2)-Padé and (1,3)-Padé approximations for e^{-z}

$$
R_{2,2}(z) = \frac{12 - 6z + z^2}{12 + 6z + z^2}, \tag{67}
$$

$$
R_{1,3}(z) = \frac{1 - \frac{z}{4}}{1 + \frac{3}{4}z + \frac{z^2}{4} + \frac{z^3}{24}}. \tag{68}
$$

$R_{2,2}(z)$ is A-acceptable and $R_{1,3}(z)$ is L-acceptable. Fig. 28 shows the behavior of the exponential function (e^{-z}), $R_{2,2}(z)$ and $R_{1,3}(z)$ approximations to e^{-z} for $z \in [0, 20]$. Fig. 29 shows the behavior of $R_{2,2}(z)$ and $R_{1,3}(z)$ for $z = x + iy \in [0, 20] \times [-10, 10]$.

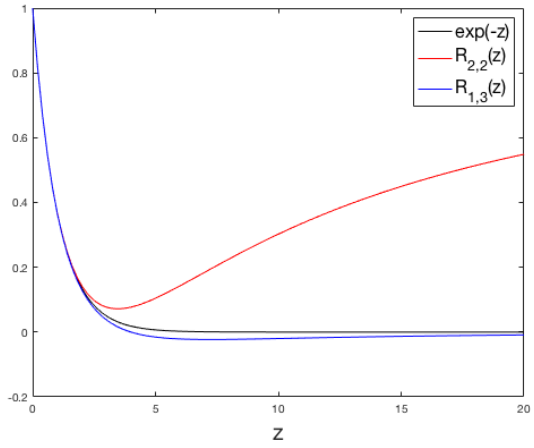

Figure 28: Behavior of the functions e^{-z}, $R_{2,2}(z)$ and $R_{1,3}(z)$ for $z \in [0, 20]$.

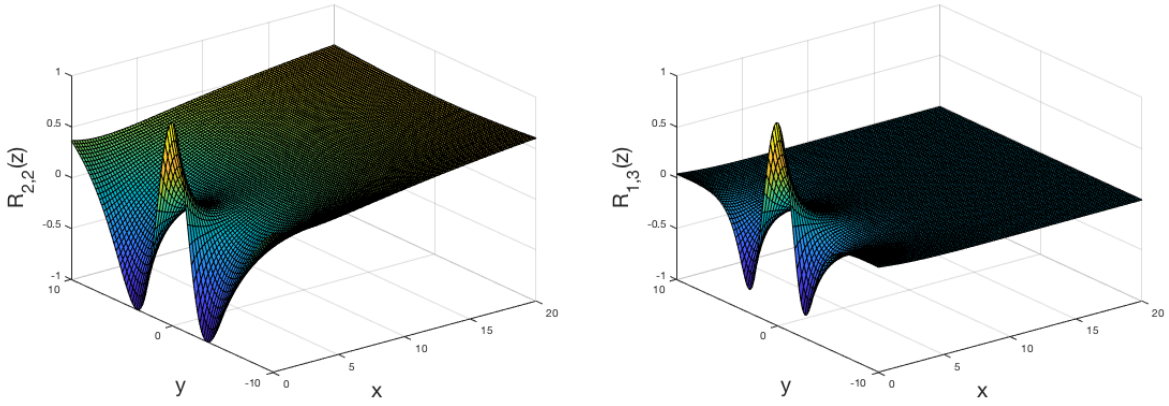

Figure 29: Behavior of $R_{2,2}(z)$ and $R_{1,3}(z)$ approximations of e^{-z} for $z \in [0, 20] \times [-10, 10]$.

By plugging (67) and (68) in (66), we obtain the following two schemes.

5.3.1 *A*-stable scheme (ETD-Padé(2,2))

Using the (2,2)-Padé approximation in (67) to $e^{-kA^{\alpha/2}}$ in (66), we get the ETD-Padé(2,2) scheme [164]

$$\begin{aligned} u_{n+1} = \; & R_{2,2}\big(kA^{\alpha/2}\big)u_n + P_1\big(kA^{\alpha/2}\big)f(u_n,t_n) \\ & + P_2\big(kA^{\alpha/2}\big)\left[f\left(a_n,t_n+\frac{k}{2}\right)+f\left(b_n,t_n+\frac{k}{2}\right)\right] \\ & + P_3\big(kA^{\alpha/2}\big)f(c_n,t_n+k), \end{aligned} \tag{69}$$

where

$$R_{2,2}\big(kA^{\alpha/2}\big) = \big(12I-6kA^{\alpha/2}+\big(kA^{\alpha/2}\big)^2\big)\big(12I+6kA^{\alpha/2}+\big(kA^{\alpha/2}\big)^2\big)^{-1},$$

$$P_1\big(kA^{\alpha/2}\big) = k\big(2I-kA^{\alpha/2}\big)\big(12I+6kA^{\alpha/2}+\big(kA^{\alpha/2}\big)^2\big)^{-1},$$

$$P_2\big(kA^{\alpha/2}\big) = 4k\big(12I+6kA^{\alpha/2}+\big(kA^{\alpha/2}\big)^2\big)^{-1},$$

$$P_3\big(kA^{\alpha/2}\big) = k\big(2I+kA^{\alpha/2}\big)\big(12I+6kA^{\alpha/2}+\big(kA^{\alpha/2}\big)^2\big)^{-1},$$

and

$$\begin{aligned} a_n &= \tilde{R}_{2,2}(kA^{\alpha/2})u_n + \tilde{P}\big(kA^{\alpha/2}\big)f(u_n,t_n), \\ b_n &= \tilde{R}_{2,2}\big(kA^{\alpha/2}\big)u_n + \tilde{P}\big(kA^{\alpha/2}\big)f\left(a_n,t_n+\frac{k}{2}\right), \\ c_n &= \tilde{R}_{2,2}\big(kA^{\alpha/2}\big)a_n + \tilde{P}\big(kA^{\alpha/2}\big)\left[2f\left(b_n,t_n+\frac{k}{2}\right)-f(u_n,t_n)\right], \end{aligned}$$

with

$$\tilde{R}_{2,2}\big(kA^{\alpha/2}\big) = \big(48I-12kA^{\alpha/2}+\big(kA^{\alpha/2}\big)^2\big)\big(48I+12kA^{\alpha/2}+\big(kA^{\alpha/2}\big)^2\big)^{-1},$$

$$\tilde{P}\big(kA^{\alpha/2}\big) = 24k\big(48I+12kA^{\alpha/2}+\big(kA^{\alpha/2}\big)^2\big)^{-1}.$$

5.3.2 L-stable scheme (ETD-Padé(1,3))

Similarly, using the (1,3)-Padé approximation in (68) to $e^{-kA^{\alpha/2}}$ in (66), we get the ETD-Padé(1,3) scheme [164]

$$\begin{aligned} u_{n+1} = \; & R_{1,3}\big(kA^{\alpha/2}\big)u_n + P_1\big(kA^{\alpha/2}\big)f(u_n,t_n) \\ & + P_2\big(kA^{\alpha/2}\big)\left[f\left(a_n,t_n+\frac{k}{2}\right)+f\left(b_n,t_n+\frac{k}{2}\right)\right] \\ & + P_3\big(kA^{\alpha/2}\big)f(c_n,t_n+k), \end{aligned} \tag{70}$$

where

$$R_{1,3}\big(kA^{\alpha/2}\big) = \big(24I-6kA^{\alpha/2}\big)\big(24I+18kA^{\alpha/2}+6\big(kA^{\alpha/2}\big)^2+\big(kA^{\alpha/2}\big)^3\big)^{-1},$$

$$P_1\big(kA^{\alpha/2}\big) = k\big(4I-kA^{\alpha/2}\big)\big(24I+18kA^{\alpha/2}+6\big(kA^{\alpha/2}\big)^2+\big(kA^{\alpha/2}\big)^3\big)^{-1},$$

$$P_2\big(kA^{\alpha/2}\big) = 2k\big(4I+kA^{\alpha/2}\big)\big(24I+18kA^{\alpha/2}+6\big(kA^{\alpha/2}\big)^2+\big(kA^{\alpha/2}\big)^3\big)^{-1},$$

$$P_3\big(kA^{\alpha/2}\big) = k\big(4I+3kA^{\alpha/2}+\big(kA^{\alpha/2}\big)^2\big)\big(24I+18kA^{\alpha/2}+6\big(kA^{\alpha/2}\big)^2+\big(kA^{\alpha/2}\big)^3\big)^{-1},$$

and

$$\begin{aligned} a_n &= \tilde{R}_{1,3}\big(kA^{\alpha/2}\big)u_n + \tilde{P}\big(kA^{\alpha/2}\big)f(u_n,t_n), \\ b_n &= \tilde{R}_{1,3}\big(kA^{\alpha/2}\big)u_n + \tilde{P}\big(kA^{\alpha/2}\big)f\left(a_n,t_n+\frac{k}{2}\right), \\ c_n &= \tilde{R}_{1,3}\big(kA^{\alpha/2}\big)a_n + \tilde{P}\big(kA^{\alpha/2}\big)\left[2f\left(b_n,t_n+\frac{k}{2}\right)-f(u_n,t_n)\right], \end{aligned}$$

with

$$\tilde{R}_{1,3}\big(kA^{\alpha/2}\big) = 24\big(8I-kA^{\alpha/2}\big)\big(192I+72kA^{\alpha/2}+12\big(kA^{\alpha/2}\big)^2+\big(kA^{\alpha/2}\big)^3\big)^{-1},$$

$$\tilde{P}\big(kA^{\alpha/2}\big) = k\big(96I+12kA^{\alpha/2}+\big(kA^{\alpha/2}\big)^2\big)\big(192I+72kA^{\alpha/2}+12\big(kA^{\alpha/2}\big)^2+\big(kA^{\alpha/2}\big)^3\big)^{-1}.$$

5.3.3 The partial fraction form of ETD schemes

The schemes considered above contain inverses of higher-order matrix polynomials, which would produce computational challenges such as inaccuracies as a result of roundoff error and high condition numbers while computing the power of these matrices. To avoid these difficulties, we employ the partial fraction decomposition proposed by Gallopoulos and Saad [148], and Khaliq *et al.* [149]. This approach is able to alleviate ill-conditioning issues since only implicit Euler solvers are needed.

5.3.3.1 The efficient version of the ETD-Padé(2,2) scheme

To compute u_{n+1} in (69), we consider the following partial fraction forms of $R_{2,2}$ and P_i

$$R_{2,2}(z) = (-1)^2 + \sum_{j=1}^{q_1} \frac{w_j}{z - c_j} + 2 \sum_{j=1+q_1}^{q_1+q_2} \Re\left(\frac{w_j}{z - c_j} \right),$$

$$P_i(z) = k \sum_{j=1}^{q_1} \frac{w_{ij}}{z - c_j} + 2k \sum_{j=1+q_1}^{q_1+q_2} \Re\left(\frac{w_{ij}}{z - c_j} \right), \quad i = 1, 2, 3,$$

where $\{c_j\}$ is the complex pole of $R_{2,2}$ with $q_1 + 2q_2 = 2$, and w_j and w_{ij} are the corresponding weights.

In order to compute a_n, b_n, and c_n, we apply

$$\tilde{R}_{2,2}(z) = (-1)^2 + \sum_{j=1}^{q_1} \frac{\tilde{w}_j}{z - \tilde{c}_j} + 2 \sum_{j=1+q_1}^{q_1+q_2} \Re\left(\frac{\tilde{w}_j}{z - \tilde{c}_j} \right),$$

$$\tilde{P}(z) = k \sum_{j=1}^{q_1} \frac{\tilde{\Omega}_j}{z - \tilde{c}_j} + 2k \sum_{j=1+q_1}^{q_1+q_2} \Re\left(\frac{\tilde{\Omega}_j}{z - \tilde{c}_j} \right),$$

where $\{\tilde{c}_j\}$ is the complex pole of $\tilde{R}_{2,2}$ with $q_1 + 2q_2 = 2$, and $\tilde{w}_j$ and $\tilde{\Omega}_j$ are the corresponding weights.

In order to implement the partial fraction form of the fourth-order schemes, poles and corresponding weights were computed as

$c_1 = -3.0 + i1.73205080756887729352,$

$w_1 = -6.0 - i10.3923048454132637611,$

$w_{11} = -0.5 - i1.44337567297406441127,$

$w_{21} = -i1.15470053837925152901,$

$w_{31} = 0.5 + i0.28867513459481288225,$

$\tilde{c}_1 = -6.0 + i3.4641016151377545870548,$

$\tilde{w}_1 = -12.0 - i20.78460969082652752232935,$

$\tilde{\Omega}_1 = -i3.46410161513775458705.$

5.3.3.2 The ETD-Padé(2,2) algorithm

For $i = 1, \ldots, q_1 + q_2$, where $q_1 = 0$, and $q_2 = 1$.

Algorithm 5 ETD-Padé(2,2) algorithm

1: Efficiently precompute $B_1 = \left(kA^{\alpha/2} - \tilde{c}_i I\right)^{-1}$, and $B_2 = \left(kA^{\alpha/2} - c_i I\right)^{-1}$.

2: **for** $m = 1, 2, \ldots, M = T/k$, **do**

3: Step 1: solve $R_{a_i} = B_1(\tilde{w}_i u_n + k\tilde{\Omega}_i f(u_n, t_n))$, and then compute a_n as $a_n = u_n + \sum_{i=1}^{q_1} R_{a_i} + 2\sum_{i=1+q_1}^{q_1+q_2} Re(R_{a_i})$.

4: Step 2: solve $R_{b_i} = B_1(\tilde{w}_i u_n + k\tilde{\Omega}_i f(a_n, t_n + k/2))$, and then compute b_n as $b_n = u_n + \sum_{i=1}^{q_1} R_{b_i} + 2\sum_{i=1+q_1}^{q_1+q_2} Re(R_{b_i})$.

5: Step 3: solve $R_{c_i} = B_1(\tilde{w}_i a_n + k\tilde{\Omega}_i(2f(b_n, t_n + k/2) - f(u_n, t_n)))$, and then compute c_n as $c_n = a_n + \sum_{i=1}^{q_1} R_{c_i} + 2\sum_{i=1+q_1}^{q_1+q_2} Re(R_{c_i})$.

6: Step 4: solve $R_{u_i} = B_2(w_i u_n + kw_{1i} f(u_n, t_n) + kw_{2i}(f(a_n, t_n + k/2) + f(b_n, t_n + k/2)) + kw_{3i} f(c_n, t_n + k))$, and then compute u_{n+1} as $u_{n+1} = u_n + \sum_{i=1}^{q_1} R_{u_i} + 2\sum_{i=1+q_1}^{q_1+q_2} Re(R_{u_i})$.

7: **end for**

5.3.3.3 The efficient version of the ETD-Padé(1,3) scheme

To compute u_{n+1} in (70), we consider the following partial fraction forms of $R_{1,3}$ and P_i

$$R_{1,3}(z) = \sum_{j=1}^{q_1} \frac{w_j}{z - c_j} + 2 \sum_{j=1+q_1}^{q_1+q_2} \Re\left(\frac{w_j}{z - c_j}\right),$$

$$P_i(z) = k \sum_{j=1}^{q_1} \frac{w_{ij}}{z - c_j} + 2k \sum_{j=1+q_1}^{q_1+q_2} \Re\left(\frac{w_{ij}}{z - c_j}\right), \quad i = 1, 2, 3,$$

where $\{c_j\}_{j=1}^{2}$ are the complex poles of $R_{1,3}$ with $q_1 + 2q_2 = 3$, and w_j and w_{ij} are the corresponding weights.

In order to compute a_n, b_n, and c_n, we apply

$$\tilde{R}_{1,3}(z) = \sum_{j=1}^{q_1} \frac{\tilde{w}_j}{z - \tilde{c}_j} + 2 \sum_{j=1+q_1}^{q_1+q_2} \Re\left(\frac{\tilde{w}_j}{z - \tilde{c}_j}\right),$$

$$\tilde{P}(z) = k \sum_{j=1}^{q_1} \frac{\tilde{\Omega}_j}{z - \tilde{c}_j} + 2k \sum_{j=1+q_1}^{q_1+q_2} \Re\left(\frac{\tilde{\Omega}_j}{z - \tilde{c}_j}\right),$$

where $\{\tilde{c}_j\}_{j=1}^{2}$ are the complex poles of $\tilde{R}_{1,3}$ with $q_1 + 2q_2 = 3$, and $\tilde{w}_j$ and $\tilde{\Omega}_j$ are the corresponding weights.

In order to implement the partial fraction form of the fourth-order schemes, poles and corresponding weights were computed as

$c_1 = -2.6258168189584667160,$

$c_2 = -1.6870915905207666420 - i2.5087317549248805108,$

$w_1 = 5.5407990186788211678,$

$w_2 = -2.7703995093394105839 - i0.1591864442851235025,$

$w_{11} = 0.92346650311313686128,$

$w_{12} = -0.46173325155656843064 - i0.026531074047520583750,$

$w_{21} = 0.38305077592917562056,$

$w_{22} = -0.19152538796458781028 + i0.47027336073401897817,$

$w_{31} = 0.42055591813817669094,$

$w_{32} = 0.28972204093091165453 - i0.18298527878713726274,$

$\tilde{c}_1 = -5.2516336379169334320,$

$\tilde{c}_2 = -3.3741831810415332840 - i5.0174635098497610217,$

$\tilde{w}_1 = 11.081598037357642334,$

$\tilde{w}_2 = -5.5407990186788211672 - i0.31837288857024700490,$

$\tilde{\Omega}_1 = 2.1101239731096647932,$

$\tilde{\Omega}_2 = -0.55506198655483239660 + i0.73103036863338010983.$

5.3.3.4 The ETD-Padé(1,3) algorithm

For $i = 1, \ldots, q_1 + q_2$, where $q_1 = 1$, and $q_2 = 1$.

Algorithm 6 ETD-Padé(1,3) algorithm

1: Efficiently precompute $B_1 = \left(kA^{\alpha/2} - \tilde{c}_i I\right)^{-1}$, and $B_2 = \left(kA^{\alpha/2} - c_i I\right)^{-1}$.

2: **for** $m = 1, 2, \ldots, M = T/k$, **do**

3: Step 1: solve $R_{a_i} = B_1(\tilde{w}_i u_n + k\tilde{\Omega}_i f(u_n, t_n))$, and then compute a_n as $a_n = \sum_{i=1}^{q_1} R_{a_i} + 2\sum_{i=1+q_1}^{q_1+q_2} Re(R_{a_i})$.

4: Step 2: solve $R_{b_i} = B_1(\tilde{w}_i u_n + k\tilde{\Omega}_i f(a_n, t_n + k/2))$, and then compute b_n as $b_n = \sum_{i=1}^{q_1} R_{b_i} + 2\sum_{i=1+q_1}^{q_1+q_2} Re(R_{b_i})$.

5: Step 3: solve $R_{c_i} = B_1(\tilde{w}_i a_n + k\tilde{\Omega}_i(2f(b_n, t_n + k/2) - f(u_n, t_n)))$, and then compute c_n as $c_n = \sum_{i=1}^{q_1} R_{c_i} + 2\sum_{i=1+q_1}^{q_1+q_2} Re(R_{c_i})$.

6: Step 4: solve $R_{u_i} = B_2(w_i u_n + kw_{1i} f(u_n, t_n) + kw_{2i}(f(a_n, t_n + k/2) + f(b_n, t_n + k/2)) + kw_{3i} f(c_n, t_n + k))$, and then compute u_{n+1} as $u_{n+1} = \sum_{i=1}^{q_1} R_{u_i} + 2\sum_{i=1+q_1}^{q_1+q_2} Re(R_{u_i})$.

7: **end for**

Remark. *To lessen the computational efforts, we precompute the inverse of the matrices* $\left(kA^{\alpha/2} - \tilde{c}_i I\right)^{-1}$, *and* $\left(kA^{\alpha/2} - c_i I\right)^{-1}$ *once outside the "for loop" then at each time step implement four matrix-vector multiplications which only require* $\mathcal{O}(n^2)$ *operations.*

5.4 Reliability and stability analysis

When discontinuities exist between the initial and boundary conditions, unwanted finite oscillations are observed. For example, using the (1,1)-Padé approximation to e^{-z}, the A-stable scheme (Crank-Nicolson) is known to produce oscillations since as z becomes large, $R_{1,1} = (4(2+z)^{-1} - 1)$ approaches (-1). In order to avoid these oscillations, Lawson and Morris [165] found out that the oscillations diminish as the highest frequency components, which are the oscillatory components, decay to zero faster than the lowest frequency components, which are the primary components. Khaliq *et al.* [55] provided an estimate on the choice of the time step for the CN scheme using the second-order MTT for discretizing the fractional Laplacian. Moreover, this estimate is extended in [55] to diagonal Padé approximations, which is similar to the estimates given in Lawson and Morris [165] and Khaliq *et al.* [149] for the corresponding integer-order PDEs.

5.4.1 Reliability Constraint

Here, we provide an estimate on the choice of the time step for the ETD-Padé(2,2) scheme (69) using the fourth-order compact scheme MTT for the space discretization.

Theorem 5.4.1.1. *[164]. Oscillations are guaranteed to dampen in the solution of the ETD-Padé(2,2) scheme (69) if*

$$k < 1.73\ \frac{1}{\kappa_\alpha}\left(\frac{h}{d}\sqrt{\frac{12X^2 - (\pi h)^2}{72\pi^2}}\right)^{\alpha/2},\ \text{where } X = (b-a)^d,\quad d = 1, 2, 3. \tag{71}$$

Proof. Let $R_{2,2}(z)$ denote the (2,2)-Padé approximation of e^z. Then, by Theorem 1 in [149], for $w < v < 0$, $wv < \min_{1\le j\le 2}|c_j|^2$, where c_j are the roots of the (2,2)-Padé approximant, we have

$$|R_{2,2}(w)| < |R_{2,2}(v)|. \tag{72}$$

If $d = 1$, let $v = k\kappa_\alpha(\frac{\sigma_1}{h^2})^{\frac{\alpha}{2}}$, and $w = k\kappa_\alpha(\frac{\sigma_{m-1}}{h^2})^{\frac{\alpha}{2}}$ where σ_1 and σ_{m-1} are given in (62). For large m,

$$v \approx k\kappa_\alpha\left(\frac{1}{h^2}\frac{4\ (\pi/2m)^2}{1-(1/3)(\pi/2m)^2}\right)^{\alpha/2}, \tag{73}$$

$$w \approx k\kappa_\alpha\left(\frac{1}{h^2}\frac{4}{1-(1/3)}\right)^{\alpha/2}.$$

Thus, (72) is true if

$$wv = k^2\kappa_\alpha^2\left(\frac{1}{h^2}\frac{72\pi^2}{12(mh)^2-(\pi h)^2}\right)^{\alpha/2} < \min_{1\le j\le 2}|c_j|^2.$$

This implies that

$$\begin{aligned} k &< \sqrt{12}\ \ \frac{1}{\kappa_\alpha}\left(h\sqrt{\frac{12X^2-(\pi h)^2}{72\pi^2}}\right)^{\alpha/2} \\ &\approx 1.73\ \ \frac{1}{\kappa_\alpha}\left(h\sqrt{\frac{12X^2-(\pi h)^2}{72\pi^2}}\right)^{\alpha/2}. \end{aligned}$$

Following the same steps, the results for $d = 2$ and 3 are obtained. □

5.4.2 Linear stability analysis

Next, we discuss the linear stability of the proposed schemes by plotting their stability regions as in [66]. We consider the nonlinear ODE

$$u_t = -cu + f(u). \tag{74}$$

Here, u is a complex valued function and $f(u)$ is the nonlinear part. We assume that there exists a fixed point u_0 such that $-cu_0 + f(u_0) = 0$. Then, by linearizing about

u_0, we get

$$u_t = -cu + \lambda u, \tag{75}$$

where u is the perturbation of u_0, and $\lambda = f'(u_0)$. The fixed point u_0 is stable if $Re(\lambda - c) < 0$ for all λ.

Let $y = -ck$ and $x = \lambda k$, where k is the time step size. The amplification symbol for the A-stable scheme is obtained in Chapter 3 by applying (69) to (75) and letting $r(x, y) = \frac{u_{n+1}}{u_n}$.

Similarly, by applying (70) to (75) we obtain the following amplification symbol for the L-stable scheme

$$r(x, y) = \frac{u_{n+1}}{u_n} = c_0 + c_1 x + c_2 x^2 + c_3 x^3 + c_4 x^4, \tag{76}$$

where

$$\begin{aligned}
c_0 &= \frac{(24 + 6y)}{(24 - 18y + 6y^2 - y^3)}, \\
c_1 &= \frac{(4 + y)}{(24 - 18y + 6y^2 - y^3)} + \frac{96(4 - y)(8 + y)}{(24 - 18y + 6y^2 - y^3)(192 - 72y + 12y^2 - y^3)} \\
&\quad + \frac{576(8 + y)^2(4 - 3y + y^2)}{(24 - 18y + 6y^2 - y^3)(192 - 72y + 12y^2 - y^3)^2}, \\
c_2 &= \frac{2(96 - 12y + y^2)(4 - y)}{(24 - 18y + 6y^2 - y^3)(192 - 72y + 12y^2 - y^3)} \\
&\quad + \frac{48(96 - 12y + y^2)(4 - y)(8 + y)}{(24 - 18y + 6y^2 - y^3)(192 - 72y + 12y^2 - y^3)^2} \\
&\quad + \frac{72(96 - 12y + y^2)(4 - 3y + y^2)(8 + y)}{(24 - 18y + 6y^2 - y^3)(192 - 72y + 12y^2 - y^3)^2} \\
&\quad - \frac{(96 - 12y + y^2)(4 - 3y + y^2)}{(24 - 18y + 6y^2 - y^3)(192 - 72y + 12y^2 - y^3)}, \\
c_3 &= \frac{2(96 - 12y + y^2)^2(4 - y)}{(24 - 18y + 6y^2 - y^3)(192 - 72y + 12y^2 - y^3)^2} \\
&\quad + \frac{48(96 - 12y + y^2)^2(4 - 3y + y^2)(8 + y)}{(24 - 18y + 6y^2 - y^3)(192 - 72y + 12y^2 - y^3)^3}, \\
c_4 &= \frac{2(96 - 12y + y^2)^3(4 - 3y + y^2)}{(24 - 18y + 6y^2 - y^3)(192 - 72y + 12y^2 - y^3)^3}.
\end{aligned}$$

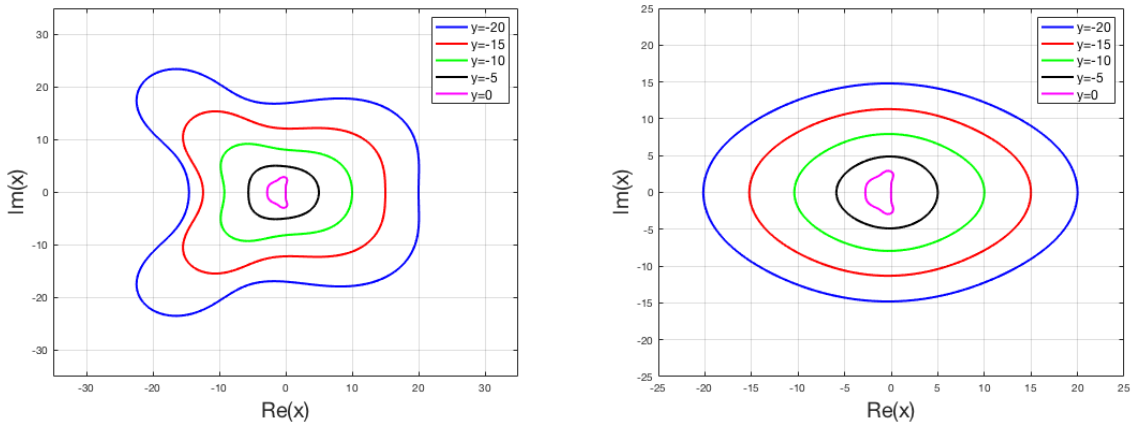

Figure 30: Stability regions of the ETD-Padé(2,2)(left) and ETD-Padé(1,3) (right) in the complex x-plane.

The curves of $r(x, y) = 1$ are shown in Fig. 30 for a complex value of x and some negative values of y. According to Beylkin *et al.* [131], for the scheme to be useful, the stability regions should grow as $y \to -\infty$. It is observed that when $y = 0$, the stability regions of the schemes correspond to the ETDRK4 scheme in [66]. Fig. 30 shows that the stability regions for the ETD-Padé(2,2) and ETD-Padé(1,3) schemes grow larger as $y \to -\infty$, which assert the stability of the schemes.

5.5 Numerical experiments

This section has several numerical test problems with smooth and non-smooth initial data. We consider a benchmark test problem with smooth initial data to verify the fourth-order accuracy of the schemes in space and time. We also consider some other problems with non-smooth data to validate our theoretical analysis. In the following, we use $\|.\|$ to denote either the L_2 or L_∞ norms. When the exact solution is known, the order of convergence in space and time is computed as

$$\text{order} = \frac{\log_{10}\left(E_{h,k}/E_{h/2,k/2}\right)}{\log_{10}(2)},$$

where $E_{h,k} = \|(u - u_{h,k})\|$ and $E_{h/2,k/2} = \left\|\left(u - u_{h/2,k/2}\right)\right\|$, u is the exact solution and $u_{h,k}$ is the numerical solution with space step size h and time step size k. When the exact solution is not known or available, the order of convergence in time with fixed space step size h is computed as

$$\text{order } = \frac{\log_{10}\left(E_{h,k}/E_{h,k/2}\right)}{\log_{10}(2)},$$

where $E_{h,k} = \left\|\left(u_{h,k} - u_{h,2k}\right)\right\|$ and $E_{h,k/2} = \left\|\left(u_{h,k/2} - u_{h,k}\right)\right\|$, $u_{h,k}$ and $u_{h,2k}$ are the numerical solutions with time step size k and $2k$, respectively.

5.5.1 Test Problem 1: a benchmark problem with an exact solution

We consider the following space-fractional reaction-diffusion equation with an exact solution [157] to validate the fourth-order accuracy of our ETD schemes

$$\frac{\partial u}{\partial t} = -\kappa_\alpha(-\Delta)^{\frac{\alpha}{2}}u + f(x,t,u),\ 1 < \alpha \leq 2,\ 0 < x < 1, \tag{77}$$

$$u(x,0) = 0,$$

$$u(0,t) = u(1,t) = 0,\ t > 0,$$

where

$$f(x,t,u) = \frac{\kappa_\alpha}{4}t^\alpha\{3[1+(2\pi)^\alpha]\sin(2\pi x) - [1+(6\pi)^\alpha]\sin(6\pi x)\} + \alpha t^{\alpha-1}\sin^3(2\pi x) - \kappa_\alpha u,$$

and $\kappa_\alpha > 0$. The exact solution to (77) is

$$u(x,t) = t^\alpha \sin^3(2\pi x).$$

The problem in (77) is chosen with an exact solution and smooth data to validate that our developed schemes exhibit the fourth-order accuracy in space and time. Fig. 31 shows the solutions up to $T = 1$ obtained via the ETD-Padé(2,2) and ETD-Padé(1,3) vs. the exact solution at $h = k = 0.01$, $\kappa_\alpha = 1$ and various values of α. Due to the smoothness of the initial data, the constraint (71) is not applicable for this problem.

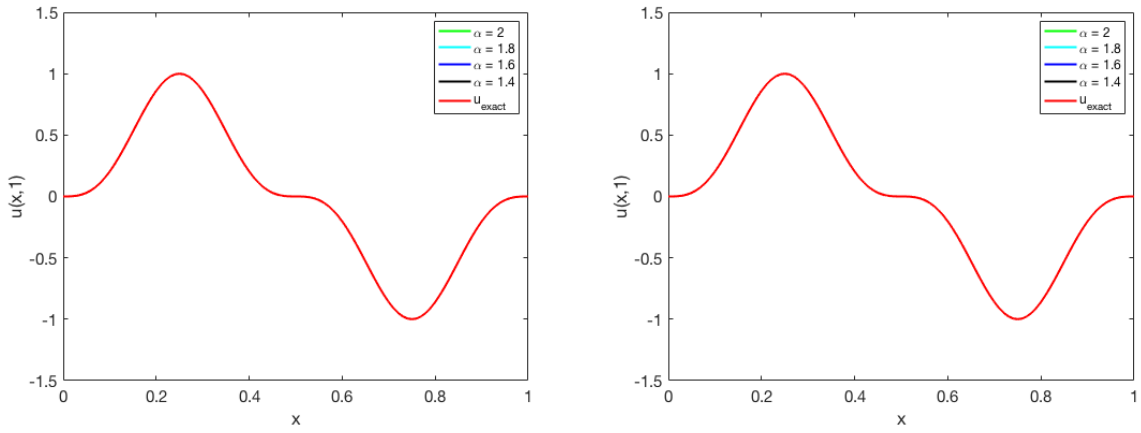

Figure 31: Numerical solutions of (77) as obtained by the ETD-Padé(2,2) (left) and ETD-Padé(1,3) (right) vs. the exact solution.

Thus, the solutions of the A-stable scheme are expected to be oscillation-free for any reasonable choice of h and k. The L_2, L_∞ errors, order of convergence and CPU(s) are listed in Tables 13 and 14 for a sequence of temporal and spatial steps starting at $k = 0.1$ and $h = 0.1$; both of them are halved for each subsequent sequence.

5.5.2 Test Problem 2: a problem from biochemistry

The following problem has a discontinuity between its initial and boundary conditions

$$\frac{\partial u}{\partial t} = -\kappa_\alpha(-\Delta)^{\frac{\alpha}{2}}u - \frac{u}{1+u}, \qquad x \in [0,1], \tag{78}$$

Table 13: Errors, convergence rates in space and time and CPU(s) for the ETD-Padé(2,2).

α	$h = k$	L_2 error	order	$L_\infty error$	order	CPU(s)
2	0.10000	1.0838e-02	-	1.4294e-02	-	0.0171
	0.05000	6.2221e-04	4.1225	9.0360e-04	3.9836	0.0261
	0.02500	3.8628e-05	4.0097	5.5754e-05	4.0185	0.0350
	0.01250	2.2569e-06	4.0972	3.2453e-06	4.1027	0.0542
1.8	0.10000	9.6407e-03	-	1.2729e-02	-	0.0584
	0.05000	5.4477e-04	4.1454	7.9213e-04	4.0063	0.0694
	0.02500	3.2731e-05	4.0569	4.7515e-05	4.0593	0.0791
	0.01250	1.9296e-06	4.0843	2.8002e-06	4.0848	0.1011
1.6	0.10000	8.4201e-03	-	1.1122e-02	-	0.0244
	0.05000	4.7226e-04	4.1562	6.8752e-04	4.0159	0.030
	0.02500	2.8352e-05	4.0581	4.1279e-05	4.0579	0.0352
	0.01250	1.7236e-06	4.0399	2.5099e-06	4.0397	0.0499
1.4	0.10000	7.2018e-03	-	9.5150e-03	-	0.0266
	0.05000	4.0460e-04	4.1538	5.8926e-04	4.0132	0.0328
	0.02500	2.4479e-05	4.0468	3.5671e-05	4.0461	0.0379
	0.01250	1.5111e-06	4.0179	2.2022e-06	4.0177	0.0519

$$u(x, 0) = 1,$$

$$u(0, t) = u(1, t) = 0.$$

Fig. 32 shows the time evolution graphs of both of the proposed schemes for $0 \leq t \leq 1$ and $\kappa_\alpha = 1$ using h = 0.01 and k= 0.01. When the A-stable scheme is used, unwanted oscillations are observed near the boundaries as the constraint (71) is not satisfied when $\alpha = 2,\ 1.8$, and 1.6. These oscillations diminish as the fractional-order decreases. No oscillation is observed in the solution when $\alpha = 1.4$ since the reliability constraint (71) is met. However, the solutions obtained by the L-stable scheme are shown to be oscillation-free for any value of α.

Table 14: Errors, convergence rates in space and time and CPU(s) for the ETD-Padé(1,3).

α	$h = k$	L_2 error	order	$L_\infty error$	order	CPU(s)
2	0.10000	1.0702e-02	-	1.4156e-02	-	0.0340
	0.05000	5.9643e-04	4.1654	8.6103e-04	4.0392	0.0452
	0.02500	3.5428e-05	4.0734	5.0858e-05	4.0815	0.0779
	0.01250	1.9187e-06	4.2067	2.7503e-06	4.2088	0.2771
1.8	0.10000	9.5434e-03	-	1.2622e-02	-	0.0328
	0.05000	5.3179e-04	4.1656	7.7111e-04	4.0329	0.0439
	0.02500	3.1342e-05	4.0847	4.5414e-05	4.0857	0.1396
	0.01250	1.7967e-06	4.1247	2.6065e-06	4.1229	0.2593
1.6	0.10000	8.3689e-03	-	1.1065e-02	-	0.0336
	0.05000	4.6663e-04	4.1647	6.7851e-04	4.0274	0.0464
	0.02500	2.7797e-05	4.0693	4.0446e-05	4.0683	0.0771
	0.01250	1.6836e-06	4.0453	2.4513e-06	4.0444	0.2458
1.4	0.10000	7.1796e-03	-	9.4898e-03	-	0.0299
	0.05000	4.0234e-04	4.1574	5.8569e-04	4.0182	0.0400
	0.02500	2.4308e-05	4.0489	3.5412e-05	4.0478	0.0636
	0.01250	1.5019e-06	4.0166	2.1885e-06	4.0162	0.2316

The L_2, L_∞ errors, order of convergence in time and CPU(s) for the A-stable and L-stable schemes are listed in Tables 15 and 16. In order to see the effect of the reliability constraint (71) in our numerical test, we fix h and vary the time steps k. We observe that the accuracy of the A-stable scheme is deteriorated for $\alpha = 2,\ 1.8$ and 1.6 when the reliability constraint is violated but becomes better with $\alpha = 1.4$. The L-stable scheme maintains the expected fourth-order accuracy in time for all values of α.

Table 15: Errors, convergence rates in time and CPU(s) for the ETD-Padé(2,2).

α	h	k	L_2error	order	L_∞error	order	CPU(s)
2	0.25000	0.25000	-	-	-	-	0.0165
	0.25000	0.12500	1.23e-02	-	1.74e-02	-	0.0255
	0.25000	0.06250	7.41e-06	10.70	9.24e-06	10.88	0.0281
	0.25000	0.03125	4.56e-08	7.34	6.45e-08	7.16	0.0311
	0.25000	0.01562	2.76e-09	4.05	3.90e-09	4.05	0.0392
1.8	0.25000	0.25000	-	-	-	-	0.0137
	0.25000	0.12500	3.28e-03	-	4.58e-03	-	0.0277
	0.25000	0.06250	2.01e-06	10.67	2.78e-06	10.69	0.0302
	0.25000	0.03125	1.16e-07	4.12	1.64e-07	4.09	0.0333
	0.25000	0.01562	7.03e-09	4.04	9.94e-09	4.04	0.0442
1.6	0.25000	0.25000	-	-	-	-	0.0142
	0.25000	0.12500	4.49e-04	-	5.34e-04	-	0.0224
	0.25000	0.06250	3.34e-06	7.07	4.73e-06	6.82	0.0250
	0.25000	0.03125	1.96e-07	4.09	2.77e-07	4.09	0.0282
	0.25000	0.01562	1.20e-08	4.04	1.69e-08	4.04	0.0367
1.4	0.25000	0.25000	-	-	-	-	0.0127
	0.25000	0.12500	8.01e-05	-	1.03e-04	-	0.0213
	0.25000	0.06250	4.06e-06	4.30	5.75e-06	4.16	0.0235
	0.25000	0.03125	2.41e-07	4.07	3.42e-07	4.07	0.0282
	0.25000	0.01562	1.48e-08	4.03	2.09e-08	4.03	0.0382

Table 16: Errors, convergence rates in time and CPU(s) for the ETD-Padé(1,3).

α	h	k	L_2 error	order	L_∞error	order	CPU(s)
2	0.25000	0.25000	-	-	-	-	0.0232
	0.25000	0.12500	7.14e-06	-	1.01e-05	-	0.0370
	0.25000	0.06250	6.60e-07	3.44	9.33e-07	3.44	0.0401
	0.25000	0.03125	4.97e-08	3.73	7.02e-08	3.73	0.0445
	0.25000	0.01562	3.42e-09	3.86	4.83e-09	3.86	0.0563
1.8	0.25000	0.25000	-	-	-	-	0.0181
	0.25000	0.12500	2.30e-05	-	3.25e-05	-	0.0298
	0.25000	0.06250	1.85e-06	3.63	2.62e-06	3.63	0.0328
	0.25000	0.03125	1.34e-07	3.80	1.89e-07	3.80	0.0375
	0.25000	0.01562	8.99e-09	3.89	1.27e-08	3.89	0.0495
1.6	0.25000	0.25000	-	-	-	-	0.0273
	0.25000	0.12500	4.56e-05	-	6.46e-05	-	0.0393
	0.25000	0.06250	3.44e-06	3.73	4.86e-06	3.73	0.0428
	0.25000	0.03125	2.39e-07	3.84	3.39e-07	3.84	0.0496
	0.25000	0.01562	1.58e-08	3.92	2.24e-08	3.92	0.0665
1.4	0.25000	0.25000	-	-	-	-	0.0161
	0.25000	0.12500	6.40e-05	-	9.06e-05	-	0.0274
	0.25000	0.06250	4.60e-06	3.80	6.51e-06	3.80	0.0304
	0.25000	0.03125	3.12e-07	3.88	4.42e-07	3.88	0.0351
	0.25000	0.01562	2.04e-08	3.94	2.89e-08	3.94	0.0469

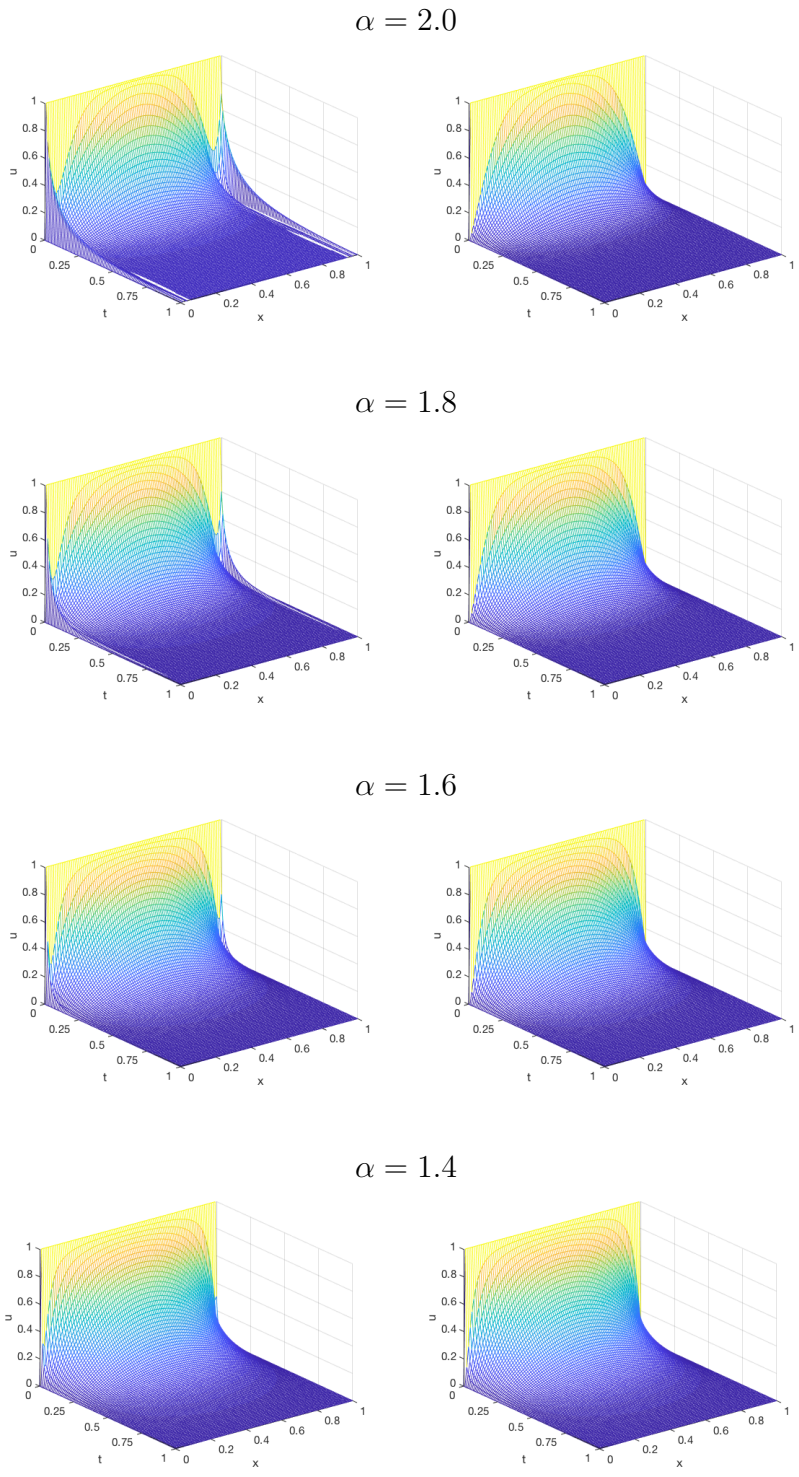

Figure 32: Solution profiles of (78) as obtained by the ETD-Padé(2,2) (left) and ETD-Padé (1,3) (right).

5.5.3 Test Problem 3: a problem with step initial condition

We consider the following problem with homogeneous Dirichlet boundary conditions and step initial condition

$$\frac{\partial u}{\partial t} = -\kappa_\alpha(-\Delta)^{\frac{\alpha}{2}}u, \qquad x \in [0,1], \tag{79}$$

$$u(x,0) = \begin{cases} 0, & 0 < x < \frac{1}{4}, \\ 1, & \frac{1}{4} \le x < \frac{3}{4}, \\ 0, & \frac{3}{4} \le x < 1. \end{cases} \qquad u(0,t) = u(1,t) = 0.$$

The exact solution is

$$u(x,t) = \sum_{n=1}^{\infty} \frac{4}{n\pi} \sin\left(\frac{n\pi}{2}\right) \sin\left(\frac{n\pi}{4}\right) \sin(n\pi x) \exp(-\kappa_\alpha (n\pi)^\alpha t).$$

Fig. 33 shows the comparison between the exact solution and the solutions obtained by the A-stable and L-stable schemes at $T = 1$, $h = 0.025$, $k = 0.025$ and $\kappa_\alpha = 1$. Spurious oscillations are observed near the discontinuity points in the solutions when the A-stable scheme is employed. The unwanted oscillations diminish when α decreases. With $\alpha = 1.6$ and 1.4, the constraint (71) is satisfied and the solution is oscillation-free. No oscillations are present in the solutions when the L-stable is applied.

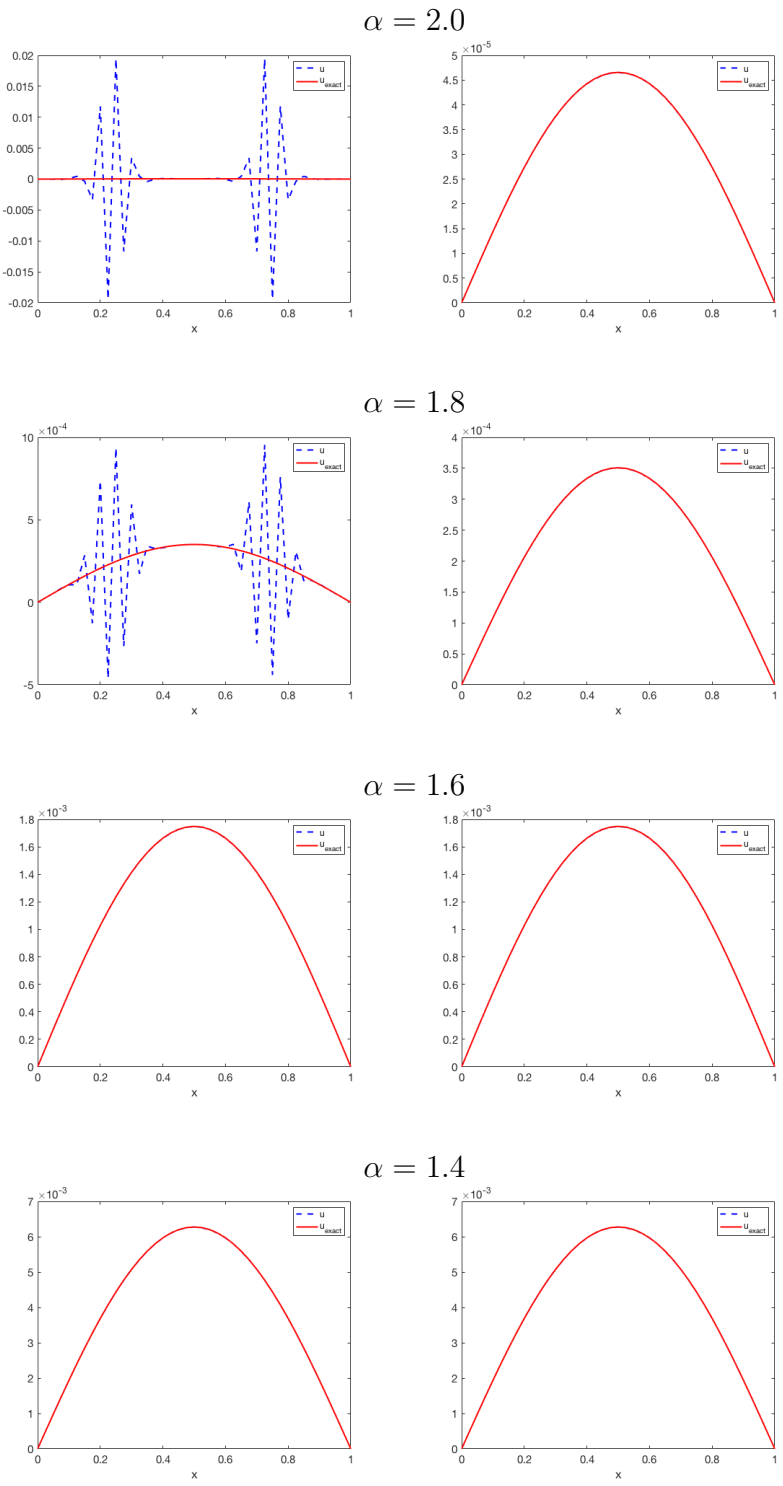

Figure 33: Solution profiles of (79) as obtained by the ETD-Padé(2,2) (left) and ETD-Padé(1,3) (right).

5.5.4 Test Problem 4: the Gray-Scott model (Pulse splitting)

We consider the system of the Gray-Scott model [100, 102, 106]

$$\begin{aligned}\frac{\partial u}{\partial t} &= -\kappa_u(-\Delta)^{\frac{\alpha}{2}}u - uv^2 + F(1-u),\\ \frac{\partial v}{\partial t} &= -\kappa_v(-\Delta)^{\frac{\alpha}{2}}v - (F+\kappa)v,\end{aligned} \tag{80}$$

with mismatched initial and boundary conditions

$$\begin{aligned}u(x,0) &= 1 - \frac{1}{2}\sin^{100}(\pi x),\\ v(x,0) &= \frac{1}{4}\sin^{100}(\pi x),\\ u(0,t) &= u(1,t) = v(0,t) = v(1,t) = 0,\end{aligned}$$

where κ_u and κ_v are the diffusion coefficients, and $x \in (0,1)$. Different patterns can be obtained depending on the values of F and κ. Figs. 34 and 35 show the time evolution of u and v for both of the derived schemes. The simulations ran up to $T = 10$ using $\kappa_u = 10^{-3}$, $\kappa_v = 10^{-5}$, $h = 0.001$, $k = 0.625$, $F = 0.024$ and $\kappa = 0.06$, where F and κ were chosen similar to [166]. Oscillations close to the boundaries can be seen in the solutions obtained by the ETD-Padé(2,2) at $\alpha = 2$, decrease at $\alpha = 1.7$ and 1.5, and are killed off at $\alpha = 1.3$, whereas no oscillations are present in the solutions when the ETD-Padé(1,3) is employed.

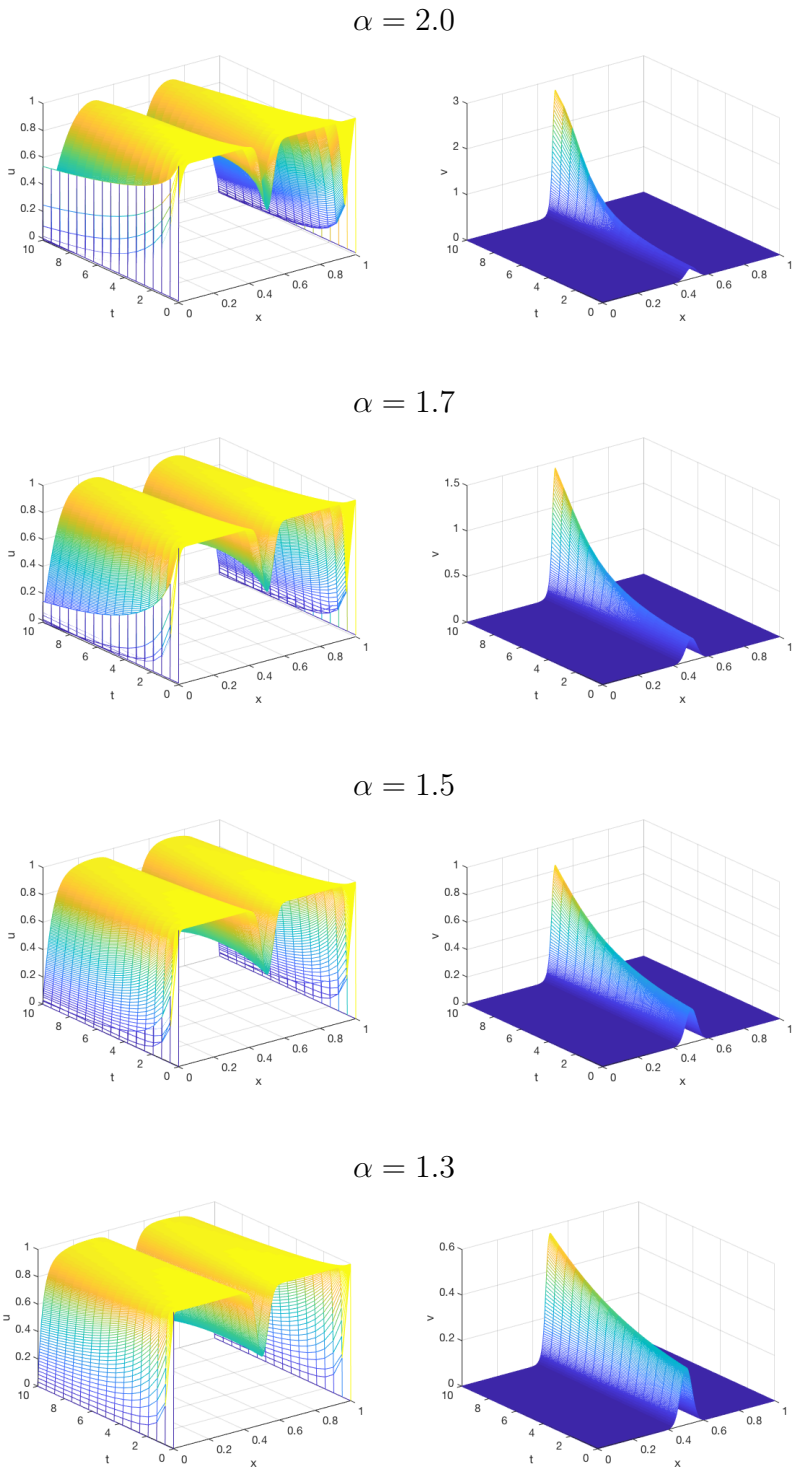

Figure 34: Solution profiles of the Gray-Scott model (80) as obtained by the ETD-Padé(2,2) (u left column and v right column) at $T = 10$.

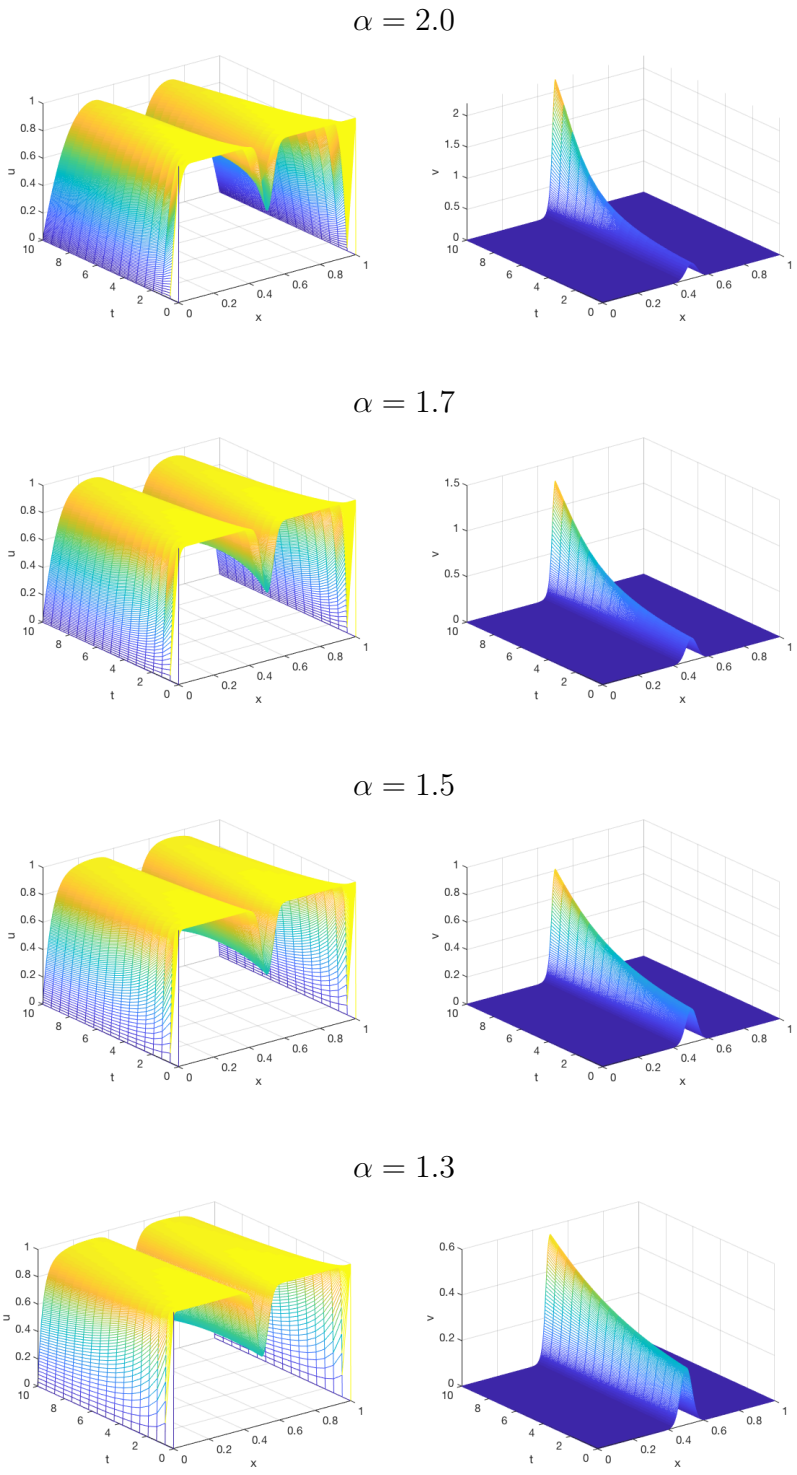

Figure 35: Solution profiles of the Gray-Scott model (80) as obtained by the ETD-Padé(1,3) (u left column and v right column) at $T = 10$.

5.5.5 Test problem 5: the 2D Fisher's equation

The following problem is the 2D space-fractional Fisher's equation

$$\frac{\partial u}{\partial t} = -\kappa_\alpha(-\Delta)^{\frac{\alpha}{2}}u + u(1-u), \quad 0 < x, y \leq 2, \tag{81}$$

$\kappa_\alpha = 1$, with homogeneous Dirichlet boundary conditions and the following initial condition

$$u(x, y, 0) = \sin\left(\frac{\pi y}{2}\right).$$

The initial and boundary conditions of (81) are mismatched. The solution for the 2D problem is shown in Fig. 36 at $T = 1$, $h = 0.05$ and $k = 0.25$. It is observed that the oscillations in the solution obtained by the ETD-Padé(2,2) scheme diminish with slow diffusion when α decreases, and the solutions produced by the ETD-Padé(1,3) scheme are oscillation-free.

In Table 17, we compare the L_2 error, order of convergence in time and CPU time of the ETD-Padé(2,2), ETD-Padé(1,3) and ETDRK4 with $h = 0.125$, $\alpha = 1.4$ and $\kappa = 3$. It is observed that the ETDRK4 scheme consumes more CPU time than the proposed schemes. Tables 18 and 19 show the L_2, L_∞ errors, order of convergence in time and CPU(s) of the A-stable and L-stable schemes at $T = 1$ and $\kappa_\alpha = 2$. It is shown that the L-stable scheme provides better accuracy than the A-stable scheme. When α decreases to 1.5, the A-stable scheme maintains the expected order of accuracy at each time step.

Table 17: A comparison of errors, convergence rates in time and CPU(s).

	ETD-Padé(2,2)			ETD-Padé(1,3)			ETDRK4		
k	L_2error	order	CPU(s)	L_2error	order	CPU(s)	L_2error	order	CPU(s)
0.12500	-	-	0.0645	-	-	0.0763	-	-	1.1205
0.06250	5.46e-05	-	0.1780	4.50e-05	-	0.2186	3.32e-06	-	2.6696
0.03125	2.27e-06	4.59	0.3920	3.56e-06	3.66	0.5185	3.93e-07	3.08	5.2742
0.01562	1.36e-07	4.06	0.8753	2.76e-07	3.69	1.0553	4.47e-08	3.14	9.7653
0.00781	8.32e-09	4.03	1.7524	2.01e-08	3.78	2.1504	3.78e-09	3.57	17.4680

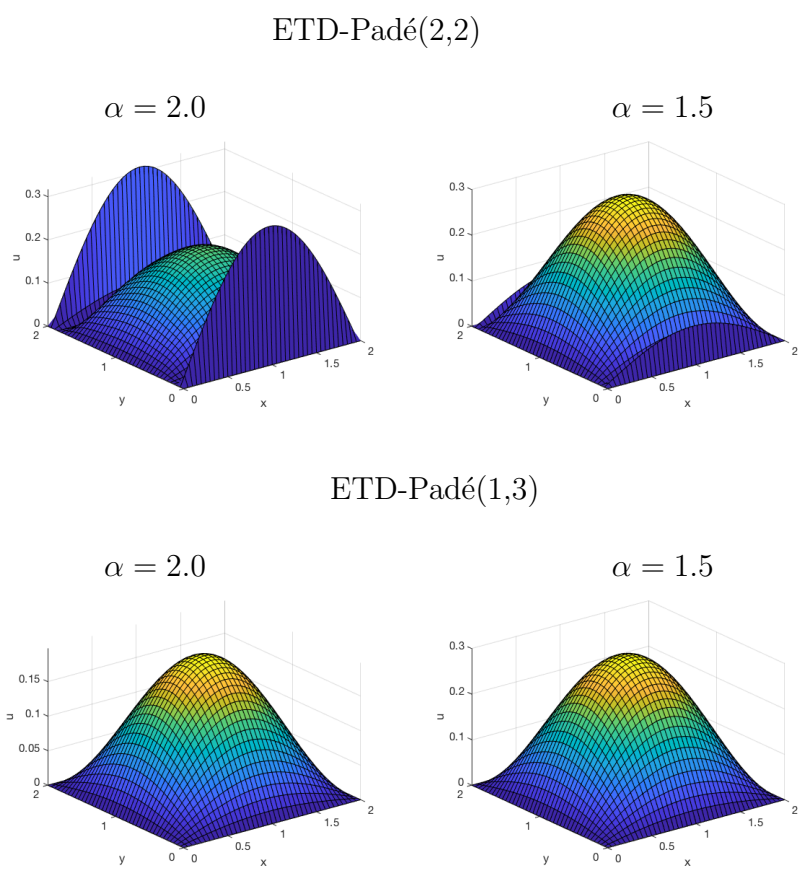

Figure 36: Solution profiles of the 2D Fisher's equation (81) at $T = 1$.

Table 18: Errors, convergence rates in time and CPU(s) for the ETD-Padé(2,2).

α	h	k	L_2error	order	L_∞error	order	CPU(s)
2	0.25000	0.25000	-	-	-	-	0.0065
	0.25000	0.12500	1.17e-02	-	5.74e-03	-	0.0119
	0.25000	0.06250	2.85e-05	8.68	1.50e-05	8.58	0.0246
	0.25000	0.03125	1.73e-06	4.04	8.67e-07	4.12	0.0460
	0.25000	0.01562	9.99e-08	4.12	5.00e-08	4.12	0.0849
1.5	0.25000	0.25000	-	-	-	-	0.0150
	0.25000	0.12500	4.20e-04	-	2.30e-04	-	0.0248
	0.25000	0.06250	2.20e-05	4.25	1.07e-05	4.42	0.0389
	0.25000	0.03125	1.37e-06	4.00	6.73e-07	3.99	0.0577
	0.25000	0.01562	8.71e-08	3.98	4.28e-08	3.98	0.0922

Table 19: Errors, convergence rates in time and CPU(s) for the ETD-Padé(1,3).

α	h	k	L_2error	order	L_∞error	order	CPU(s)
2	0.25000	0.25000	-	-	-	-	0.0196
	0.25000	0.12500	3.89e-04	-	1.94e-04	-	0.0327
	0.25000	0.06250	3.47e-05	3.49	1.73e-05	3.49	0.0436
	0.25000	0.03125	3.08e-06	3.49	1.53e-06	3.49	0.0680
	0.25000	0.01562	2.66e-07	3.53	1.32e-07	3.53	0.1396
1.5	0.25000	0.25000	-	-	-	-	0.0244
	0.25000	0.12500	3.47e-04	-	1.66e-04	-	0.0408
	0.25000	0.06250	2.94e-05	3.56	1.40e-05	3.56	0.0559
	0.25000	0.03125	2.25e-06	3.71	1.07e-06	3.71	0.0949
	0.25000	0.01562	1.58e-07	3.83	7.54e-08	3.83	0.1787

5.5.6 Test problem 6: the 3D Fisher's equation

The following problem is the 3D space-fractional Fisher's equation

$$\frac{\partial u}{\partial t} = -\kappa_\alpha(-\Delta)^{\frac{\alpha}{2}}u + u(1-u), \quad 0 < x, y, z \leq 1, \tag{82}$$

$\kappa_\alpha = 1/6$, with homogeneous Dirichlet boundary conditions and the following initial condition

$$u(x, y, z, 0) = \sin\left(\frac{\pi y}{2}\right)\sin\left(\frac{\pi z}{2}\right).$$

The initial and boundary conditions of (82) are mismatched. The solution for the 3D problem is shown in Fig. 37 at $T = 1$, $h = 0.05$ and $k = 0.5$. It is shown that the ETD-Padé(1,3) scheme is able to damp the oscillations due to the high frequency components in the solution. On the other hand, due to mismatched boundary and initial conditions, the ETD-Padé(2,2) scheme suffers with spurious oscillations near the boundary. The spurious oscillations diminish as α decreases.

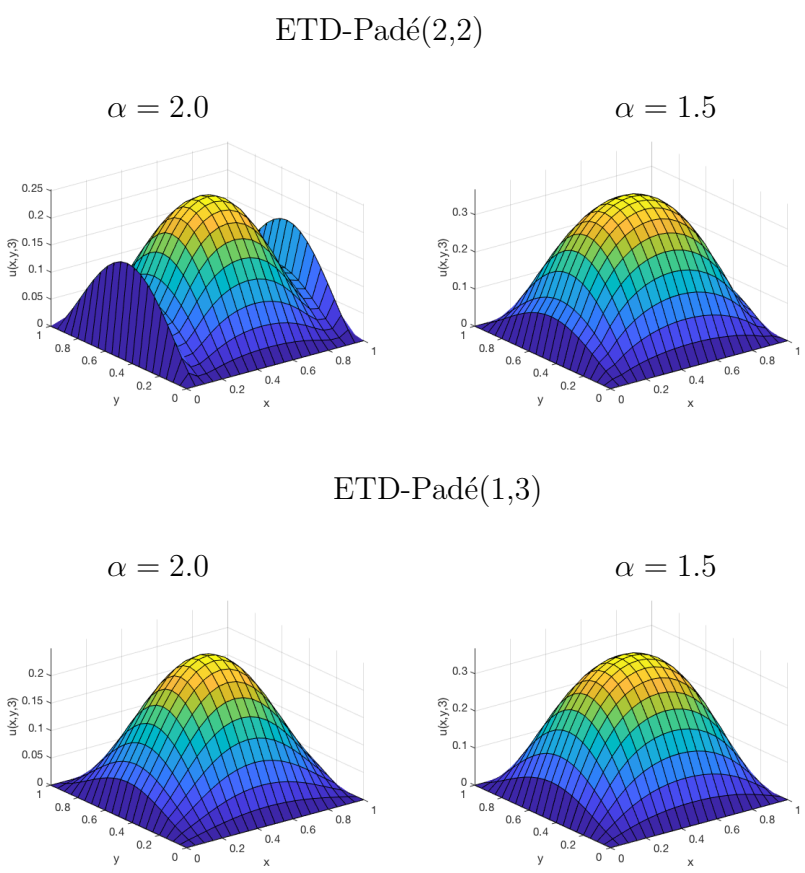

Figure 37: Solution profiles of the 3D Fisher's equation (82) at $T = 1$.

5.6 Conclusion

Two fourth-order schemes have been developed for solving space-fractional reaction-diffusion equations. The schemes are based on the fourth-order MTT in space and the fourth-order ETD in time. It is shown that when the initial data is non-smooth, the A-stable scheme produces spurious oscillations and is thus unreliable. On the other hand, the L-stable scheme is reliable for any time step and maintains its expected fourth-order accuracy. Numerical examples demonstrated the fourth-order accuracy in space and time, and showed the efficiency, accuracy and reliability of the developed schemes.

CHAPTER 6

CONCLUSIONS AND FUTURE WORK

In this dissertation, we have investigated several efficient numerical approximations for solving multidimensional space-fractional reaction-diffusion systems. We have developed and analyzed second-order ETD schemes of approximating the matrix exponential by (1,1)-Padé and (0,2)-Padé approximations, which are combined with the Fourier spectral approach to solve space-fractional partial differential equations with non-smooth initial data. A fourth-order ETD scheme of approximating the matrix exponential by the (2,2)-Padé approximation is also developed in combination with the Fourier spectral approach. Since the Fourier spectral approach, which is used for discretizing the fractional operator, can not handle the non-homogeneous boundary conditions, we consider using the MTT with homogeneous and non-homogeneous boundary conditions. Fourth-order ETD schemes were developed and combined with the MTT for solving the nonlinear multidimensional systems where the partial fraction decomposition is used to alleviate the difficulty due to ill-conditioning. When the A-stable schemes were applied with non-smooth initial data, unwanted oscillations were observed due to high frequency components. These oscillations diminished as the fractional-order decreased, we have proposed a novel reliability constraint to avoid the oscillations present in the solutions. Thus, the L-stable schemes are shown to be more reliable than the A-stable schemes when the initial data is non-smooth. The stability of the schemes was analyzed by plotting the stability regions. The error analysis, convergence, and stability of the schemes have been examined on several numerical experiments of well-known mathematical models, which exhibited the reliability, accuracy and efficiency of the schemes compared with some other numerical schemes in the literature. Our future work will include developing highly efficient numerical approximations to the time-space-fractional partial differential equations with non-homogeneous Neumann and Robin boundary conditions.

BIBLIOGRAPHY

References

[1] D. A. Benson, M. M. Meerschaert, and J. Revielle. Fractional calculus in hydrologic modeling: A numerical perspective. *Adv. Water Resour.*, 51:479–497, 2013.

[2] G. W. Leibniz. *Leibniz: Mathematische Schriften.* Olms, Hildesheim, 1962.

[3] K. B. Oldham and J. Spanier. *The Fractional Calculus.* Academic Press, New York, 1974.

[4] K. S. Miller and B. Ross. *An Introduction to the Fractional Calculus and Fractional Differential Equations.* Wiley, New York, 1993.

[5] G. Boling, P. Xueke, and H. Fenghui. *Fractional Partial Differential Equations and Their Numerical Solutions.* World Scientific, 2015.

[6] C. Pozrikidis. *The Fractional Laplacian.* CRC Press, 2016.

[7] V. V. Afanasiev, R. Z. Sagdeev, and G. M. Zaslavsky. Chaotic jets with multifractal space-time random walk. *Chaos*, 1(2):143–159, 1991.

[8] S. Fomin, V. Chugunov, and T. Hashida. Mathematical modeling of anomalous diffusion in porous media. *Fract. Differ. Calc.*, 1(1):1–28, 2011.

[9] D. A. Benson, S. W. Wheatcraft, and M. M. Meerschaert. The fractional-order governing equation of Lévy motion. *Water Resour. Res.*, 36(6):1413–1423, 2000.

[10] D. A. Benson, R. Schumer, M. M. Meerschaert, and S. W. Wheatcraft. Fractional dispersion, Lévy motion, and the made tracer tests. *Transp. Porous Media*, 42(1-2):211–240, 2001.

[11] A. Compte. Stochastic foundations of fractional dynamics. *Phys. Rev. E*, 53(4):4191, 1996.

[12] D. del Castillo-Negrete, B. A. Carreras, and V. E. Lynch. Front dynamics in reaction-diffusion systems with Levy flights: a fractional diffusion approach. *Phys. Rev. Lett.*, 91(1):018302, 2003.

[13] M. M. Meerschaert, D. A. Benson, H. P. Scheffler, and P. Becker-Kern. Governing equations and solutions of anomalous random walk limits. *Phys. Rev. E*, 66(6):060102, 2002.

[14] M. M. Meerschaert, D. A. Benson, H. P. Scheffler, and B. Baeumer. Stochastic solution of space-time fractional diffusion equations. *Phys. Rev. E*, 65(4):1103–1106, 2002.

[15] R. Metzler and J. Klafter. The random walk's guide to anomalous diffusion: a fractional dynamics approach. *Phys. Rep.*, 339(1):1–77, 2000.

[16] D. Frenkel and B. Smit. *Understanding Molecular Simulation: From Algorithms to Applications*. Elsevier, 2001.

[17] G. Iaffaldano, M. Caputo, and S. Martino. Experimental and theoretical memory diffusion of water in sand. *Hydrol. Earth Sys. Sci. Discuss.*, 2(4):1329–1357, 2005.

[18] J. Bai and X. Feng. Fractional-order anisotropic diffusion for image denoising. *IEEE Trans. Image Process.*, 16(10):2492–2502, 2007.

[19] M. Bologna, C. Tsallis, and P. Grigolini. Anomalous diffusion associated with nonlinear fractional derivative Fokker-Planck-like equation: Exact time-dependent solutions. *Phys. Rev. E*, 62(2):2213, 2000.

[20] O. G. Bakunin. *Turbulence and Diffusion: Scaling Versus Equations*. Springer Science & Business Media, 2008.

[21] S. Dipierro, G. Palatucci, and E. Valdinoci. Dislocation dynamics in crystals: a macroscopic theory in a fractional Laplace setting. *Commun. Math. Phys.*, 333(2):1061–1105, 2015.

[22] M. Raberto, E. Scalas, and F. Mainardi. Waiting-times and returns in high-frequency financial data: an empirical study. *Phys. A*, 314(1):749–755, 2002.

[23] E. Scalas, R. Gorenflo, and F. Mainardi. Fractional calculus and continuous-time finance. *Phys. A*, 284(1-4):376–384, 2000.

[24] Q. Meng, D. Ding, and Q. Sheng. Preconditioned iterative methods for fractional diffusion models in finance. *Numer. Methods Partial Differential Equations*, 31(5):1382–1395, 2015.

[25] W. Wang, X. Chen, D. Ding, and S. L. Lei. Circulant preconditioning technique for barrier options pricing under fractional diffusion models. *Int. J. Comput. Math.*, 92(12):2596–2614, 2015.

[26] W. Chen. Soft matter and fractional mathematics: insights into mesoscopic quantum and time-space structures. *arXiv preprint cond-mat/0405345*, 2004.

[27] E. Barkai, R. Metzler, and J. Klafter. From continuous time random walks to the fractional Fokker-Planck equation. *Phys. Rev. E*, 61(1):132, 2000.

[28] S. B. Yuste and K. Lindenberg. Subdiffusion-limited A+ A reactions. *Phys. Rev. Lett.*, 87(11):118301, 2001.

[29] S. B. Yuste, L. Acedo, and K. Lindenberg. Reaction front in an A+ B $\rightarrow$ C reaction-subdiffusion process. *Phys. Rev. E*, 69(3):036126, 2004.

[30] B. Baeumer, M. Kovács, and M. M. Meerschaert. Fractional reproduction-dispersal equations and heavy tail dispersal kernels. *Bull. Math. Biol.*, 69(7):2281–2297, 2007.

[31] F. Liu, V. Anh, and I. Turner. Numerical solution of the space fractional Fokker–Planck equation. *J. Comput. Appl. Math.*, 166(1):209–219, 2004.

[32] S. Momani and Z. Odibat. Numerical solutions of the space-time fractional advection-dispersion equation. *Numer. Methods Partial Differential Equations*, 24(6):1416–1429, 2008.

[33] E. E. Adams and L. W. Gelhar. Field study of dispersion in a heterogeneous aquifer: 2. spatial moments analysis. *Water Resour. Res.*, 28(12):3293–3307, 1992.

[34] D. A. Benson, S. W. Wheatcraft, and M. M. Meerschaert. Application of a fractional advection-dispersion equation. *Water Resour. Res.*, 36(6):1403–1412, 2000.

[35] B. Baeumer, D. A. Benson, M. M. Meerschaert, and S. W. Wheatcraft. Subordinated advection–dispersion equation for contaminant transport. *Water Resour. Res.*, 37(6):1543–1550, 2001.

[36] Y. Zhang, X. Liu, M. R. Belić, W. Zhong, Y. Zhang, and M. Xiao. Propagation dynamics of a light beam in a fractional Schrödinger equation. *Phys. Rev. Lett.*, 115(18):180403, 2015.

[37] D. del Castillo-Negrete and L. Chacón. Parallel heat transport in integrable and chaotic magnetic fields. *Phys. Plasmas*, 19(5):056112, 2012.

[38] Y. Zhang, M. M. Meerschaert, and R. M. Neupauer. Backward fractional advection dispersion model for contaminant source prediction. *Water Resour. Res.*, 52(4):2462–2473, 2016.

[39] Y. A. Rossikhin and M. V. Shitikova. Application of fractional calculus for dynamic problems of solid mechanics: novel trends and recent results. *Appl. Mech. Rev.*, 63(1):010801, 2010.

[40] Ł. Płociniczak. Analytical studies of a time-fractional porous medium equation. Derivation, approximation and applications. *Commun. Nonlinear Sci. Numer. Simul.*, 24(1-3):169–183, 2015.

[41] R. Metzler, J. H. Jeon, A. G. Cherstvy, and E. Barkai. Anomalous diffusion models and their properties: non-stationarity, non-ergodicity, and ageing at the centenary of single particle tracking. *Phys. Chem. Chem. Phys.*, 16(44):24128–24164, 2014.

[42] M. Yamamoto. Asymptotic expansion of solutions to the dissipative equation with fractional Laplacian. *SIAM J. Math. Anal.*, 44(6):3786–3805, 2012.

[43] N. Laskin. Fractional quantum mechanics and Lévy path integrals. *Phys. Lett. A*, 268(4-6):298–305, 2000.

[44] P. Constantin and J. Wu. Behavior of solutions of 2D Quasi-geostrophic equations. *SIAM J. Math. Anal.*, 30(5):937–948, 1999.

[45] A. de Pablo, F. Quirós, A. Rodríguez, and J. L. Vázquez. A fractional porous medium equation. *Adv. Math.*, 226(2):1378–1409, 2011.

[46] N. S. Landkof. *Foundations of Modern Potential Theory*. Springer, New York, 1972.

[47] S. G. Samko, A. A. Kilbas, and O. I. Marichev. *Fractional Integrals and Derivatives: Theory and Applications*. Gordon and Breach, Amsterdam, 1993, Translation from the Russian.

[48] E. D. Nezza, G. Palatucci, and E. Valdinoci. Hitchhikers guide to the fractional Sobolev spaces. *Bull. Sci. Math.*, 136(5):521–573, 2012.

[49] A. Lischke, G. Pang, M. Gulian, F. Song, C. Glusa, X. Zheng, Z. Mao, W. Cai, M. M. Meerschaert, M. Ainsworth, and G. E. Karniadakis. What is the Fractional Laplacian? *arXiv preprint arXiv:1801.09767*, 2018.

[50] G. M. Bisci, V. D. R**u**adulescu, and R. Servadei. *Variational Methods for Nonlocal Fractional Problems*. Cambridge University Press, 2016.

[51] A. Atangana and I. Koca. Chaos in a simple nonlinear system with Atangana–Baleanu derivatives with fractional order. *Chaos Solitons Fractals*, 89:447–454, 2016.

[52] A. Bueno-Orovio, D. Kay, and K. Burrage. Fourier spectral methods for fractional-in-space reaction-diffusion equations. *BIT Numer. Math.*, 54(4):937–954, 2014.

[53] T. Bakkyaraj and R. Sahadevan. Invariant analysis of nonlinear fractional ordinary differential equations with Riemann–Liouville fractional derivative. *Nonlinear Dyn.*, 80(1-2):447–455, 2015.

[54] M. Zheng, F. Liu, I. Turner, and V. Anh. A novel high order space-time spectral method for the time fractional Fokker–Planck equation. *SIAM J. Sci. Comput.*, 37(2):A701–A724, 2015.

[55] A. Q. M. Khaliq, T. A. Biala, S. S. Alzahrani, and K. M. Furati. Linearly implicit predictor–corrector methods for space-fractional reaction–diffusion equations with non-smooth initial data. *Comput. Math. Appl.*, 75(8):2629–2657, 2018.

[56] C. Li and A. Chen. Numerical methods for fractional partial differential equations. *Int. J. Comput. Math.*, 95(6-7):1048–1099, 2018.

[57] R. Gorenflo and F. Mainardi. Random walk models for space-fractional diffusion processes. *Fract. Calc. Appl. Anal.*, 1(2):167–191, 1998.

[58] M. Ilic, F. Liu, I. Turner, and V. Anh. Numerical approximation of a fractional-in-space diffusion equation (II)–with non-homogeneous boundary conditions. *Fract. Calc. Appl. Anal.*, 9(4):333–349, 2006.

[59] Q. Yang, F. Liu, and I. Turner. Numerical methods for fractional partial differential equations with Riesz space fractional derivatives. *Appl. Math. Model.*, 34(1):200–218, 2010.

[60] A. Q. M. Khaliq, X. Liang, and K. M. Furati. A fourth-order implicit-explicit scheme for the space fractional nonlinear Schrödinger equations. *Numer. Algorithms*, 75(1):147–172, 2017.

[61] M. D. Ortigueira. Riesz potential operators and inverses via fractional centred derivatives. *Int. J. Math. Math. Sci.*, 63(3):1–12, 2006.

[62] I. Podlubny, A. Chechkin, T. Skovranek, Y. Chen, and B. M. V. Jara. Matrix approach to discrete fractional calculus II: Partial fractional differential equations. *J. Comput. Phys.*, 228(8):3137–3153, 2009.

[63] S. Hamdi, W. E. Schiesser, and G. W. Griffiths. Method of lines. *Scholarpedia*, 2(7):2859, 2007.

[64] W. E. Schiesser and G. W. Griffiths. *A Compendium of Partial Differential Equation Models: Method of Lines Analysis with Matlab*. Cambridge University Press, 2009.

[65] J. Certaine. The solution of ordinary differential equations with large time constants. *Math. Methods Digital Comput.*, 128–132, 1960.

[66] S. M. Cox and P. C. Matthews. Exponential time differencing for stiff systems. *J. Comput. Phys.*, 176(2):430–455, 2002.

[67] C. Klein and K. Roidot. Fourth order time-stepping for Kadomtsev–Petviashvili and Davey–Stewartson equations. *SIAM J. Sci. Comput.*, 33(6):3333–3356, 2011.

[68] A. Kassam and L. N. Trefethen. Fourth-order time-stepping for stiff PDEs. *SIAM J. Sci. Comput.*, 26(4):1214–1233, 2005.

[69] A. Q. M. Khaliq, J. Martin-Vaquero, B. A. Wade, and M. Yousuf. Smoothing schemes for reaction-diffusion systems with nonsmooth data. *J. Comput. Appl. Math.*, 223(1):374–386, 2009.

[70] H. P. Bhatt and A. Q. M. Khaliq. Fourth-order compact schemes for the numerical simulation of coupled Burgers' equation. *Comput. Phys. Commun.*, 200:117–138, 2016.

[71] J. D. Lambert. *Numerical Methods for Ordinary Differential Systems: The Initial Value Problem*. John Wiley & Sons, Inc., 1991.

[72] M. Ilic, F. Liu, I. Turner, and V. Anh. Numerical approximation of a fractional-in-space diffusion equation, (I). *Fract. Calc. Appl. Anal.*, 8(3):323–341, 2005.

[73] I. Turner, M. Ilic, and P. Perre. The use of fractional-in-space diffusion equations for describing microscale diffusion in porous media. *In: 11th International Drying Conference, Magdeburg, Germany*, 2010.

[74] P. Constantin and M. Ignatova. Remarks on the fractional Laplacian with Dirichlet boundary conditions and applications. *Int. Math. Res. Notices*, 2017(6):1653–1673, 2017.

[75] F. Song, C. Xu, and G. E. Karniadakis. Computing fractional Laplacians on complex-geometry domains: algorithms and simulations. *SIAM J. Sci. Comput.*, 39(4):A1320–A1344, 2017.

[76] D. A. Voss and A. Q. M. Khaliq. A linearly implicit predictor-corrector method for reaction-diffusion equations. *Comput. Math. Appl.*, 38(11-12):207–216, 1999.

[77] J. Cao, G. Song, J. Wang, Q. Shi, and S. Sun. Blow-up and global solutions for a class of time fractional nonlinear reaction–diffusion equation with weakly spatial source. *Appl. Math. Lett.*, 91:201–206, 2019.

[78] C. Li and A. Chen. Numerical methods for fractional partial differential equations. *Int. J. Comput. Math.*, 95(6-7):1048–1099, 2018.

[79] M. M. Meerschaert and C. Tadjeran. Finite difference approximations for two-sided space-fractional partial differential equations. *Appl. Numer. Math.*, 56(1):80–90, 2006.

[80] H. Wang, K. Wang, and T. Sircar. A direct O (N $\log^2$ N) finite difference method for fractional diffusion equations. *J. Comput. Phys.*, 229(21):8095–8104, 2010.

[81] K. Burrage, N. Hale, and D. Kay. An efficient implicit FEM scheme for fractional-in-space reaction-diffusion equations. *SIAM J. Sci. Comput.*, 34(4):A2145–A2172, 2012.

[82] Q. Yang, I. Turner, F. Liu, and M. Ilić. Novel numerical methods for solving the time-space fractional diffusion equation in two dimensions. *SIAM J. Sci. Comput.*, 33(3):1159–1180, 2011.

[83] L. Aceto and P. Novati. Rational approximation to the fractional Laplacian operator in reaction-diffusion problems. *SIAM J. Sci. Comput.*, 39(1):A214–A228, 2017.

[84] A. Saadatmandi, M. Dehghan, and M. Azizi. The Sinc–Legendre collocation method for a class of fractional convection–diffusion equations with variable coefficients. *Commun. Nonlinear Sci. Numer. Simul.*, 17(11):4125–4136, 2012.

[85] M. Dehghan and M. Abbaszadeh. Numerical study of three-dimensional Turing patterns using a meshless method based on moving Kriging element free Galerkin (EFG) approach. *Comput. Math. Appl.*, 72(3):427–454, 2016.

[86] M. Dehghan and M. Abbaszadeh. Variational multiscale element free Galerkin (VMEFG) and local discontinuous Galerkin (LDG) methods for solving two-

dimensional Brusselator reaction–diffusion system with and without cross-diffusion. *Comput. Methods Appl. Mech. Eng.*, 300:770–797, 2016.

[87] M. Dehghan, M. Abbaszadeh, and W. Deng. Fourth-order numerical method for the space–time tempered fractional diffusion-wave equation. *Appl. Math. Lett.*, 73:120–127, 2017.

[88] H. G. Lee. A second-order operator splitting Fourier spectral method for fractional-in-space reaction–diffusion equations. *J. Comput. Appl. Math.*, 333:395–403, 2018.

[89] M. Marek and I. Schreiber. *Chaotic Behaviour of Deterministic Dissipative Systems*. Cambridge University Press, New York, 1991.

[90] G. Nicolis and I. Prigogine. *Self-Organization in Non-Equilibrium Systems*. Wiley-Interscience, New York, 1977.

[91] R. Fazio and A. Jannelli. Second order numerical operator splitting for 3D advection–diffusion-reaction models. *Numer. Math. Adv. Appl.*, 317–324, 2009.

[92] A. L. Hodgkin and A. F. Huxley. A quantitative description of membrane current and its application to conduction and excitation in nerve. *J. Physiol.*, 117(4):500–544, 1952.

[93] M. Courtemanche, W. Skaggs, and A. T. Winfree. Stable three-dimensional action potential circulation in the FitzHugh-Nagumo model. *Phys. D*, 41(2):173–182, 1990.

[94] C. Henze, E. Lugosi, and A. T. Winfree. Helical organizing centers in excitable media. *Can. J. Phys.*, 68(9):683–710, 1990.

[95] J. P. Keener and J. J. Tyson. The dynamics of scroll waves in excitable media. *SIAM Rev.*, 34(1):1–39, 1992.

[96] V. N. Biktashev and A. V. Holden. Reentrant arrhythmias and their control in models of mammalian cardiac tissue. *J. Electrocardiol.*, 32:76–83, 2001.

[97] A. Bueno-Orovio, E. M. Cherry, and F. H. Fenton. Minimal model for human ventricular action potentials in tissue. *J. Theor. Biol.*, 253(3):544–560, 2008.

[98] R. FitzHugh. Impulses and physiological states in theoretical models of nerve membrane. *Biophys. J.*, 1(6):445–466, 1961.

[99] J. Nagumo, S. Arimoto, and S. Yoshizawa. An active pulse transmission line simulating nerve axon. *Proc. Inst. Radio Eng.*, 50(10):2061–2070, 1962.

[100] P. Gray and S. K. Scott. Autocatalytic reactions in the isothermal, continuous stirred tank reactor: Oscillations and instabilities in the system A+ 2B→ 3B; B→ C. *Chem. Eng. Sci.*, 39(6):1087–1097, 1984.

[101] J. K. Hale, L. A. Peletier, and W. C. Troy. Exact Homoclinic and Heteroclinic solutions of the Gray–Scott Model for Autocatalysis. *SIAM J. Appl. Math.*, 61(1):102–130, 2000.

[102] A. Doelman, T. J. Kaper, and P. A. Zegeling. Pattern formation in the one-dimensional Gray-Scott model. *Nonlinearity*, 10(2):523–563, 1997.

[103] W. N. Reynolds, S. Ponce-Dawson, and J. E. Pearson. Self-replicating spots in reaction-diffusion systems. *Phys. Rev. E*, 56(1):185–198, 1997.

[104] K. J. Lee, W. D. McCormick, J. E. Pearson, and H. L. Swinney. Experimental observation of self-replicating spots in a reaction–diffusion system. *Nature*, 369(6477):215–218, 1994.

[105] W. N. Reynolds, J. E. Pearson, and S. Ponce-Dawson. Dynamics of self-replicating patterns in reaction diffusion systems. *Phys. Rev. Lett.*, 72(17):2797–2800, 1994.

[106] J. E. Pearson. Complex patterns in a simple system. *Science*, 261(5118):189–192, 1993.

[107] J. Lefèvre and J. Mangin. A reaction-diffusion model of human brain development. *PLoS Comput. Biol.*, 6(4):e1000749, 2010.

[108] J. J. Tyson. Some further studies of nonlinear oscillations in chemical systems. *J. Chem. Phys.*, 58(9):3919–3930, 1973.

[109] G. Adomian. The diffusion-Brusselator equation. *Comput. Math. Appl.*, 29(5):1–3, 1995.

[110] D. Iron, J. Wei, and M. Winter. Stability analysis of Turing patterns generated by the Schnakenberg model. *J. Math. Biol.*, 49(4):358–390, 2004.

[111] J. Schnakenberg. Simple chemical reaction systems with limit cycle behaviour. *J. Theor. Biol.*, 81(3):389–400, 1979.

[112] J. D. Murray. *Mathematical Biology II: Spatial Models and Biochemical Applications*. Springer-Verlag Berlin, 2003.

[113] M. Ghergu and V. D. Radulescu. *Nonlinear PDEs: Mathematical Models in Biology, Chemistry and Population Genetics*. Springer, Heidelberg, 2012.

[114] C. Moler and C. Van Loan. Nineteen dubious ways to compute the exponential of a matrix, twenty-five years later. *SIAM Rev.*, 45(1):3–49, 2003.

[115] M. M. Meerschaert and C. Tadjeran. Finite difference approximations for fractional advection–dispersion flow equations. *J. Comput. Appl. Math.*, 172(1):65–77, 2004.

[116] C. Çelik and M. Duman. Crank–Nicolson method for the fractional diffusion equation with the Riesz fractional derivative. *J. Comput. Phys.*, 231(4):1743–1750, 2012.

[117] Q. Yu, F. Liu, I. Turner, and K. Burrage. Numerical investigation of three types of space and time fractional Bloch–Torrey equations in 2D. *Cent. Eur. J. Phys.*, 11(6):646–665, 2013.

[118] Q. Yu, F. Liu, I. Turner, and K. Burrage. Stability and convergence of an implicit numerical method for the space and time fractional Bloch–Torrey equation. *Phil. Trans. R. Soc. A*, 371(1990):20120150, 2013.

[119] Z. Yang, Z. Yuan, Y. Nie, J. Wang, X. Zhu, and F. Liu. Finite element method for nonlinear Riesz space fractional diffusion equations on irregular domains. *J. Comput. Phys.*, 330:863–883, 2017.

[120] K. M. Owolabi and A. Atangana. Analysis of mathematics and numerical pattern formation in superdiffusive fractional multicomponent system. *Adv. Appl. Math. Mech.*, 9(6):1438–1460, 2017.

[121] K. M. Owolabi and A. Atangana. Numerical simulations of chaotic and complex spatiotemporal patterns in fractional reaction–diffusion systems. *Comput. Appl. Math.*, 37(2):2166–2189, 2018.

[122] Q. Yang, I. Turner, T. Moroney, and F. Liu. A finite volume scheme with preconditioned Lanczos method for two-dimensional space-fractional reaction–diffusion equations. *Appl. Math. Model.*, 38(15-16):3755–3762, 2014.

[123] F. Liu, P. Zhuang, and Q. Liu. *Numerical Methods of Fractional Partial Differential Equations and Applications*. Science Press, China, 2015.

[124] J. Shen, T. Tang, and L. Wang. *Spectral Methods: Algorithms, Analysis and Applications*. Springer Science & Business Media, 2011.

[125] L. N. Trefethen. *Spectral Methods in MatLab*. SIAM, Philadelphia, 2000.

[126] W. L. Briggs and V. E. Henson. *The DFT: An Owner's Manual for the Discrete Fourier Transform*. SIAM, 1995.

[127] A. Bueno-Orovio and V. M. Pérez-García. Spectral smoothed boundary methods: the role of external boundary conditions. *Numer. Methods Partial Differential Equations*, 22(2):435–448, 2006.

[128] B. Kleefeld, A. Q. M. Khaliq, and B. A. Wade. An ETD Crank-Nicolson method for reaction-diffusion systems. *Numer. Methods Partial Differential Equations*, 28(4):1309–1335, 2012.

[129] M. Yousuf, A. Q. M. Khaliq, and B. Kleefeld. The numerical approximation of nonlinear Black–Scholes model for exotic path-dependent American options with transaction cost. *Int. J. Comput. Math.*, 89(9):1239–1254, 2012.

[130] S. S. Alzahrani and A. Q. M. Khaliq. Fourier spectral exponential time differencing methods for multi-dimensional space-fractional reaction–diffusion equations. *J. Comput. Appl. Math.*, 361:157–175, 2019.

[131] G. Beylkin, J. M. Keiser, and L. Vozovoi. A new class of time discretization schemes for the solution of nonlinear PDEs. *J. Compu. Phys.*, 147(2):362–387, 1998.

[132] Y. Cherruault, M. Choubane, J. M. Valleton, and J. C. Vincent. Stability and asymptotic behavior of a numerical solution corresponding to a diffusion-reaction equation solved by a finite difference scheme (Crank–Nicolson). *Comput. Math. Appl.*, 20(11):37–46, 1990.

[133] S. M. Allen and J. W. Cahn. A microscopic theory for antiphase boundary motion and its application to antiphase domain coarsening. *Acta Metall. Mater.*, 27(6):1085–1095, 1979.

[134] F. Liu, P. Zhuang, I. Turner, V. Anh, and K. Burrage. A semi-alternating direction method for a 2-D fractional Fitzhugh–Nagumo monodomain model on an approximate irregular domain. *J. Comput. Phys.*, 293:252–263, 2015.

[135] R. I. Fernandes and G. Fairweather. An ADI extrapolated Crank-Nicolson orthogonal spline collocation method for nonlinear reaction–diffusion systems. *J. Comput. Phys.*, 231(19):6248–6267, 2012.

[136] E. Hairer and G. Wanner. *Solving ordinary Differential Equations, II: Stiff and Differential–Algebraic Problems*. Springer-Verlag Berlin, 1991.

[137] B. Yin, Y. Liu, H. Li, and S. He. Fast algorithm based on TT-M FE system for space fractional Allen-Cahn equations with smooth and non-smooth solutions. *J. Comput. Phys.*, 379:351 – 372, 2019.

[138] M. Hederi, A. L. Islas, K. Reger, and C. M. Schober. Efficiency of exponential time differencing schemes for nonlinear Schrödinger equations. *Math. Comput. Simul.*, 127:101–113, 2016.

[139] S. S. Alzahrani and A. Q. M. Khaliq. High-order time stepping Fourier spectral method for multi-dimensional space-fractional reaction–diffusion equations. *Comput. Math. Appl.*, 77(3):615–630, 2019.

[140] K. Burrage, N. Hale, and D. Kay. An efficient implicit FEM scheme for fractional–in–space reaction–diffusion equations. *SIAM J. Sci. Comput.*, 34(4):A2145–A2172, 2012.

[141] B. Fornberg and T. A. Driscoll. A fast spectral algorithm for nonlinear wave equations with linear dispersion. *J. Comput. Phys.*, 155(2):456–467, 1999.

[142] P. Gray and S. K. Scott. Autocatalytic reactions in the isothermal, continuous stirred tank reactor: isolas and other forms of multistability. *Chem. Eng. Sci.*, 38(1):29–43, 1983.

[143] P. Gray and S. K. Scott. Sustained oscillations and other exotic patterns of behavior in isothermal reactions. *J. Phys. Chem.*, 89(1):22–32, 1985.

[144] E. Hairer, S. P. Norsett, and G. Wanner. *Solving Ordinary Differential Equations, I: Nonstiff Problems*. Springer-Verlag Berlin, 1993.

[145] W. R. Holmes. An efficient, nonlinear stability analysis for detecting pattern formation in reaction diffusion systems. *Bull. Math. Biol.*, 76(1):157–183, 2014.

[146] V. J. Ervin, N. Heuer, and J. P. Roop. Numerical approximation of a time dependent, nonlinear, space-fractional diffusion equation. *SIAM J. Numer. Anal.*, 45(2):572–591, 2007.

[147] P. Zhuang, F. Liu, V. Anh, and I. Turner. Numerical methods for the variable-order fractional advection-diffusion equation with a nonlinear source term. *SIAM J. Numer. Anal.*, 47(3):1760–1781, 2009.

[148] E. Gallopoulos and Y. Saad. On the parallel solution of parabolic equations. *CSRD Report, University of Illinois, Urbana, Chumpaign*, 1988.

[149] A. Q. M. Khaliq, E. H. Twizell, and D. A. Voss. On parallel algorithms for semidiscretized parabolic partial differential equations based on subdiagonal Padé approximations. *Numer. Methods Partial Differential Equations*, 9(2):107–116, 1993.

[150] X. Cabré and J. Tan. Positive solutions of nonlinear problems involving the square root of the Laplacian. *Adv. Math.*, 224(5):2052–2093, 2010.

[151] R. L. Frank and E. Lenzmann. Uniqueness of non-linear ground states for fractional Laplacians in $\mathbb{R}$. *Acta Math.*, 210(2):261–318, 2013.

[152] X. Cabré and Y. Sire. Nonlinear equations for fractional Laplacians II: existence, uniqueness, and qualitative properties of solutions. *Trans. Amer. Math. Soc.*, 367(2):911–941, 2015.

[153] R. H. Nochetto, E. Otárola, and A. J. Salgado. A PDE approach to fractional diffusion in general domains: a priori error analysis. *Found. Comput. Math.*, 15(3):733–791, 2015.

[154] C. Tadjeran, M. M. Meerschaert, and H. P. Scheffler. A second-order accurate numerical approximation for the fractional diffusion equation. *J. Comput. Phys.*, 213(1):205–213, 2006.

[155] W. Deng. Finite element method for the space and time fractional Fokker–Planck equation. *SIAM J. Numer. Anal.*, 47(1):204–226, 2008.

[156] X. Zhang, M. Lv, J. W. Crawford, and I. M. Young. The impact of boundary on the fractional advection–dispersion equation for solute transport in soil: Defining the fractional dispersive flux with the Caputo derivatives. *Adv. Water Resour.*, 30(5):1205–1217, 2007.

[157] S. Zhai, D. Gui, J. Zhao, and X. Feng. High accuracy spectral method for the space-fractional diffusion equations. *J. Math. Study*, 47(3):274–286, 2014.

[158] B. Yu, X. Jiang, and H. Xu. A novel compact numerical method for solving the two-dimensional non-linear fractional reaction-subdiffusion equation. *Numer. Algorithms*, 68(4):923–950, 2015.

[159] M. E. Farquhar, T. J. Moroney, Q. Yang, and I. W. Turner. GPU accelerated algorithms for computing matrix function vector products with applications to exponential integrators and fractional diffusion. *SIAM J. Sci. Comput.*, 38(3):C127–C149, 2016.

[160] E. O. Asante-Asamani, A. Q. M. Khaliq, and B. A. Wade. A real distinct poles exponential time differencing scheme for reaction–diffusion systems. *J. Comput. Appl. Math.*, 299:24–34, 2016.

[161] H. P. Bhatt and A. Q. M. Khaliq. Higher order exponential time differencing scheme for system of coupled nonlinear Schrödinger equations. *Appl. Math. Comput.*, 228:271–291, 2014.

[162] H. Ding and Y. Zhang. New numerical methods for the Riesz space fractional partial differential equations. *Comput. Math. Appl.*, 63(7):1135–1146, 2012.

[163] Y. Hu, C. Li, and H. Li. The finite difference method for Caputo-type parabolic equation with fractional Laplacian: more than one space dimension. *Int. J. Comput. Math.*, 95(6-7):1114–1130, 2018.

[164] S. S. Alzahrani, A. Q. M. Khaliq, T. A. Biala, and K. M. Furati. Fourth-order time stepping methods with matrix transfer technique for space-fractional reaction-diffusion equations. *Appl. Numer. Math.*, 146:123–144, 2019.

[165] J. D. Lawson and J. L. Morris. The extrapolation of first order methods for parabolic partial differential equations. *SIAM J. Numer. Anal.*, 15(6):1212–1224, 1978.

[166] P. A. Zegeling and H. P. Kok. Adaptive moving mesh computations for reaction–diffusion systems. *J. Comput. Appl. Math.*, 168(1-2):519–528, 2004.